Nordic Volcanological Institute 9501
University of Iceland

The Nordic-Baltic Scholarship Scheme

Petrology and Petrogenesis of the Thverartindur Plutonic Formation, SE Iceland

by

Alvar Soesoo*

Reykjavík 1995

*Present address: Institute of Geology, Academy of Sciences of Estonia, Estonia pst. 7, EE0100, Tallinn, Estonia

Nordic Volcanological Institute 9501
University of Iceland

The Nordic-Baltic Scholarship Scheme

Petrology and Petrogenesis of the Thverartindur Plutonic Formation, SE Iceland

by
Alvar Soesoo*

Reykjavík 1995

*Present address: Institute of Geology, Academy of Sciences of Estonia, Estonia pst. 7, EE0100, Tallinn, Estonia

Content

1. Introduction

The geology of Iceland reflect igneous activity back to 16 m.y. Due to heavy glacial erosion in the south-eastern part of the Iceland, up to 500 m may have been removed from the mountain tops exposing sections down to 2000 m original depth in glacial valleys (Walker, 1974). This section offers a unique opportunity to study the part of crust where intrusions are beginning to dominate over lava flows. A diversity of plutonic rocks exposed allows to evaluate the mechanism of magmatic intrusion and differentiation.

The Thverartindur formation is a deeply eroded Tertiary central volcanic complex situated on a volcanic lineament parallel to the Eastern Neovolcanic Zone (Fig. 1.). Three gabbro - granophyre composite intrusions -- Hvannadalur, Fellsa and Vedurardalur are exposed in glacial valleys in addition to several generations of dikes and inclined sheets. The complicated intrusive relationships exhibit a multitude of small gabbroic sill-like intrusions, while abundant granophyres form the separate bodies.

Ocean floor gabbros are commonly described as highly cumulative rocks, and it is inferred that gabbro formation follows fractional crystallization path along distinctive mineral sequences. A distinctive feature of the Thverartindur gabbros is the lack of cumulus textures, and whole rock chemistry close to unmodified magmatic liquid composition. The present study describes the less common situation in the ocean floor environment -- non-cumulus gabbros. An attempt is made to evaluate the crustal processes that produced the Thverartindur plutonic formation.

Several methods have been employed to establish the observed crystallization trends and links between primitive and evolved basaltic compositions. Thermodynamic models have been applied to demonstrate how the common quartz-tholeiites may be formed. It will be shown that the quartz-tholeiites may form after 40-55% equilibrium crystallization of olivine-tholeiite close to the QFM oxygen buffer and may be affected by minor assimilation and mixing effects. Clinopyroxene compositions have been studied in detail. Using interelement relationships and multivariate statistics, the clinopyroxenes can be used as an indicator for crystallization and mixing histories.

2. General Geology of Iceland and Thverartindur formation

A combination of an oceanic ridge and the Icelandic hot spot active during the Tertiary, has created the Icelandic crust during the last 16 my. At the present, Iceland is cut by the North-Atlantic plate boundary which is exposed in several rift segments of roughly NE-SW direction. The crust gets younger towards the rift-zones but as the relative position of the hot spot and the plate boundary in Iceland have changed by time a series of ridge jumps and ridge propagation episodes have taken place. The half-spreading rate in Iceland is 10 mm/y. Due to higher mantle temperatures (White and McKenzie, 1986), the range of rock types are more varied. Estimates of the thickness of the crust in Iceland varies from 8 to over 20 km being anomalously thick compared with the range of 3-8 km for a normal oceanic crust.

The recent volcano-tectonic activity is concentrated in elongated rift segments and to few off-rift volcanic systems. Each volcano-tectonic system is composed of a set of parallel volcanic lineaments, constituting a fissure swarm that varies in length from 20 to 100 km, and in width from 5 to 30 km (Jakobsson, 1979). The centres of these swarms may develop into a central volcano that has lifetime about from 0,3 to 1 My (Saemundsson, 1979). Shield volcanoes or lava shields of various size (up to15 km^3) are found randomly within the rift zones.

Glacial activity during the Quaternary has created most of the Holocene landforms in Iceland. In addition to the formation of subglacial volcanic rocks (ridges and table-mountains) the Quaternary glaciation produced the alluvial planes which constitute the coastal lowland in Iceland.

In SE Iceland, glacial erosion has exposed nineteen central volcanic complexes (Kristjansson and Helgason, 1988). Two prominent geological features occur in this region: i) major intrusions of gabbro, granophyre and granites, some of which post-date the lava pile considerably (Freidleifsson, 1983) and ii) a monocline flexure which runs from Breidamerjökull in the south-west some 250 km north to Vopnafjordur. The flexure is commonly defined as the zone where the dip of lavas is greater than 10°. Many authors have discussed the structural and geologic nature of this zone (e.g. Walker, 1964, 1974; Annels, 1967; Newman, 1967; Ward, 1971; Torfason, 1979; Fridleifsson, 1983).

The area investigated in the present study is on the south-east coast of Iceland, between the Vatnajökull glacier and the coast line (Fig. 1.). The topography of the glacially eroded landscape reaches from sea level up to maximum elevation of 1554 m and displays excellent exposure. The area is cut by four valleys which are oriented roughly NW-SE. The Thverartindur area (Fig. 1) is dominated by late Tertiary plateau basalts and hyaloclastites, which to the north-west and at an elevation of 900-1100 m

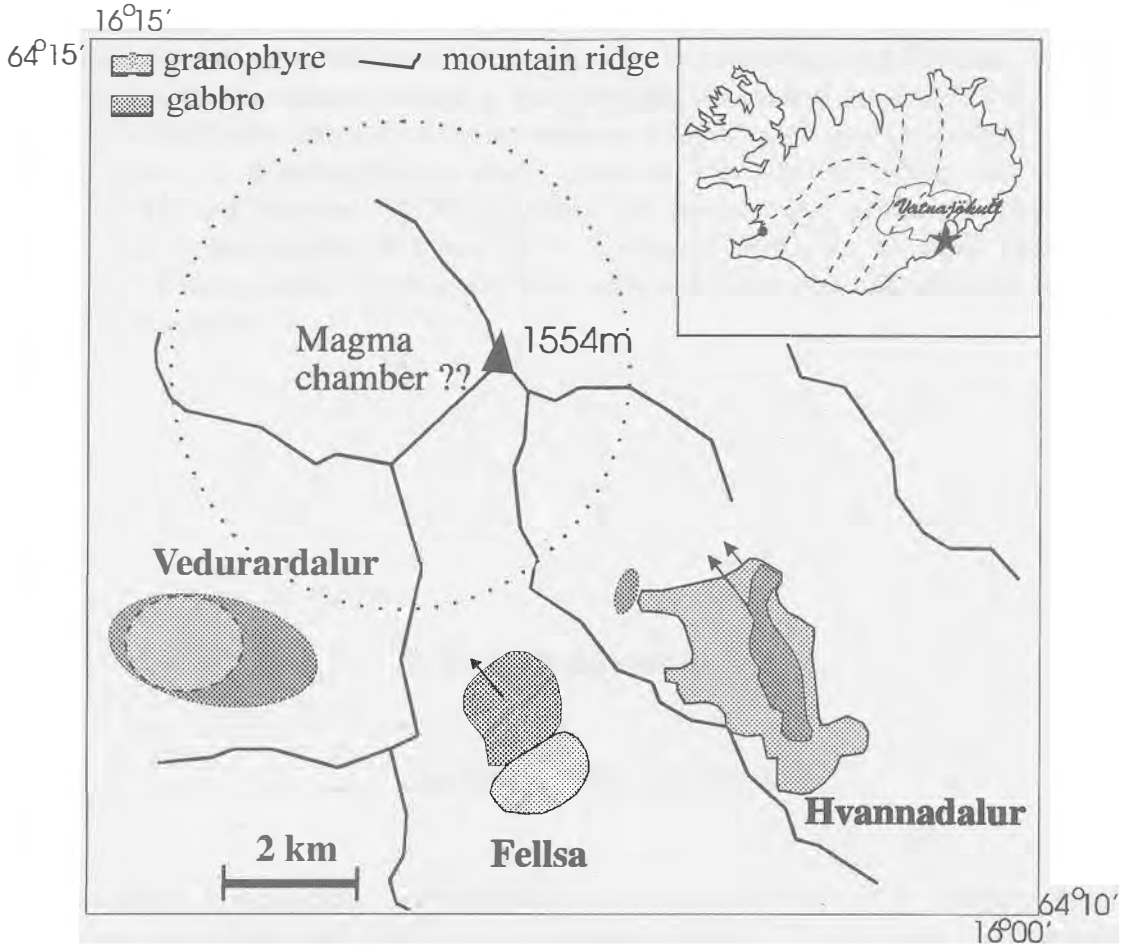

Figure 1. Sketch map of the Thverartindur central volcanic complex, showing the location in Iceland (inset), and three composite intrusions. Dashed circle indicates a possible outline of magma chamber as established by cone sheet major dipping direction. Arrows show dipping direction of plutonic (gabbro) formation.

are uncomformably overlain by early Plio-Pleistocene hyaloclastites. The regional dip of Tertiary lavas is 10-14° towards the NNE. An erosional depth is around 2000 m as suggested according to the regional laumontite-zone metamorphism by Walker, (1964). Only a few age determinations have been made on the plutonic rock suit in SE Iceland. These estimates give a time span of 2.2--7 Ma (Gale et al, 66; Moorbath et al, 68), the granophyres from the Hvannadalur pluton being the youngest.

2.1. Previous Studies

Several investigations have been carried out on the volcanic systems in SE Iceland (e.g. Walker, 1964, 1974; Moorbath et al, 68; Blake, 1964, 1966; Newman, 1967; Annels, 1967; Torfason, 1979; Fridleifsson, 1983; Mattson et al., 1986; Furman et al., 1992a; 1992b;). These studies include petrology and structure of the intrusive and

extrusive units of the area. Magnetic field measurements on two intrusions (Hvannadalur and Geitafell) were documented by Schönharting and Petersen, (1979). The Hvannadalur composite intrusion was mapped and studied by Annels (1967) and Newman (1967) who interpreted the intrusion as a separate structure embodied by four phases such as quartz-gabbros, acid, ultrabasic and minor dikes and sheets. Schönharting and Petersen, (1979) described the Hvannadalur gabbros as sheet like bodies. The Fellsa intrusion was mapped by Torfason (1979), but no detail geological work were accomplished. The Vedurardalur composite intrusion has not been mapped and described before.

3. Field Relationship

3.1. The Hvannadalur Intrusion

The complex Hvannadalur intrusion (ca 4 km^2) is exposed in a Tertiary basalt succession in a deep NNW stricking glacial valley (Fig. 2). The intrusion cuts majority of the cone sheets, and the intrusive relations are very complex. The formation may be divided into five main rock types: ultramafic, gabbro, hybrid rocks, granophyric, and a very fine grained basic intrusive rock type, which is referred to as a basic envelope.

Gabbros, hybrid rocks and ultramafic rocks form the central part of the intrusion which is surrounded by granophyres, extending up to altitude 850 m along the western slope, and up to 350-400 m on the eastern slope of the valley (Fig. 2). Exposure of the gabbro is roughly 2 km by length, but rarely exceeds 400 m in width. The granophyres are almost everywhere surrounded by very fine grained black basic envelope. Sometimes, the gabbros contain texturally distinct gabbroic, fine-grained basaltic and ultramafic xenoliths. In the northern margin of the intrusion, the gabbro reveals breccia-like features.

Ultramafic rocks form an half to three meters thick layers showing gradual to sharp contacts with the surrounding gabbros. These sill-like bodies dip about 15-20° towards NW - NNW. Very frequently, the ultramafic sills are spatially closely related to the very coarse grained (pegmatitic) gabbros and hybrid rocks.

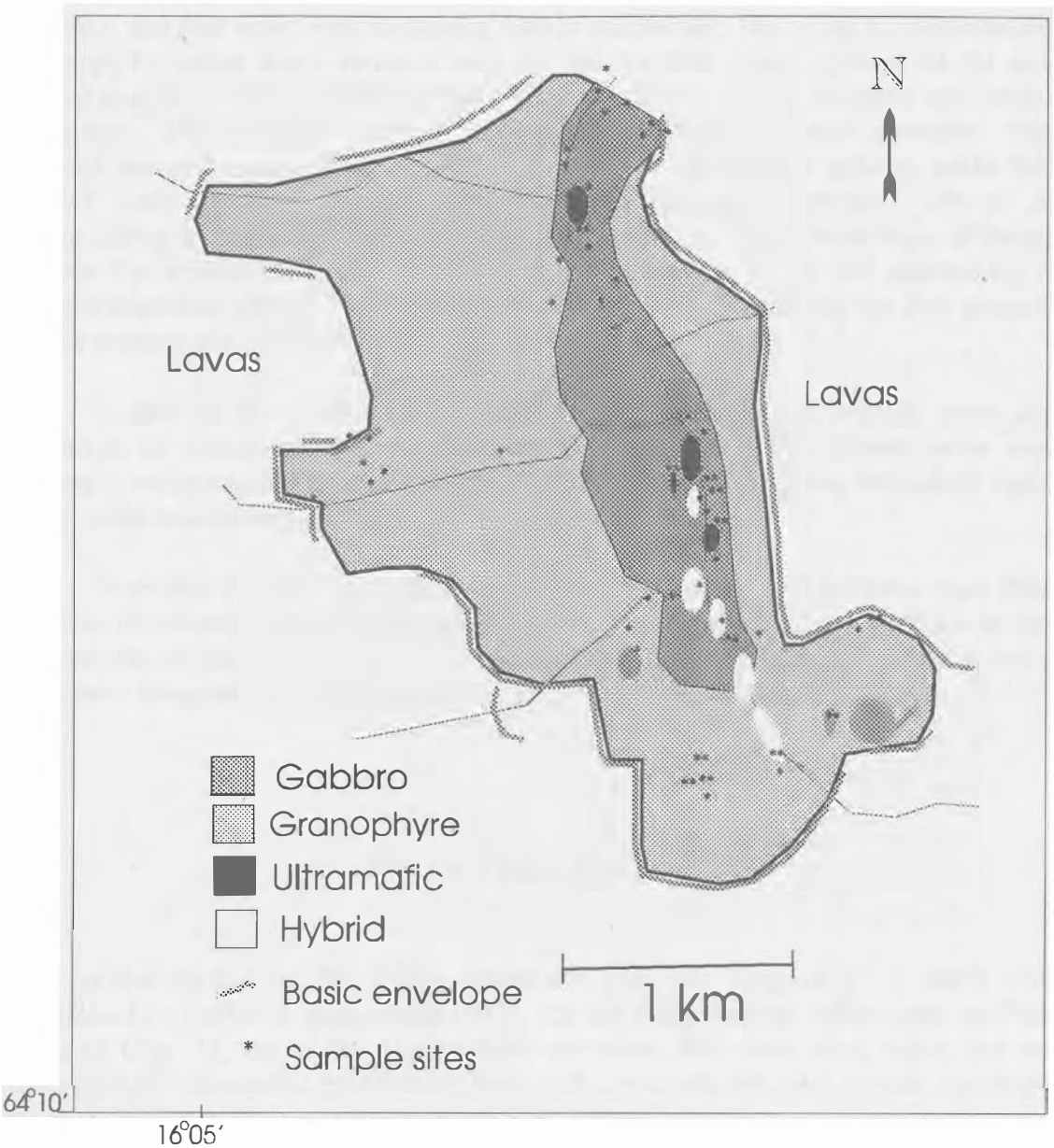

Figure 2. Geological sketch map of the Hvannadalur intrusive complex. Rock types and sample sites are shown. Fine dashed lines indicate the rivers.

The exposed silicic rocks (granophyres) occupy a volume of 2-3 km^3, but could be much more voluminous if it is assumed that they continue towards Fellsa valley forming a common body for both the major intrusions (see also Figs. 2 and 4). Granophyre intrusions appear to be build up by multiple injections. At the southern end, a number of separate layers (injections), 10-60 cm thick, are observed, while at the northern end intrusion, the thickness of single injections reach up to 20 m. Commonly, granophyres contain roughly 0.1 - 10 vol% rounded fragments of basic xenoliths.

At the central and southern part of the intrusive, a net veined complex (NVC) has developed displaying similarities with those described in the Austurhorn (Blake, 1964, 1966; Furman et al, 1992a, 1992b) and Vesturhorn intrusions. A central net veined complex shows two different types of veins -- typical NVC, with abundant

xenoliths, and less wide veins containing mainly plagioclase. The veins are distinctively separated by rather sharp contacts with the surrounding rocks, both in lateral and vertical directions. The main features of NVC are the basic pillows enclosed and cut by granophyre, and generally smaller, angular and texturally unzoned xenoliths. The pillowed masses consist almost entirely of peridotite and olivine gabbro, while the angular xenoliths are of gabbro-dolerites and diorites (Newman, 1967). A distinguishing feature of the pillows is their textural zoning, and around most of them, a dense fine grained margin is developed, never exceeding 8 mm and maintaining a uniform thickness with a single pillow (Newman, 1967). Away from the fine grained margin towards the centre of the pillow, the grain size increases.

Further to the south, away from the well-developed net veining, there are exposures of hybrid rocks. Field relations indicate, that NVC, hybrid rocks and ultramafic rocks may have a petrogenetic relationship. In some places, the hybrid veins are intruded into ultramafic rock (sill) near the contacts.

From less than one to thirty meters thick fine grained basic intrusive rock type envelops the Hvannadalur intrusive complex being spatially and temporally close to the granophyric rocks. The contacts between those are commonly sharp, but have sometimes irregularities caused by limited granophyric injections.

3.2. The Fellsa Intrusion

The general outline of the Fellsa composite intrusive complex (< 3 km^2) was established by Torfason (pers.comm.1993), but the valley has not before been studied in detail (Fig. 3). As in the Hvannadalur intrusion, five main rock types can be distinguished: ultramafic, gabbroic, hybrid rocks, granophyres, and a basic envelope surrounding the entire intrusive complex (Fig. 3.).

The gabbro intrusion consist of several subparallel 15-60 m thick sill-like melanocratic to leucocratic zones, which are cut by ultramafic dikes and sills. The Fellsa gabbros are texturally more variable than the Hvannadalur gabbros. The alternation of petrographically distinctive types of gabbros can be clearly observed at the south-western part of intrusion (Fig. 4.). Coarse grained, sometimes pegmatitic gabbros form the lowest part of the exposure. Some coarse gabbros at the north-western part of the intrusion reach an altitude of nearly 800 m. Coarse to medium-grained leucogabbros, spotted gabbros and gabbros with elongated euhedral plagioclase crystals form the stratigraphic central part of this cross section. The boundaries between different types of gabbros are distinctive; but only in two cases chilled margins are found. Sometimes, the contact is diffuse, but in a larger scale, the two gabbro types are distinguished by their textural characteristics. It appears that the gabbroic part of intrusion represents the combination of sills, emplaced within a rather long time interval. The multiple emplacement history is supported by the occurrence of different gabbroic xenoliths in leucocratic gabbros, which in general have gradual boundaries, but in some instances sharp contacts. In some places, the breccia-like

gabbros are found. Rounded ultramafic xenoliths, commonly partly assimilated, are found in the northern part of pluton. These xenoliths vary in diameter from a few mm up to 1-2 m. Close spatial relationship of ultramafic sills and very coarse grained and spotted gabbros may suggest their possible petrogenetic relation.

Hybrid rocks of the Fellsa formation are usually indistinguishable from the normal gabbros in hand specimens, and differ from those of Hvannadalur.

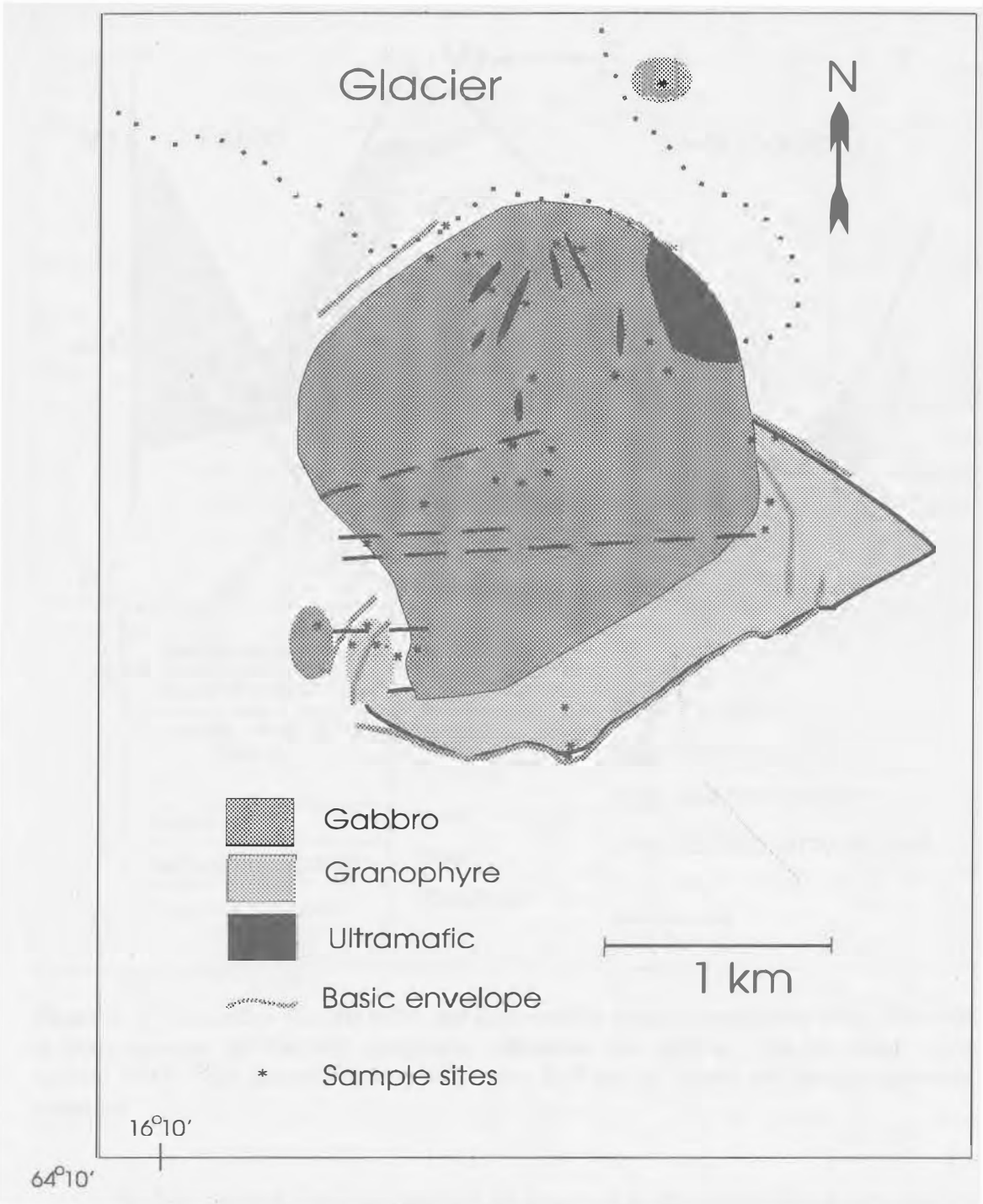

Figure 3. Geological sketch map of the Fellsa intrusive complex. Rock types and sample sites are shown. Dashed lines indicate the late vertical gabbroic dikes. Hybrid rocks are not shown.

Silicic rocks are represented by granophyres and granites. Reddish and greyish miarolithic granophyres usually contain basaltic xenoliths with diameter up to 4 cm. As in the Hvannadalur intrusion, the granophyres are always accompanied with fine grained basic rock envelope, which separates the main intrusive from the surrounding basaltic lavas. Some granitic veins and injections cut this envelope, but usually the contact between granophyres and basic envelope is sharp.

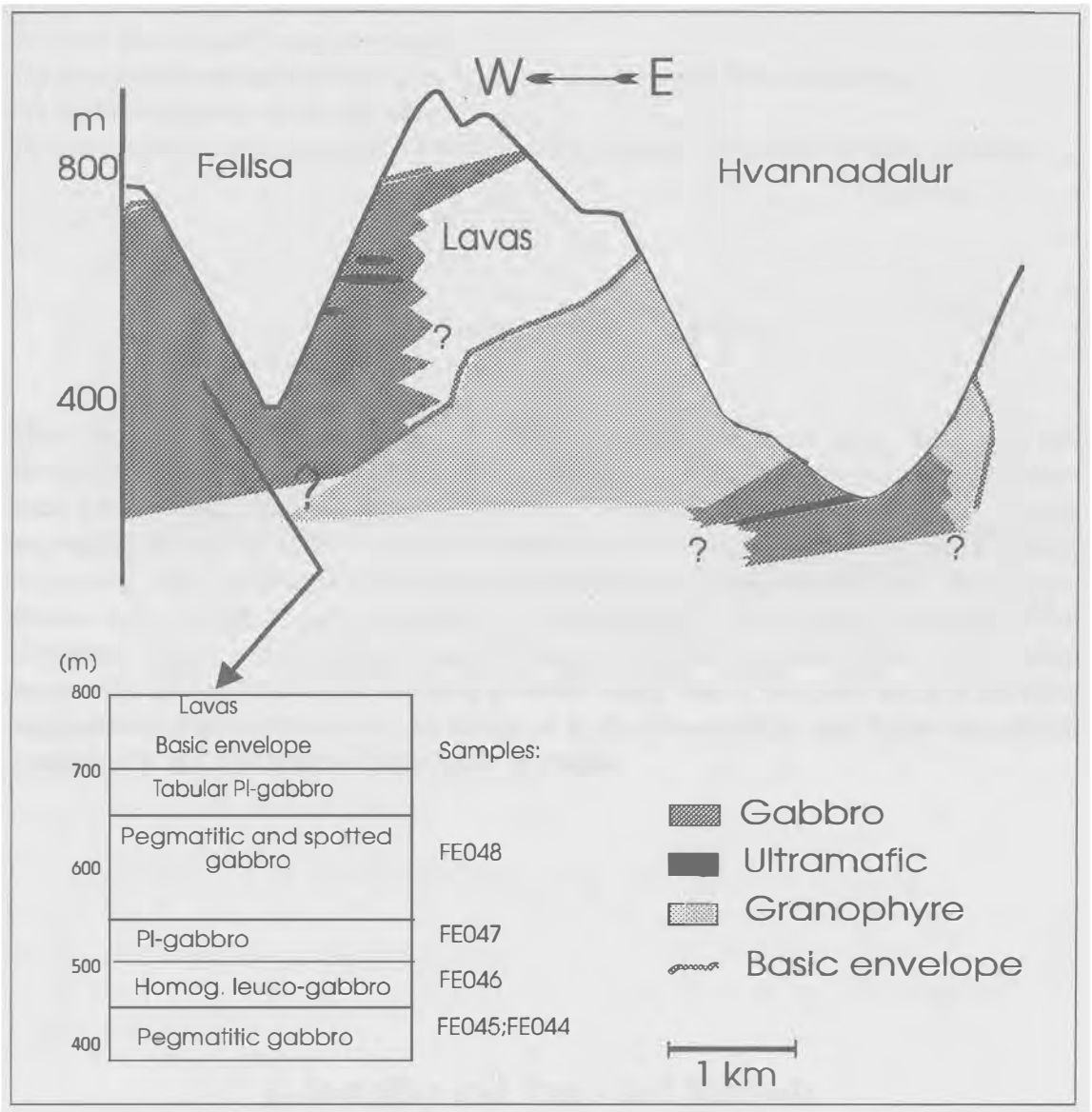

Figure 4. Cross-section over the Fellsa and Hvannadalur intrusive complexes. Silicic intrusion is likely common for the both complexes. Ultramafic and gabbroic sills are tilted 15-20' towards NNW. The alternation of gabbro types in Fellsa is shown and sample references presented.

Well-developed net vein complex as observed in the Hvannadalur intrusion, is not found in the Fellsa intrusion. Two zones of granitic veins penetrating gabbros are exposed in the western and eastern part of the intrusion. Several fine grained gabbroic veins (up to 4 cm) oriented roughly N and NNW, cut the entire gabbro complex.

As mentioned earlier, the gabbros have a multiple emplacement history. A long time span is assumed to be needed for cooling of a single 20-30m thick gabbroic intrusion to form a chilled margin by a later injection. The field evidence suggests the following emplacement sequence:

(1) several gabbroic sill-like injections, (possible three main pulses);
(2) minor sheets with average width of 0.5-1 m;
(3) gabbroic megasheets (some of tens meters thick);
(4) very fine grained basic envelope;
(5) granophyres along the boundary between gabbros and basic envelope;
(6) shallow-dipping ultrabasic sills;
(7) latest vertical and subvertical gabbroic dikes, which cut whole intrusive complex.

3.3. The Vedhurardalur Intrusion

This intrusion was discovered in 1993 around an ice-margin lake of the Breidamerkurjökull glacier. Gabbros and granophyres are exposed on a roughly 3 km^2 area. Due to steep cliffs around the ice lake, where the best outcrops occur, it was impossible to map intrusion in detail. Generally, the same rock types and emplacement sequences were confirmed. Gabbros are usually leuco- to melanocratic, a very coarse grained gabbro body is exposed roughly 2 km towards N, in the uppermost part of the Draugagil valley, just below the glacier tongue. The granophyres form a large body around the lake extending in diameter possible more than 2 km, and show a multiple emplacement macro-structures. As observed in the Hvannadalur and Fellsa intrusions, granophyres are accompanied by a basic envelope.

4. Sampling and Analytical Methods

Rock samples were collected in the Thverartindur Hvannadalur, Fellsa and Vedurardalur volcanic complexes. Samples cover the variation in rock subtypes and the representative samples were selected for whole rock chemical analysis and mineral analysis. The analyses of major and trace elements (Cr, Ni, Co, Sc, V, Cu, Zn, Ba, Sr, Zr, Y) were performed by ICP spectrometry. Rb was analyzed by AAS, (Nordic Volcanological Institute), and 28 samples were analyzed for Nb, Ga, and repeatedly for Sr and Rb using X-ray fluerensence technique at the Institute of Geology in Estonia. Petrological calculations were made with the NewPet software. Statistical analysis

were made with CSS-software. The COMAGMAT-computer model was used to describe the crystallization history and assess the pressure, water content, oxygen fugacity and crystallization mechanism´ influences.

Sixteen samples were selected for electron microprobe study. Analyses were performed on an ARL-SEMQ instrument at Nordic Volcanological Institute, Reykjavik. Analytical conditions for olivine (200 analyses), oxides (400) and clinopyroxene (350) were: beam potential 15 kV, sample current 80 nA and a counting time 10 seconds for peak and 4 seconds for background. Plagioclases (300) were analysed at 15 kV and 25 nA, with 20 seconds (peak) and 4 seconds (background) counting times.

5. Petrography of Thverartindur

Most of the plutonics of Thverartindur have undergone some alteration, but these effects are minor, and are typically restricted to slight chemical replacement along margins and internal cracks of clinopyroxene and olivine. Plagioclase is not or very slightly affected by alteration. A brief description of ultramafic, gabbroic, hybrid, and granitic rocks are presented below.

The ***ultramafic*** rocks are medium to coarse grained consisting of olivine either clinopyroxene with minor plagioclase and minor amounts of magnetite, ilmenite and Cr-spinel. The olivine frequently contains melt inclusions. Euhedral Cr-spinel occurs as an inclusion in olivine, and sometimes in interstitial zones, where euhedral to rounded plagioclase and anhedral augite are most common. Occasionally, olivine has trapped the earliest generation of highly anorthitic plagioclase. A few ortopyroxenes have been observed. Commonly they are partly resorbed into clinopyroxen. The common crystallization sequence of this rock type is: spinel $\Rightarrow$ magnetite $\Rightarrow$ olivine $\Rightarrow$ plagioclase $\Rightarrow$ clinopyroxene.

The Thverartindur ***gabbros*** are fine to coarse grained, melano- to leucocratic rocks containing plagioclase and clinopyroxene (modal 80-95 vol%), and magnetite and ilmenite (< 10%) as the main phases. Accessory phases are olivine, quartz, apatite, hornblende, biotite and alteration minerals, such as iddingsite, calcite and chlorite. The texture range from granular to ophitic. The Thverartindur gabbros classify as quartz- and olivine-gabbros, where small olivine grains are commonly replaced by iddingsite and/or serpentine+magnetite. A slight differences in the mineralogical assemblage between these two groups are mainly expressed by an increased quantity of quartz and apatite in the quartz-gabbros. This classification is supported by whole rock chemical composition (see Chapter 6.).

The clinopyroxene is unzoned or slightly zoned and occasionally partly replaced by amphibole around the margins within more evolved gabbros. Typically, plagioclase forms euhedral and elongated grains, while interstitial plagioclase is commonly rounded. Both unzoned and zoned (normal and reverse) plagioclase are often found within the same sample. Amongst the quartz-gabbro samples, plagioclase appears to have been locally affected by alteration processes, as indicated by restricted myrmecitization. The main crystallisation sequence of the Thverartindur gabbros is: (olivine and magnetite) $\Rightarrow$ plagioclase $\Rightarrow$ (magnetite and ilmenite) $\Rightarrow$ clinopyroxene.

The ***granitic rocks*** contain up to 60 vol% modal quartz and 20--60 vol% feldspar with 10--16 vol% normative orthoclase. Magnetite and ilmenite form up to 4 vol%, while pyroxene, hornblende, apatite, epidote, sphene, zircon and alteration minerals such as chlorite, uralite, calcite and pyrite are common as accessories. The granitic rocks often show petrographic evidence of local hydrothermal alteration. Granophyric inter-growth and myrmecite are common textural features, but are not characteristic for all granites. Most granites contain roughly 0.1 - 10 vol% of rounded basalt fragments with diameter between 1 to 300 mm.

The Thverartindur ***hybrid rocks*** consist of plagioclase, clinopyroxene, magnetite, ilmenite ∓quartz as the main phases while hornblende, apatite, epidote, sphene, zircon and alteration minerals are accessories. Frequently, this rock type exhibits compositionally different plagioclase and/or clinopyroxene with normal and reverse zoning within the same sample. Further details concerning the hybrid rocks will be discussed in Chapter 6.

The Thverartindur gabbros do not display distinctive cumulate textures. An exception could arise concerning poicilitic Ca-rich pyroxene which encloses plagioclases. This is indicated where residual liquid has crystallized as clinopyroxene, whereas plagioclase may been locally transported, and mechanically mixed with that liquid. After an intensive plagioclase separation, the liquid likely reaches the density of 2.70-2.67 g/cm^3. An_{76} with density of 2.67 g/cm^3 can therefore be floated. Low abundances of incompatible trace elements in some primitive gabbros suggest a certain escape (1-2%) of an intercumulus liquid left after clinopyroxene crystallization. In case the temperature falls slowly, as supported by coarse grained texture, the cumulus phases may re-equilibrate at lower temperatures. As shown later, slightly lower An and En numbers are evident compared with idealized thermodynamic calculations. Despite of certain scatter in incompatible elements, the sill forming gabbros can be treated as *in situ* crystallized non-cumulate rocks, but also resemble adcumulates according to Irvine's (1980; 1982) classification.

6. Petrochemistry of Thverartindur

The Thverartindur rocks define a tholeiitic evolutionary trend comparable to other rift zone generated Icelandic central volcanic systems (Figs. 5, 6). Major elements versus MgO abundances of Thverartindur rocks outline a broad linear trend for calcium, curvilinear for silicon and total iron, widely scattered for potassium and sodium, and complex covariation for aluminium (Fig. 6). Only few samples cover the intermediate range from 54-63wt% SiO_2.

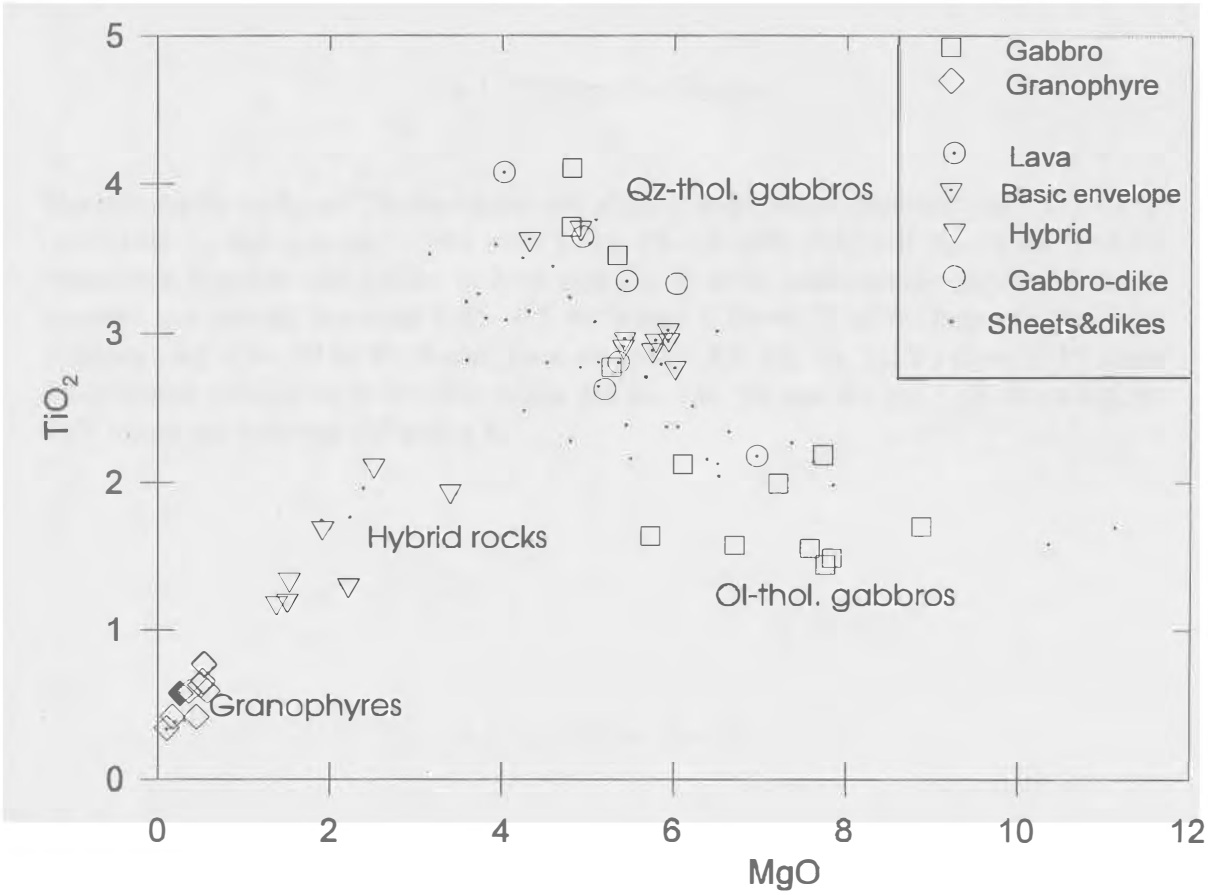

Figure 5. Chemical range of the Thverartindur rocks shown on MgO vs. TiO_2 (wt%) plot. Five rock types are distinguished. Note, that the sheet and dike compositions cover the plutonic rock types revealing gradual change in magma chemistry. Ultramafic rocks show MgO and TiO_2 abundances between 20-32wt% and 0,7-1,1wt%, respectively.

The whole-rock analysis are presented in Tables 1, 2, 3, 4, 5, and 6 (Appendix 1). The compositions of the dikes/sheets and major plutonic rocks overlap (see Tabs. 1 - 5, and Figs. 5,6). The dikes cover the entire range between the two gabbro types. The dikes may thus represent different stages in evolution of magma reservoirs. If the dikes represent magma composition, it can be assumed, that the gabbros are close to unfractionated magma compositions. Slight fractionation effects may be caused by a different removal of plagioclase and clinopyroxene within a sill, and only slightly modify the original magma composition. This feature is not observed in other Tertiary central volcanic complexes in SE Iceland (Furman et al., 1992a, 1992b). The fact, that the plutonic rocks have higher Ti content than corresponding dikes, may be explained by a more extensive Fe-Ti oxide separation in plutonics being common feature of a Fenner-type differentiation of tholeiitic magmas. Thus, most of the plutonic rock samples studied are good candidates for petrogenetic investigations of the processes at a plate margin.

6.1. Ultramafic Rocks

The ultramafic rocks of Thverartindur are slightly nepheline-normative (*ne*= 0-3 wt%) (see Table 1), and contain 37--44 wt% SiO_2, 10--19 wt% FeO and 22--31 wt% MgO. Normative diopside and olivine is 8-14 and 36-78 wt%, respectively. K_2O and Na_2O contents are usually between 0.05--0.5 wt% and 0.32--0.73 wt%, respectively. Mg# numbers vary from 69 to 83. Some trace elements (Rb, Ba, Zr, Ti, Y) show 1-10 times lower values relative to N-MORB, while the Zn, Cu, Ni, and Cr are 1-10 times higher. Zr/Y ratios are between 4.0 and 4.4.

6.2. Gabbroic Rocks

The gabbroic rocks are restricted within the main basaltic range of 47 - 53 wt% SiO_2 (Tabs. 2 and 3). The subdivision into the olivine- and quartz-tholeiitic gabbro types is shown on the MgO - TiO_2 diagram (Fig. 5). Olivine-tholeiitic gabbros are more primitive in composition (MgO>5.7wt%; TiO_2<2-2.2wt%) and depleted in incompatible elements, commonly containing normative olivine (*ol*=1-16 wt%); with *high* normative anorthite, and with rare modal secondary quartz. The quartz-tholeiitic gabbros contain modal magmatic quartz, and have the high Fe-Ti contents, and lower

MgO. This evolved gabbro type is referred to as oxide-gabbro.

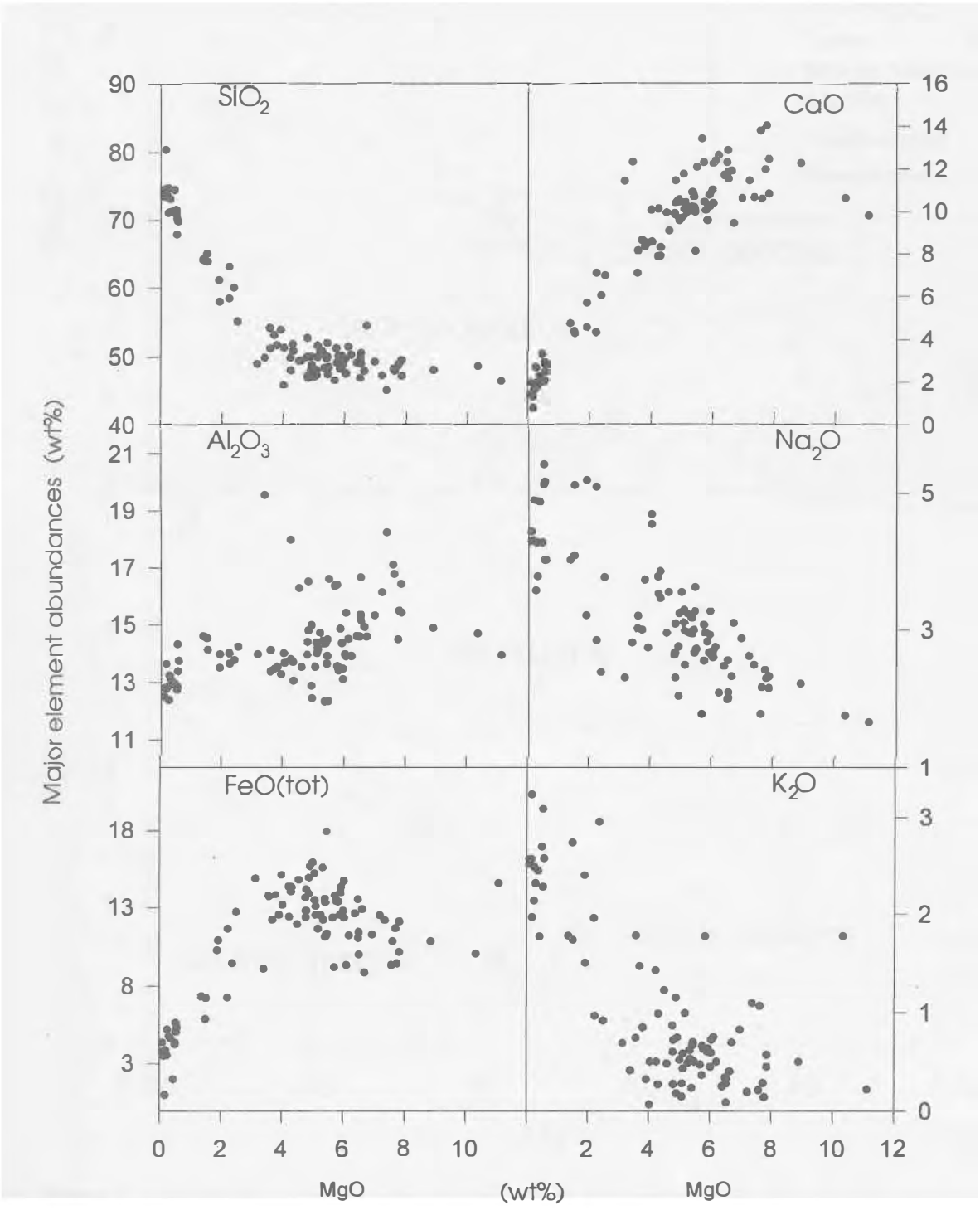

Figure 6. Major element abundances vs. MgO (wt%) of the Thverartindur plutonic rocks and dikes/sheets. Notice the large scattering of basaltic/gabbroic samples.

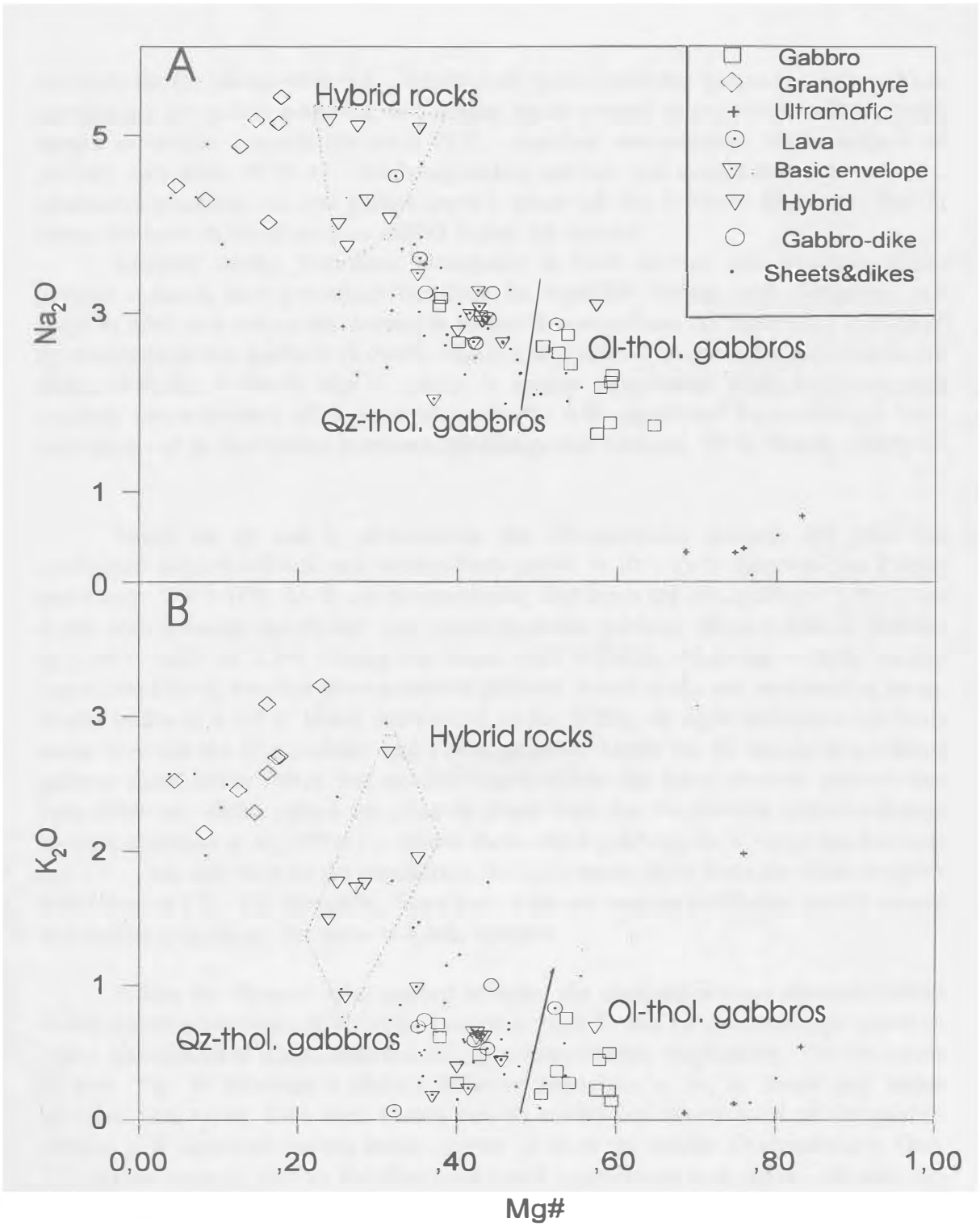

Figure 7. Variation in sodium (A) and potassium (B) contents vs. Mg# number of the Thverartindur rocks.

The Thverartindur gabbros show MnO and P_2O_5 contents similar to OIT and MORB (Mullen 1983). Abundances of P_2O_5 display a very good linear trend against

the MgO for the olivine-tholeiite -- hybrid rock types, while the quartz-tholeiitic gabbro samples are somewhat scattered, and display much steeper slope, which indicate rapid apatite saturation towards the most FeTi - enriched end-member. Mg# numbers of gabbros vary from 39 to 61, clearly separating olivine- and quartz-tholeiitic varieties. Distinctive grouping into two gabbro types is observed also in Na vs. Mg# plot (Fig. 7) where the more evolved gabbros exhibit higher Na content.

Roughly similar potassium abundance in both olivine- and quartz-tholeiitic gabbros indicate, that potassium has been incompatible during rock evolution, and could be used as a conserved element in further investigations. An interesting feature of the quartz-tholeiitic gabbros (4-5wt% MgO) is the low silica content compared to the olivine-tholeiitic (6-9wt% MgO) variety. A similar observation of tholeiitic magmas evolving towards more silica-poor compositions with significant Fe-enrichment have been observed in Skaergaard intrusion (McBirney and Naslund, 1990; Morse, 1990).

Based on Zr and Y abundances, the Thverartindur gabbros fall onto the overlapped field of MORB and Within-Plate region in Zr - Zr/Y diagram (see Pearce and Norry, 1979) (Fig. 8). It can be mentioned, that there are no significant differences in this ratio between the olivine- and quartz-tholeiitic gabbros. More primitive gabbros give Zr/Y ratios of 3.5-4.5 being consistent with MORBs, when the evolved variety (quartz-tholeiitic), but also some primitive gabbros, hybrid rocks and surrounding lavas, display ratios of 4.1-5.0, which correspond to the WPBs. A slight difference has been found between the Hvannadalur and Fellsa gabbros, where the Hvannadalur primitive gabbros show lower ratios, but no differences within the more evolved gabbros has been observed. These values are close to those from the Austurhorn central volcanic complex (Furman et al., 1992a) -- within Hvalnesfjall gabbros, Zr/Y ratios are between 3.7 -- 5.2; but also close to the transitional tholeiitic mafic dikes from the same complex with ratios of 4.2 --6.4. However, there is no evidence assume a different mantle source and melting percentage for those volcanic systems.

Within the Thverartindur gabbro samples, the compatible trace elements reflect mainly modal mineralogy of individual samples. High Sr and Ni contents correspond to higher abundances of plagioclase and clinopyroxene/olivine, respectively. The Sc versus Zr plot (Fig. 9) indicates a slightly different behaviour of Sc in minor and major intrusive rock types. Two main trends can be established where most of the gabbro samples plot separately having lower content of Sc at the similar Zr abundances. Only four gabbro samples plot on the dike/sheet trend representing both types - olivine- and quartz-tholeiites. The differences, concerning these two trends are difficult to explain solely by presence of different amount of clinopyroxene as more Sc-philic mineral having bulk/crystal partition coefficient as high as 1.7-3.2 in basaltic liquid (Fujikami et al., 1984). But there are no contrasts in normative and modal mineralogy between minor and major intrusive rock types.

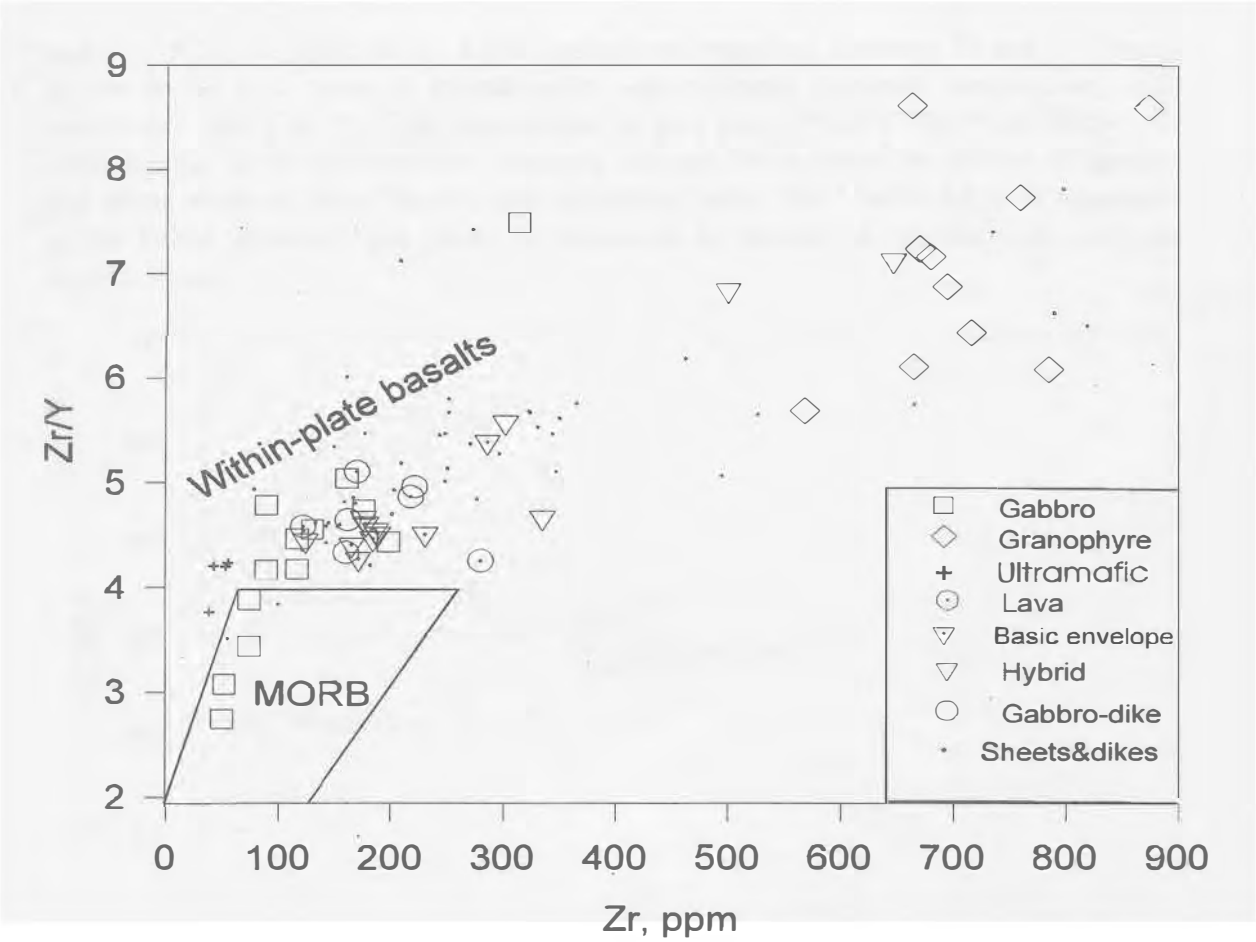

Figure 8. Zirconium vs. Zr/Y ratio plot of the Thverartindur rocks. Tectonical setting are from Pearce and Norry, (1979). Only some primitive gabbros show MORB affinities, while an essential part of the rocks fall within the WPB-field. No signs indicate highly different mantle source/primary magma.

Differing olivine loss or accumulation are not the case producing Sc shift observed, because the comparatively low partitioning coefficient - 0.17 (Gill, 1981). Comparable shift of dike and plutonic rock types is seen also by Ni vs. Zr in Figure 9. It is possible, that a minor loss of clinopyroxene through fractionation before the sill formation can cause the differences observed.

6.3. Hybrid Rocks

The Thverartindur hybrid rocks abridge the compositional gap between quartz-tholeiites and granites, and have mineral populations not in equilibrium to each other (Tab. 4; Fig. 5 and 6). They have high potassium and sodium contents-- 0.4 - 2.9wt%,

and 2.39-5.2wt%, respectively. Mg# numbers are restricted between 24 and 35. There appear to be two types of hybrid rocks with different chemical composition, and mineralogy (see Tab. 4). The intermediate to acid type (54--65(70)wt% of SiO_2) is characteristic for the Hvannadalur intrusion and may be explained by mixing of basaltic and silicic magmas. More basaltic type of hybrid rocks (49--55wt% SiO_2) is abundant in the Fellsa intrusion, and could be explained by mixing of crystals with evolved basaltic liquid.

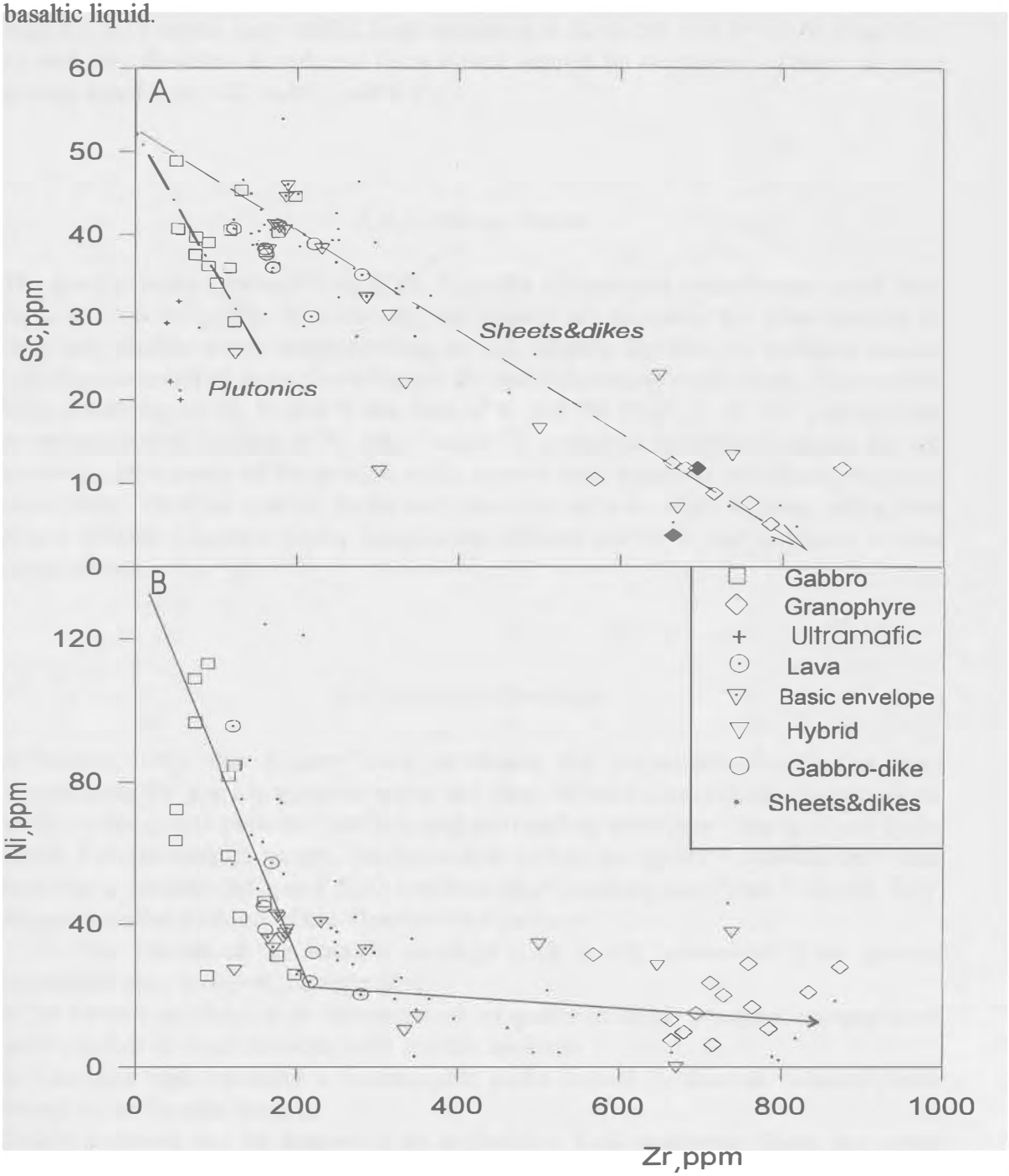

Figure 9. Thverartindur plutonic rocks and sheets/dikes on the Sc vs. Zr (A) and Ni vs. Zr (B)(ppm) plots. See text for discussion.

This type of hybrid rocks is spatially close to the gabbro sills or indistinguishable from them. It is still not clear, whether they represent a separate magma, or if they are the products of *in situ* mixing where two magmas or magma and crystals were mixed together. In compatible, and some incompatible elements, the hybrids tend to form separate trends, usually with steeper slopes, indicating more abrupt element saturation/depletion as compared with the general evolutionary trend. Showing rather different Zr/Y ratios, they exhibit huge scattering in Zr vs. Sc and Zr vs. Ni plots (Fig. 9), and may therefore be referred to as a rock formed by interaction of three or more phases; liquid1, liquid2, solid1...solid(*n*).

6.4. Granitic Rocks

The granitic rocks (granophyres) (Tab. 5) define a distinctive evolutionary trend from 65 to 80 wt% SiO_2 (Fig. 5). Generally, the granites are tholeiitic, but some samples lie on a calc-alkaline trend, corresponding to calc-alkaline rhyolites to tholeiitic dacites with aluminium-alkali ratios characteristic for meta-aluminous rocks types. They exhibit large scattering of Sr, V and Y but less of K and Na (Figs. 7, 8, 9). Variable and sometimes higher contents of Fe, Mg, Ca and Ti, compared to normal granites, are not suprising, since nearly all the granitic rocks contain basic xenoliths in different stages of assimilation. Thus the granitic rocks could be referred to as silicic hybrids, rather than proper granitic magmatic rocks. Large compositional scatter is also observed in dike compositions.

6.5. Basaltic Envelope

A basaltic, very fine grained rock envelopes the major intrusive bodies, and accompanies the granitic rocks in space and time. It has compositional characteristics similar to the quartz-tholeiitic gabbros, and surrounding lavas (see Tabs. 6, 2 and 3). In Figure 5, these samples occupy the lowermost part of the quartz - tholeiitic field, and have nearly constant SiO_2 and K_2O contents. Mg# numbers vary from 31 to 44. Zr/Y ratios are similar to those of the Thverartindur gabbros.

The genesis of the basaltic envelope rock is still unresolved. Two general hypotheses may, however, be suggested:

i) The basaltic envelope is an intrusive rock of quartz-tholeiitic composition, emplaced shortly before or simultaneously with granitic rocks; or

ii) This rock type represent a metamorphic rocks formed by thermal metamorphism caused by hot basaltic magma.

Both hypotheses can be supported by preliminary field evidences. There are some composite dikes similar to the envelope rock; and the surrounding lavas have chemical composition nearly indistinguishable from the envelope rock. Detailed petrological and isotopic investigation is needed to establish the genesis of this rock type.

7. Mineral Chemistry

Microprobe analyses of olivines, plagioclases, pyroxenes and oxide phases were conducted to establish the range of compositions within the Thverartindur plutonic rocks. Mineral data in conjunction with the whole rock chemical data, and field studies have employed to infer chemical parameters attendant to the evolution of the Thverartindur magmatic system.

7.1. Olivines

Olivines form a essential part of the ultramafic rocks investigated (4 samples) in both Hvannadalur and Fellsa intrusive complexes. The representative chemical analyses of olivines are presented in Table 7 (Appendix 2).

Forsterite content of olivines from the sheet-like ultramafic layer (FE065) varies from Fo_{66} to Fo_{73} with average Fo_{70} (Tab. 7). Reverse zonation is a common phenomenon showing core/rim differences in 2-5% of Fo component.

Ultramafic xenolith (FE063) contains olivines within Fo_{72}--Fo_{79} with average of Fo_{75}. Mainly homogenous crystals are found, a few crystals exhibit a slight normal zonation. Homogenous or in some cases slightly normally zoned olivines from the Hvannadalur ultramafic dike (AA101) show forsterite contents between Fo_{76} and Fo_{87}. However, the olivines from the ultramafic sill (HV028) display forsterite contents between Fo_{83} and Fo_{91}, with average of Fo_{89}. A slight normal zonation is common ranging from Fo_{88} to Fo_{90} and Fo_{86} to $Fo_{90\text{-}91}$, from rim to core. Small groundmass crystals are homogenous -- $Fo_{83\text{-}84}$.

There are some differences in the olivine composition between the Hvannadalur and Fellsa ultramafic rocks. Hvannadalur olivines have higher content of Ni - 0.22--0.33 wt%, and lower Mn - 0.09--0.13 wt% when compare to those of Fellsa, where Mn vary from 0.2 up to 0.7 wt%, and Ni from 0.09--0.23, respectively (Tab. 7). The content of Ca in the Thverartindur olivines varies within a large range - 0--0.5 wt%, while Fellsa olivines have either low CaO contents (0.5 wt%) or do not contain CaO at all. In sample FE065, both types of olivines are present.

Mg-Fe partitioning has been estimated using the simple relation:

$$Kd = X_{ol}\,FeO * X_{liq}\,MgO / X_{liq}\,FeO * X_{ol}\,MgO,$$

where XFeO, XMgO denote the molar proportion in olivine and in rock, respectively. Calculated crystal/rock Mg--Fe exchange coefficients occupy large range from 0.51 up to 1.0 confirming olivine growth under the non-equilibrium conditions. In case of the equilibrium partitioning of these elements, the coefficient is close to 0.3 (Roeder and Emslie, 1970; Roeder, 1974, Duke, 1976). The nearest values to the equilibrium partitioning - 0.51--0.53 are characteristic for olivines from the chilled margin of the olivine dike in the Hvannadalur intrusion. Central part of this dike show Mg -- Fe partitioning values of 0.61--0.64, which are similar to olivines of the Hvannadalur olivine sill. Fellsa olivine-bearing rocks expose much higher Kd coefficients varying from 0.87 to 0.99.

7.2. Plagioclases

Chemical analyses of the Thverartindur plagioclases are presented for the rock types distinguished in Tables 8, 9, 10, and 11. The statistical distribution of An# number within the rocks is demonstrated on the histograms in Figure 10, while an adjacent values of An, En, Fs and Wo are juxtaposed to the evolutionary index of rock (Zr in host rock) in Figure 11.

7.2.1. Ultramafic Rocks

Plagioclase is a minor phase in the ultramafic rocks presented as a small euhedral crystals, often enclosed witin clinopyroxene or olivine. Representative plagioclase compositions are listed in Table 8.

Uniform crystals or slight normal zonation is common. The cores vary from An_{59} to An_{70}; while the highest values reach An_{80}. As evident from Figure 10, plagioclases display a An# distribution peak at An_{70} following gradual decrease towards the more albitic compositions. Later may be explained by normal magmatic zoning through the decreasing Ca content in magma accompanied by decreasing crystallization temperature. The average Na -- Ca exchange distribution coefficients vary from 0.23 to 0.3 as calculated by:

$$Kd = [X_{pl}/X_{liq}]^{CaO}\ [X_{liq}/X_{pl}]^{Na_2O}$$

where X is a mole fraction.

FeO abundances range from 0.20 to 0.80wt% clustering into the two groups of low (FeO<0.4wt%) and high (FeO>0.6wt%) iron contents, which may reflect the different plagioclase generations depending upon the crystallization sequence of rock-forming minerals.

7.2.2. Olivine-tholeiitic Gabbros

Plagioclases were studied in three samples. Euhedral to anhedral plagioclase form medium to large individual crystals or form inclusions in clinopyroxene. Representative plagioclase compositions are presented in Table 9.

Both, homogenous and zoned crystals are observed. Zoning is both normal and reverse. Occasionally, two distinctive core generations are found in a single sample within the main range of $An_{60...76}$. The most calcic plagioclase reach An_{81}. Two peaks, distinguished by An component distribution are evident from Figure 10., showing rather similar symmetry to that of the ultramafic rocks. The latest plagioclases form small crystals and vary in composition between An_{50} to An_{57}. The content of FeO range from 0.50 to 0.70wt%, while sample FE081 exhibits a plagioclase of slightly lower iron abundances. The Na -- Ca Kds range from 0.49 (FE045) through 0.54 (FE044) to 0.80 (FE081). Sample FE044 exhibit a generation of plagioclase with Kd=0.21, which is similar to that of the ultramafic rocks.

7.2.3. Quartz-tholeiitic Gabbros

Plagioclases were studied in four samples -- HV012, FE047, FE079 and FE050 (xenolith). Representative chemical analyses are presented in Table 10.

Plagioclases of the quartz-tholeiitic gabbros are mainly zoned and uniform crystals are rare. The cores of zoned crystals range between An_{40} and An_{59},while rim composition varies between An_{40}-An_{50}. Several generations are detected in a single sample, the cores ranging within An_{26-36} An_{46} , An_{56-58}

It is important to note that no smooth changes in core compositions were detected for different plagioclase generations in a single sample. Some crystals show remarkable reverse zonation from cores An_{32-36} to rims An_{57-59}. The xenolith (FE050) reveal the two types of plagioclases - slightly normally, and revearsely zoned.

Kd coefficients are clustered: -- 0.51 (FE047) -- 0.63 (HV012, FE079). FeO abundances vary between 0.10 - 1.16wt%, being higher in sample HV012. Two patterns of iron distribution between core/rim occurs. Plagioclases from sample FE047 show higher FeO content in core, while sample HV012 exhibit plagioclase with iron-enriched rims. Sample FE079 displays both patterns.

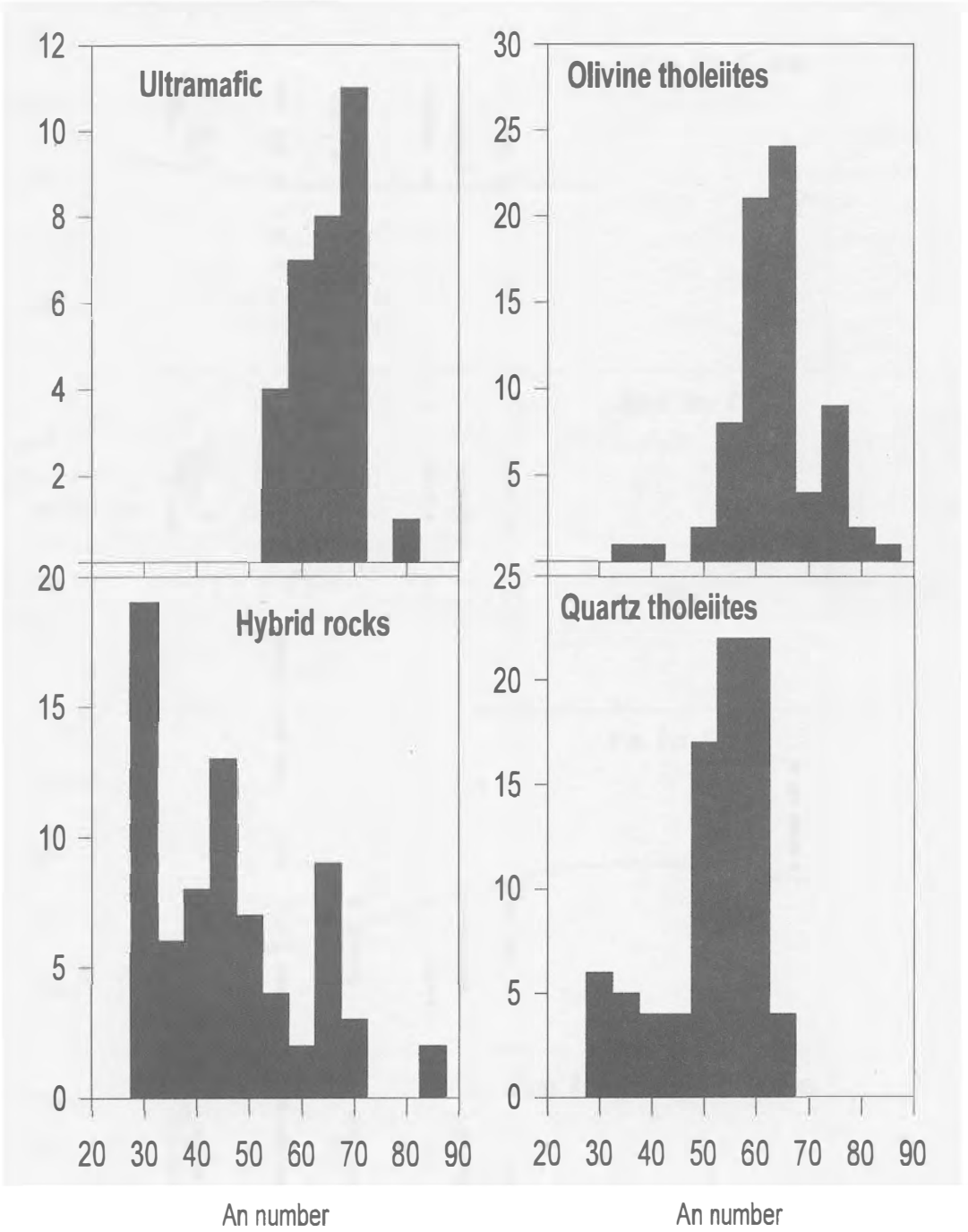

Figure 10. Histogram showing the distribution of An# number for Thverartindur plagioclases. Ultramafic, olivine- and quartz-tholeiitic gabbros, and hybrid rock types are separated.

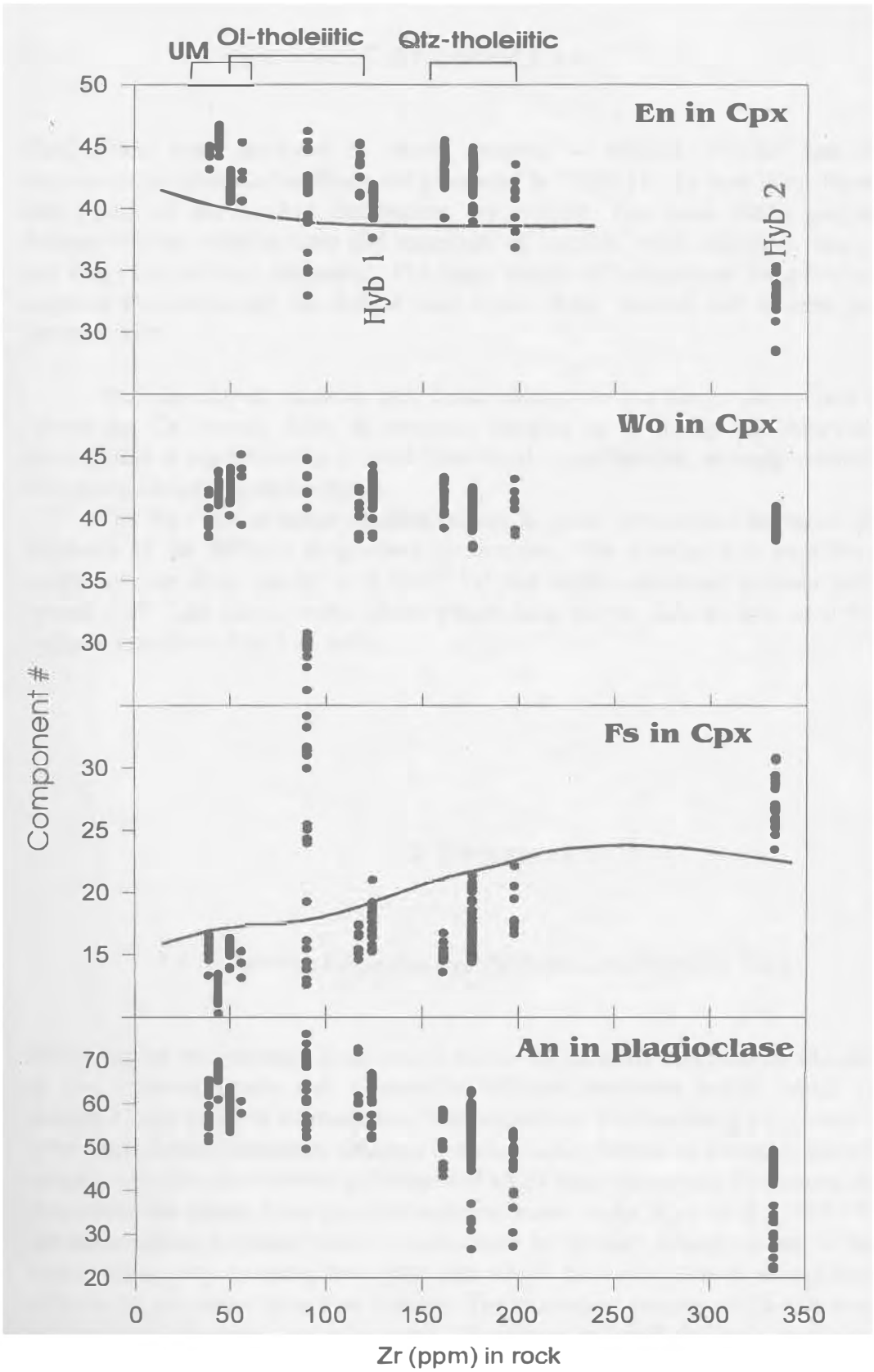

Figure 11. En, WO, Fs and An components of clinopyroxene and plagioclase, respectively, plotted against the Zr content in the host rock. Two hybrid samples display different origin.

7.2.4. Hybrid Rocks

Plagioclases were analysed in three samples -- HV035, FE046 and FE048. Representative chemical analyses are presented in Table 11. As seen from Figure 10., four peaks of An number distribution are evident. The most albitic plagioclases demonstrate the reaction rims and some altered crystals, while others -- An_{45}, An_{65} and An_{81} are primary magmatic. The large variety of plagioclase compositions is a common feature among the hybrid rock types. Both, normal and reverse zonation patterns occur.

Well developed zonation and direct change over a single plagioclase crystal (where the Ca content differ in opposite margins up to 10%) are observed. This phenomenon is considered as a result from local crystallization, strongly controlled by decreasing Ca content in the liquid.

The Na - Ca exchange coefficients are in good agreement with major element chemistry of the different plagioclase generations. The average Kds over the entire sample set are fairly similar -- 0.7-0.9, but the highly anorthitic crystals yield Kds around 2.27. The latest, more albitic plagioclase, shows Kds as low as 0.35. FeO contents vary from 0 to 0.75 wt%.

7.3. Pyroxenes

7.3.1. Common Occurrence of Pyroxenes in Magmatic Rocks

Slowly cooled and strongly fractionated bodies of tholeiitic magmas are characterized by two compositionally and structurally different pyroxene trends which co-exist through a large range of fractionation. The occurrence of co-existing pyroxenes each of which may display exsolution features is a diagnostic feature of tholeiitic intrusions in contrast with the non-exsoved pyroxenes of alkali basic intrusions. Pyroxenes showing exsolutions are absent from quickly cooled volcanic rocks (Cox et al., 1989). Usually the calcium-poor pyroxene trend is represented by primary orthopyroxene in the early stages, giving way to monoclinic pigeonite which, however, almost always inverts to orthorombic pyroxene upon slow cooling. The exsolution process of Ca-rich exsolves a calcium-poor daughter, and vice versa. Pyroxenes in small tholeiitic intrusions may show exsolution textures, although less commonly of the broad, regular lamellae variety.

The low-Ca pyroxene that crystallize from MORB at low pressure are pigionites (e.g. Shibata, 1976; Sigurdsson, 1981; Perfit and Fornaris, 1983; Elthon, 1987). The pseudoliquidus phase diagram of Grove and Bryan (1983) further shows that pigeonite is the low-Ca pyroxene that crystallizes from MORBs at 1 atm and that orthopyroxene would not crystallize from MORB-type liquids at this pressure. Experimental studies of MORB liquids indicate, however, that orthopyroxene replaces pigeonite as the low-Ca pyroxene with increasing pressure.

The Thverartindur gabbros are mainly medium to very coarse grained indicating a slow cooling rate for the sills. No exsolutions of lamellae or even blebs have been detected. A few ortopyroxenes observed by microscope in ultramafic unit occur mostly as cores inside the clinopyroxene crystals. This contradiction between assumed slow cooling rate, and the presence of one homogenous clinopyroxene (augite) strongly favours low pressures and forced cooling without convective thermal buffering.

Thverartindur clinopyroxenes are presented according to the rock types defined above. Representative chemical analyses are presented in Tables. 12, 13, 14, and 15; while statistical distribution of En, Fs and Wo components are demonstrated in Figures. 12 and 13. The geometry of these distributions gives a general petrogenetic idea. Evolutionary background can be easily followed from Figure 11., where clinopyroxenes and plagioclases have been plotted against Zr content in the host rock.

7.3.2. Ultramafic Rocks

Three samples taken from an ultramafic dike and a sill (FE065, HV028), and a xenolith (FE063) inside medium grained gabbro, were studied. Orthopyroxene analyses were obtained only from one ultramafic sample (FE065) - En_{69} Fs_{26} Wo_3. The augites from the ultramafic rocks are usually uniform or slightly zoned exhibiting average composition of En_{42-45} Fs_{12-17} Wo_{38-43} (Tab. 12). Cores of augite yield crystal/liquid rock Fe-Mg exchange coefficients - Kd from 0.73 (sample FE063), through 0.84 (FE065) to 1.76 (HV028) indicating pyroxene crystallization under the disequilibrium conditions. It is noted, that the pyroxenes from the xenolith reveal slightly more homogenous chemical composition.

7.3.3. Olivine-tholeiitic Gabbros

Within the olivine-tholeiitic gabbros, the clinopyroxenes reveal mainly uniform compositions En_{42-44} Fs_{15-16} Wo_{40-43} (Tab. 13); in a few cases reverse zonation has observed. Calculated augite/rock Kd vary from 0.41 to 0.53. Sample FE081 displays a large compositional spectrum of CPX core compositions distinguishing clearly two generations defined by En, Fs and Wo numbers in additions to the different zoning patterns expressed by En and Wo.

	En		Fs		Wo	
	core	rim	core	rim	core	rim
I generation :	36	33	33	41	30	26
II generation:	41	39	15	31	43	29

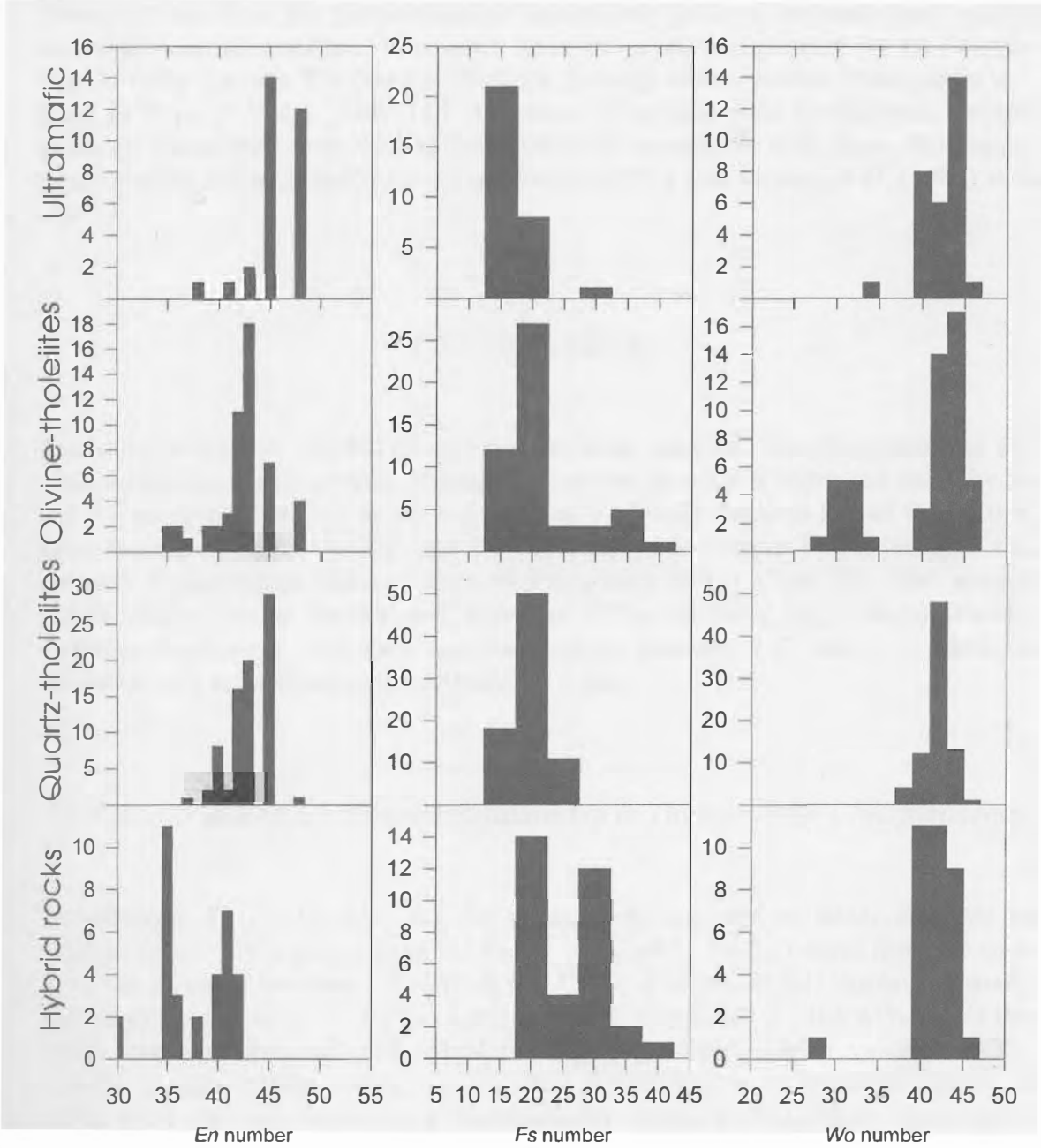

Figure 12. Distribution of En, Fs and Wo of Thverartindur clinopyroxenes. The ranking of En, Fs and Wo numbers is chosen according to the specific nature of those in order to minimize a "random" values. Most stable, En component, has counter-step 1; Wo -- 2, and Fs, as most easily modified by local alteration, has step 5.

The different CPX generations are also defined by the Fe-Mg distribution coefficients - the first generation has Kd ranging from 0.8-1.6, which is comparable with the CPXs in ultramafic rocks. The second generation display Kd's of 0.36-0.58.

7.3.4. Quartz-tholeiitic Gabbros

Three samples from the melano- to leucocratic gabbroic sills (HV012, FE079, FE047) and one from the leucocratic gabbroic xenolith (FE050) have been studied. Clinopyroxenes from the quartz-tholeiitic gabbros are uniform, but sometimes exhibit very slight normal zonation. This slight zonation is expressed either by Fs (sample FE079) or by En, and Wo (sample HV012). Average clinopyroxene composition is - En_{40-43} Fs_{15-17} Wo_{41} (Tab. 14.). The cores of augites yield crystal/liquid Fe-Mg exchange coefficients from 0.21 to 0.30, which is comparable with those determined experimentally for MORBs by Grove and Bryan (1983), and Tormey et al. (1987) at 1 atm.

7.3.5. Hybrid Rocks

Two samples (FE046, FE048) of hybrid rocks were analysed. The clinopyroxenes are small uniform or zoned crystals. Normal and reverse zonation is expressed either by Fs and Wo (sample FE046) or by En and Fs (sample FE048). Samples FE046 and FE048 have distinctively different Mg and Fe contents, while sample FE046 exhibits the common Thverartindur clinopyroxene of En_{40} Fs_{19} Wo_{41} (Tab. 15). The sample FE048 displays more Fe-rich and Mg-poor CPXs of En_{33} Fs_{28} Wo_{39}. Fe-Mg exchange coefficients are very uniform, ranging between 0.27 and 0.3, which is consistent with crystallization from MORB at 1 atm.

7.3.6. Major and Minor Element Relationship in Thverartindur Clinopyroxenes

The elements Ti, Al, Cr, Mn, and Na oxides were analysed as minor elements in clinopyroxenes. TiO_2 ranges from 0.5 to 1.3 wt%, while Al_2O_3 ranges from 0.5 to 4 wt%, but is usually between 1-3 wt%. A few CPXs of sample FE081 display unusually high Al_2O_3 contents, up to 7 wt%. MnO content is commonly 0.2-0.3 wt%, while the CPXs from the ultramafic and hybrid rocks display slightly higher values -- 0.35-0.5wt%. Cr_2O_3 content is low, varying from 0.01-0.08wt%. A common feature of CPXs from all rock types is a systematically negative TiO_2-MnO covariation. Aluminium and TiO_2 contents increase usually with increase of Mg# number. There are two trends corresponding to the olivine- and quartz-tholeiitic gabbros, while the CPX from olivine-tholeiites have a slightly higher Al_2O_3 and a steeper slope in Al_2O_3 vs. Mg# than quartz-tholeiitic gabbros (not shown).

Only in TiO_2 content is there a slight systematic difference between clinopyroxene cores and rims. Aluminium, Cr_2O_3 and Na_2O display rather random behaviour inside the cores and rims. Some olivine- and quartz-tholeiitic gabbros (samples FE047, FE045) exhibit a coupled change of TiO_2, Al_2O_3, Cr_2O_3 and Na_2O, where certain element concentration vary from rim through core to the other side of crystals. This direct change is observed also, for the En, Fs and Wo components.

The CPXs' major and minor element relationship is presented in Table 16. The correlation between CaO and FeO in the Thverartindur CPXs is always negative, although Fe-enrichment follows decreasing crystallization temperatures. MgO and CaO display negative correlation solely in the ultramafic and hybrid rocks, whereas the CPXs of the olivine-tholeiitic gabbros show good positive correlation. The weakest positive and negative correlations between major CPX constituents have been observed in the quartz-tholeiitic gabbros.

Table 16. Correlations between major and minor elements (oxide wt%) of clinopyroxenes from the Thverartindur ultramafic, olivine-tholeiitic, quartz-tholeiitic and hybrid rocks.

	SiO_2	TiO_2	Al_2O_3	Cr_2O_3	FeO	MnO	MgO	CaO	Na_2O
SiO_2	1								
TiO_2	0.09	1							
Al_2O_3	0.08	0.26	1						
Cr_2O_3	0.15	-0.14	0.30	1					
FeO	0.22	-0.30	-0.06	-0.34	1				
MnO	0.07	-0.33	-0.44	-0.47	0.79	1			
MgO	0.54	0.26	-0.06	0.13	-0.17	-0.25	1		
CaO	-0.61	0.05	-0.18	0.07	-0.58	-0.32	-0.43	1	
Na_2O	0.12	-0.04	0.15	-0.03	0.15	-0.01	-0.21	-0.15	1

The correlation between whole-rock and CPX compositions has been studied. It is important to mention, that Ca and Na in CPXs exhibit the worst correlation with all others elements. Significant positive correlation (+0.69 to 0.78) is observed between Mn in CPX and incompatible elements such as P, Ba, Y and Zr in the host rock, which may indicate the importance of manganese as an evolutionary index of CPX crystallization from tholeiitic magma. Slightly weaker, but negative correlation of Mg# number of CPX and K, P, Ba, Y and Zr in the rock supports this assumption. Phosphorous content in the host rock displays the highest correlation indicating high affinity of phosphorus in CPX' crystallization. The increases of P_2O_5 in more evolved basaltic magmas enhance a modal Pl/Px ratio as reported by Toplis et al. (1994). It seems therefore possible, that phosphorous has significant influence on CPX.

Despite of relatively uniform concentration of minor elements in the Thverartindur CPXs, the inter-element relationship is variable. Most distinctive is the variation in CPXs of the hybrid rocks displaying a good correlation between element pairs like Na-Al, Na-Ti, Na-Mg and Ti-Mg, which are usually weak and negative for all other rocks. There might be a special path of crystallization causing strong correlations between chemical constituents of CPXs in this rock variety. Na+Al+Ti alternative behaviour could possible be explained by, (i) later subsolidus reaction caused by dominant irreversible reactions (at least at the present P-T); (ii) primary crystallization feature due to magma mixing, which may lower the magma temperature, and therefore cause the rapid crystallization of CPX with different contents of Na, Al and Ti, but with a strong correlation between them.

Clinopyroxene cores exhibit much weaker major and trace elements correlations than CPX from each rock type separately. This would be expected assuming distinctive initial magma compositions, and slightly differing temperature regime of crystallization. Therefore, the petrogenetically significant interrelationship of CPX constituents will be obtained analysing each rock as a separate entity.

For comparison purposes, the Thverartindur CPXs are plotted on the pyroxene quadrilateral together with the Skaergaard trend (Fig. 13). The Thverartindur CPXs are slightly different from those of Skaergaard and Kap Edvard Holm formation in E. Greenland, by En-Wo-Fs values, but differ remarkably in the content of minor elements (see Wager and Brown, 1968; Bernstein et al.,1992). The Thverartindur CPXs form a Ca-rich cluster as compared with the Skaergaard at high En-values. Similarly the shorter Thverartindur trend shows decrease of the En-component at higher Ca value (Fig. 13.).

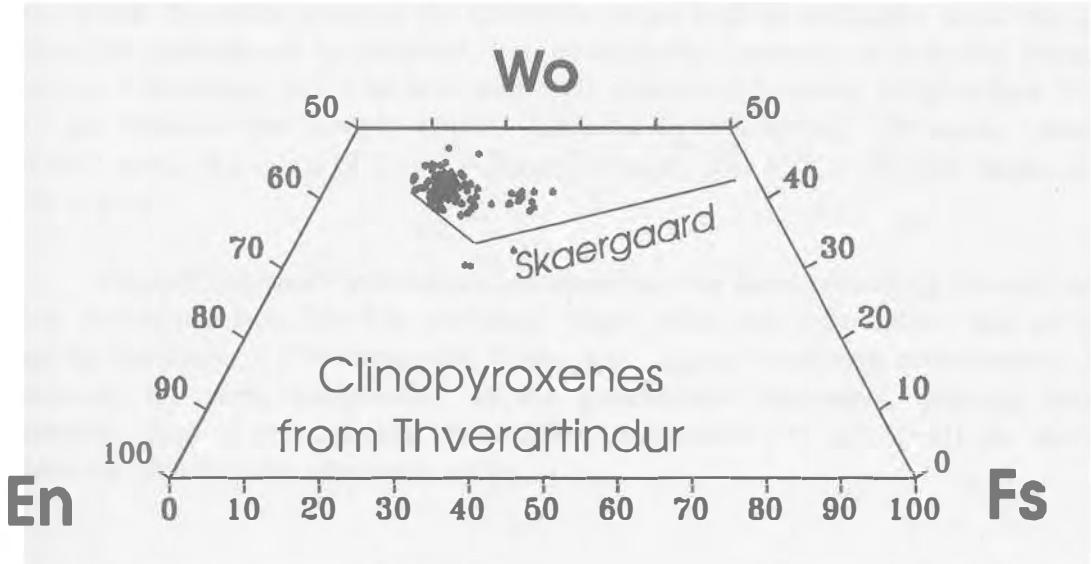

Figure 13. En-Fs-Wo plot of Thverartindur clinopyroxenes. Evolutionary trend of Skaergaard clinopyroxenes is presented for reference.

Also, Fe-enrichment trends display distinctive features. However, Thverartindur CPXs are close to the compositions crystallizing in early stages from a tholeiitic basaltic liquid - Wo_{40} $En_{43}Fs_{17}$, while a classical fractionated endmember-CPX of $Wo_{39}En_{29}Fs_{32}$ is not found. CPXs from the more evolved quartz-gabbros show those of $Wo_{41}En_{41}Fs_{16}$, not distinctively differing from the more primitive variety. Similarly to the Kap Edvard Holm layered gabbro complex and Austurhorn composite intrusion in SE Iceland, Ca-poor pyroxene was not found in Thverartindur complex. It is difficult to relate the lack of Ca-poor phase to the changing silica activity in the melt, that can in principle, terminate the crystallization of Ca-poor pyroxene balanced by reappearance of iron-rich olivine. This process is documented in the later stages of fractionation in Bushveld and Skaergaard intrusions. In the Thverartindur rocks, the olivine is a rare phase and accompanied mainly with the ultramafic rocks. There is no evidence of extensive olivine breakdown reactions. However, these reactions do not explain a unzoned and unexsolved single CPX occurring in the Thverartindur complex. This situation resembles a crystallization process in alkali basalts.

7.4. FeTi - Oxides

Oxides are abundant within groundmass and/or enclosed inside olivine, clinopyroxene and plagioclase in the Thverartindur rocks. Representative chemical analyses are presented in Tables 17 and 18. Compositions of coexisting magnetite and ilmenite were used to evaluate temperatures and oxygen fugasities using the method of Bacon and Hirchmann (1988).

7.4.1. Ultramafic Rocks

Spinels and chromites occur in the ultramafic rocks both as inclusions in olivine, and within the groundmass as euhedral, but occasionally corroded or anhedral crystals. There is a difference in Cr/Al ratio and total abundance between samples (see Table 17); for instance, the sample HV028 contains Cr-rich spinel. Ultramafic xenolith (FE063) reveal the spinel of Cr $\leftrightarrow$ Fe reaction series. The Cr/Cr+Al ratio ranges from 0,40 to 0,69.

Magnetite-ilmenite exsolutions are observed, but these coexisting minerals have often undergone later Mg-Mn exchange which rules out temperature and oxygen fugacity calculations. The magnetite, ($Usp_{0,060 - 0,090}$) occurring as inclusions, has frequently the same composition as the groundmass suggesting, primary origin. However, close to end-member composition, magnetites (96 wt% FeO) are studied within the Thveratindur ultramafic rocks.

7.4.2. Olivine- and Quartz-tholeiitic Gabbros

Within the olivine-tholeiitic gabbros, opaques are interstitial or enclosed in plagioclase or clinopyroxene. Magnetite-ilmenite exsolutions are common. Sample FE044 shows a variety of very fine exsolutions. This sample has an end-member magnetite depleted in Cr. Rutile with FeO content of 0,72 wt% was found in sample FE081 indicating severe oxidation. Ti-magnetites enclosed within plagioclase are often richer in Al compared to the groundmass crystals or exsolution pairs.

Quartz-tholeiitic gabbros reveal a large compositional variety of FeTi - oxides. Occurrence of a magnetite close to end-member composition, is a common feature, while the proportions of magnetite and ilmenite and presence or lack of exsolutions differs within individual samples. In the several big euhedral cystals (sample FE079), a good magnetite-ilmenite exsolutions having lower Cr and higher Mn abundances are found.

The gabbroic xenolith displays a sign of alteration of oxides, while no exsolutions has been detected.

7.4.3. Hybrid Rocks

Several associations of FeTi - oxides are found, distinguished by high and low MnO, Al_2O_3 and Cr_2O_3 abundances. Exsolution phenomenon is widely detected, occasionally reaching a magnetite end-member composition. Ilmenite seems to dominate in all three samples whereas magnetite sometimes form separate crystals within the groundmass. Secondary oxide generations are indicated by higher Mn content reaching up to 7 wt% and very low Cr and Al contents.

7.4.4. Estimates of Temperature and Oxygen Fugacity

Oxygen fugacity plays an important role in determining the fractionation history of magma since it controls Fe-Ti oxide precipitation and throughout magnetite/ilmenite removal from magma enriches the residual liquid in silica and depletes it in total iron. In certain cases, the magnetite/ilmenite precipitation results the FeTi-enrichment at constant silica and has a drastic effect upon the MgO/FeO ratios of residual liquids.

Partitioning of Mg and Mn between titanomagnetite and ferrian ilmenite in rock provides a test for equilibrium between the coexisting phases (Bacon and Hirshmann, 1988). This approach is based on exchange reaction:

$$Mg^{il} + Mn^{mt} = Mn^{il} + Mg^{mt}$$

In order to estimate genuine intensive parameters, the equilibrium between oxide phases is needed. In many volcanic rocks, the oxides have oxidized and exsolved into two phases. This process most likely takes place during relatively slow cooling when a vapour phase was present. Subsolidus oxidation-exsolution also is a common feature in plutonic and metamorphic rocks selectively affecting Mg and Mn distribution between new phases. Therefore, this method, is not widely applicable for rocks with complex cooling history. Only mineral pairs satisfying equilibrium were selected for temperature and fO_2 calculations which may not exclude some cases when an apparent equilibrium may have prevailed.

Oxide inclusions in olivine and pyroxene from ultramafic rocks reveal temperatures from 630 to 750 °C at log fO_2 between -13 and -19, i.e., below the QFM oxygen buffer, while an ultramafic sill displays oxides crystallized at 1122 °C slightly above the QFM oxygen buffer. However, small groundmass crystals indicate the magmatic temperature 1037 °C about two log units above the QFM buffer. Coexisting magnetite and ilmenite in the Thverartindur gabbros record the highest temperature - 1146 °C at fO_2 -9.26. Magnetite and ilmenite lamellae in both gabbro types indicate temperatures between 747 and 880 °C at fO_2 -13.1 -- -16.8, i.e., close to QFM oxygen buffer. Interstitial oxides record lower temperatures around 700 °C, being slightly above QFM buffer. The evolved hybrid sample (FE048) display magmatic temperatures 921 and 749 °C, while other magnetite-ilmenite lamellae record 649 °C at QFM+1 log

unit (NNO) buffer. Calculated parameters are in a good coincidence with Austurhorn volcanic complex (Furman et al., 1992) and Askja lavas from 1875 (Sigurdsson and Sparks, 1981), but differ from those inferred for basalts from Vestmannaeyjar (Jakobsson et. al., 1973), Vestfirdir (Meyer, 1978), Jan Mayen Island (Imsland, 1984). Relying upon calculated values, it can be concluded, that the Thverartindur gabbros are crystallized at or near the QFM buffer, in spite of likely several magma injections, while the ultramafic rocks record more variable oxygen fugacity spanning a few log units around the QFM buffer.

8. Role of Mineral Separation in Evolution of the Tverartindur Formation

Pearce element ratios have been used (Pearce, 1978, Russell, 1986, Pearce 1987) to avoid two main problems when utilizing of data on oxide-oxide wt% variation diagrams. (i) Data in wt% format is not easily related to mineral formulae, and (ii) the wt% oxide data suffer from a constant sum effect (Skala, 1979, Aitchison, 1981, 1984; Russell and Nicholls, 1988; Nicholls, 1988). The trends on the Pearce element diagrams have slopes that are a function of the stoichiometry of the mass transfer processes and therefore give an immediate indication of which minerals may have controlled the chemical variations in magmtic suite, whereas the intercepts are a function of initial magma chemistry (Pearce, 1978, Russell, 1986, Pearce 1987, Russell et al., 1990). A disadvantages is the spurious correlation arising from using conserved element that act as compatible in certain moment of magmatic evolution, and inability to consider the effects of magma mixing, which is evident from both field and mineralogical observations.

The Pearce element ratios are calculated according to the formulae

$$e_i = W_i * A_i / MW_i$$

where W_i, A_i, MW_i are wt%, the number of cations in the oxide formula and the molecular weight of oxide i, respectively. The Pearce element ratio of element i is

$$r_i = e_i / e_Z,$$

where e_Z is a conserved element. The choice of a conserved element is entirely model dependent. Typically, Ti and K satisfy this option at least during the initial stages of differentiation of basaltic magmas. Complex ratio diagrams using axes constrained to be sensitive to the fractionation of a particular mineral are used to evaluate the role of that mineral in the petrogenesis of cogenetic rocks related by fractional crystallisation. As mentioned above, K reveals conserved characteristics in both, olivine- and quartz-

tholeiitic rock types. Ti is related to clinopyroxene and forms Ti-magnetite and ilmenite phases in more evolved gabbros, which may complicate the petrologic interpretation.

Many basaltic suites are believed to be controlled by olivine fractionation (Sparks and Huppert, 1984; Nicholson and Latin, 1992). Olivine gain or loss hypotheses can be tested by plotting olivine indices (0.5*(Fe+Mg)) against the denominator K in Figure 16, where besides plutonic rocks the dike and sheet rocks are included. Other simultaneously crystallized Mg-Fe phases will do shallower the olivine stochiometric slope 1.0. The slopes obtained differ remarkable from theoretical olivine fractionation slopes (Russell and Nicholls, 1988) and it can be concluded that olivine separation has not significantly modified liquid composition, and can not play important role in magmatic evolution of the Thverartindur complex. As we see later, olivine crystallization is mainly restricted in the high temperature crystallization section followed later by a complete or partial dissolution. Only two ultramafic samples plot close to slope 1.

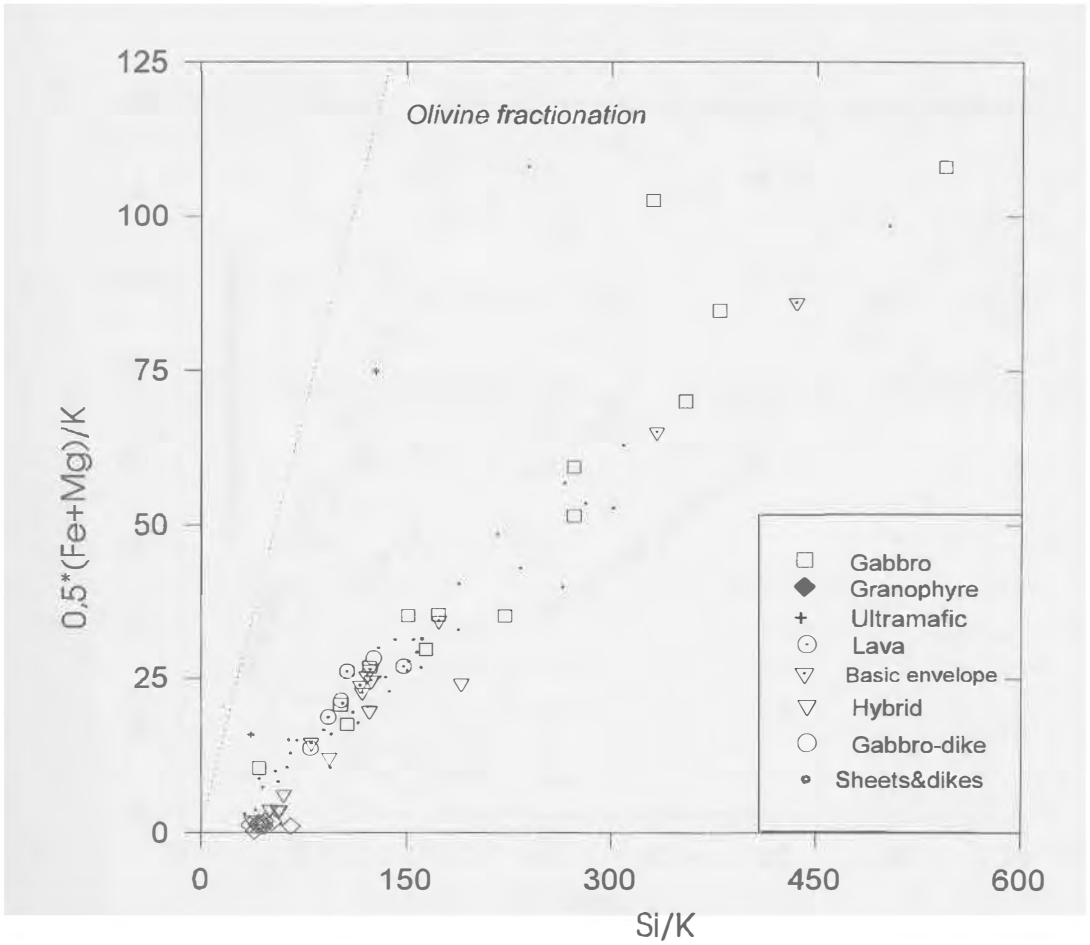

Figure. 16. Test for olivine gain or loss of the Thverartindur rocks. When olivine test (0.5*(Mg+Fe)/K) shows slope much different from 1.0, olivine fractionation cannot be responsible for magmatic differentiation, at least at upper section of the crust. This suggest that these rock are observed only during their late evolution - as also evident from their mineralogy.

An intermediate conclusion from this is that the Thverartindur basaltic suite is in reality highly evolved and that the present study only covers the latest crystallization of olivine-tholeiite. This is also consistent with the shallow crustal conditions of volcanic centres of a rift-zone. It is evident that magma mixing is extremely favourable explanation to many observed chemical parameters.

Petrographically, most gabbros consists of plagioclase and clinopyroxene as main phases. The Pearce element ratio plot [2*Ca+3*Na/Ti] vs. Si/Ti shows that rocks related solely by the separation of plagioclase will generate a slope of 1.0 (not shown here). The slope for Thverartindur basic rocks is distinctively different -- 1.5, and thereby the plagioclase separation alone can not control magma differentiation. Plagioclase fractionation may play some role in local-scale magmatic differentiation.

Employing element ratios (2*Ca+Na)/Ti vs. Al/Ti guarantees additional test for clinopyroxene and plagioclase separation or mutual gain or loss during magma evolution, where according to the mineral stochiometric formulae the olivine and oxide mineral influences are rejected (Fig. 17).

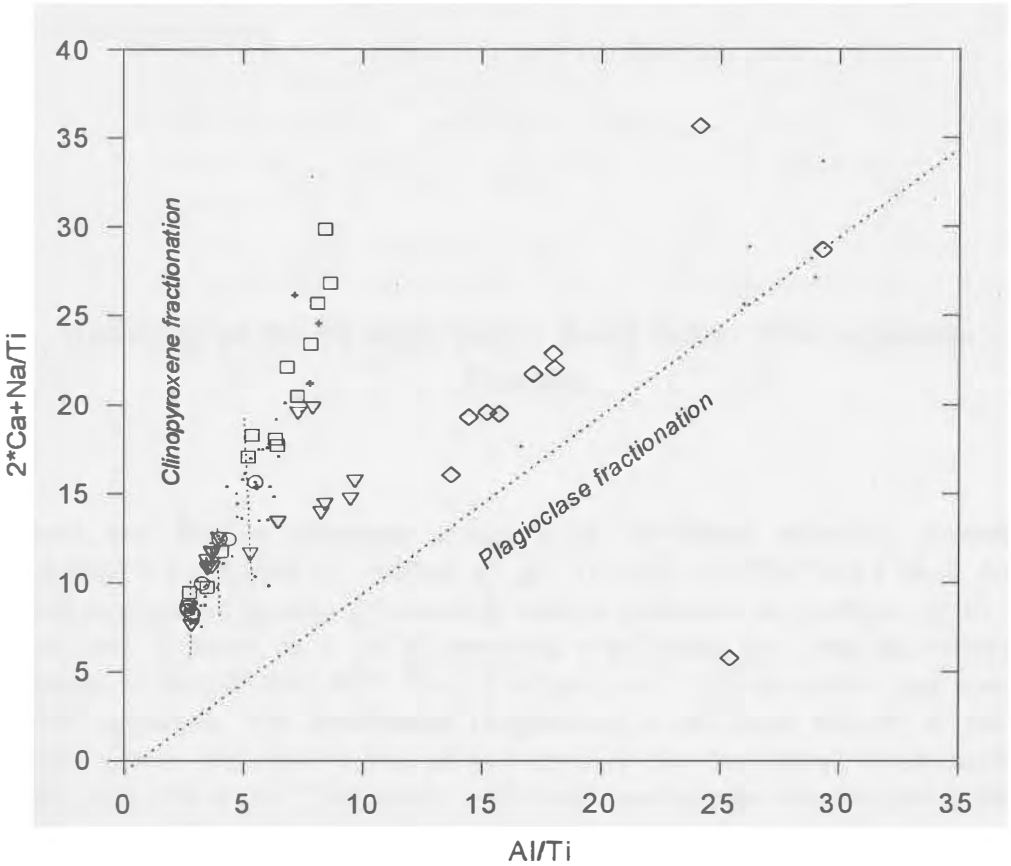

Figure.17. The plagioclase vs. clinopyroxene separation of the Thverartindur complex. Plagioclase fractionation will define slope 1.0, clinopyroxene defines infinite. Two trends separate the basaltic and silicic part of the complex. Hybrid units have a junction point (4, 11). The evolution of basaltic magma lead to simultaneous separation of plagioclase and dominantly clinopyroxene. In others words, some clinopyroxene cumulates can be present in the source region which most likely is a deeper ol-tholeiite reservoir. Symbols as defined in Fig. 16.

The trends obtained show that solely plagioclase (slope=1.0) has controlled the later stage of magmatic differentiation, particularly granites, while the gabbros have been controlled by plagioclase and dominantly by clinoyroxene separation (perfect clinopyroxene fractionation would give an infinite slope). The point (4, 11) in the Figure 17, separates the hybrid trend indicating that hybrid compositions are closer to plagioclase-controlled evolution than the basic plutonics and dike rocks are. Granitic and hybrid samples show a slope very close to 1.0. The scattering of samples may be due to magma mixing effects.

The main conclusion from the Pearce element ratios, is that the olivine separation was completed before the observed rocks were intruded. Since we do not know the composition of the mantle-derived primary melt, the olivine fractionation at deeper level can not be quantified. The clinopyroxene domination during shallow magmatic fractionation is indicated at the closing phase i.e. solidus phase incorporating appropriate residium chemistry (rest liquid, probably 1-2%, has to escape or crystallize as interstitial, if any left). However, these diagrams give a very general idea of magmatic lineage and role of mineral separation in further petrologic context, but can not efficiently contribute in detail studies or when processes reveal the complexities inherited from a repeated magmatism at thermally well-connected magmatic systems like at mid-ocean ridges.

9. Modeling of the Thverartindur Rock Suite: PT-conditions and Genesis

A resent and flexible computer program for modelling magmatic processes is COMAGMAT (compiled by Ariskin et al., (1993)). COMAGMAT is a program designed to simulate igneous processes in magma chambers at pressures up to 12 kb. The program is based on a set of empirical expressions that describe mineral-melt equilibrium in combination with basic thermodynamic considerations and non-linear empirical equations. The equilibrium temperature is unknown initially in simulated magmatic system, but may be derived as a result of the free energy minimization at a constant total crystallinity. Empirically calibrated equations for mineral-melt equilibrium include olivine, plagioclase, augite pigeonite ortopyroxene, ilmenite and magnetite. Main range of modeling extents from 45 to 60 wt% of SiO_2 when alkalies (Na_2O+K_2O) do not exceed 5wt%. The contents of Fo, An, En, Fs and Wo can be predicted within 1-3 mol% and $\mp$ 10° C (Ariskin et al., 1993). For trace elements, the partitioning expressions have been empirically corrected for the compositional dependence, and temperature and pressure.

9.1. Influence of Water

Pressure and water content affect the compositions of cotectic phase boundaries of phases crystallizing from basaltic magmas (Takashki and Kushiro, 1983; Michael and Chase, 1987). Variations between MORB differentiation trends result largely from different major element chemistry and H_2O contents of primary magmas (Michael and Chase, 1987).

Composition of sample FE045 has been modeled with the QFM+1 log units fO_2 buffer through fractional and equilibrium crystallization paths in order to define the water influence. Crystallization pressure was 0 kb which is consistent with other estimations. Crystallization increment used was 2% with total crystallinity up to 90%. The water contents applied in an initial magma were 0.1, 0.15, 0.2, 0.25% (fractional crystallization), and 0.02, 0.05, 0.1, 0.15, 0.2 and 0.25% (equilibrium crystallization). The most important results can be summarized:

I. Varying water content at low pressure does not cause the appearance of new mineral phases crystallizing but change slightly the phase proportions.

II. H_2O modifies slightly Si-depletion and Fe-Ti oxide enrichment trends in case of equilibrium crystallization and has lesser influence whether crystallization is following the fractional crystallization paths.

III. Higher water content ($H_2O \geq 0.25\%$) in magma obscures the differences between equilibrium and fractional crystallization.

IV. Aluminium is highly variable at high temperature (T>1145 C°) regardless the water content, whereas remarkable aluminium depletion in liquid is observed at 0.05% H_2O reaching $\Delta X=3.5\%$.

V. Highest Ti-Fe enrichment in liquid is found at low water content - 0.02-0.1%. Low water content in basaltic system has a drastic influence to the entire Fe-Ti-Si-Al complex which is following an equilibrium crystallization path.

VI. Initial water content in magma has no significant influence on a mineral compositions except plagioclase which tends to more calcic at higher water content.

9.2. Decompression and Intermediate Pressure Crystallization

Liquid lines of descent and element partitioning between crystals and liquid are effected by rapid rise of magma and decompression crystallization. The decompression crystallization is modeled on the samples FE045 and HV012 by decreasing the total pressure in increments of $\Delta P=0.1$ kb per 1% crystallization. Calculation was carried out through the pressure range from 6 to 0 kb, while a more detailed test was made over the pressure range from 3 to 0 kb. Applied oxygen fugacities range from QFM+2 (units of log fO_2) to QFM buffers. It can be concluded that there are no grounds to assume a pressure change during crystallization of the modeled compositions.

The case of primitive plutonic composition -FE045 - being modified through high pressure crystallization from a more primitive parental liquid was evaluated. Two

primitive dikes containing 8,9 and 11,1 wt% of MgO, respectively, were used in both decompression and intermediate pressure modeling. The results obtained from crystallization above QFM buffer, of water content up to 0,2 wt% in magma, and at equilibrium and fractional crystallization do not give a good fit neither major nor trace elements with the olivine-tholeiitic samples, particularly sample FE045. The more primitive dike sample (11,1% MgO), modeled under decompression crystallization from 6 to 0 kb, decreasing the total pressure in increments of ΔP=0.1 kb per 1% crystallization reveals bifurcation of K+Na+Si from Al+Mg+Ca. The best fit of Al+Mg+Ca is observed at crystallinity about 10-14%, while K+Na+Si can fit to sample FE045 at crystallinity of about 35%. A distribution of Co+V+Rb+Cu can be satisfied at 30-35% crystallinity, which does not make any logical extension to the K+Na+Si element group which are close to the same stage of crystallinity. Two explanations for failure of the model to explain observed compositions can be considered:

(i) The primitive gabbro composition (FE045) may be formed from the more primitive magma through decompression crystallization in very complex way, where after 10-14% mineral fractionation the rest melt will mix with much more evolved (40% crystallized, magma of the same parent) liquid, i.e. fractionation plus mixing

(ii) There is no compositional lineage between the primitive dike liquid and the primitive gabbro liquid which seems more applicable, since the first scenario has difficulties in explaining TiFe-oxides of the resulting liquid. Inference from this later suggestion is that the primitive dike composition is not at all an appropriate choice for a parental magma at Thverartindur.

9.3. Fractional vs. Equilibrium Crystallization

Calculations of equilibrium crystallization and fractional crystallization of the two Thverartindur tholeiitic compositions have been performed, which shows significant differences only for Si, Ti and Fe in the evolving magma. Through the whole range of crystallization, three elements -- K, Mg, Na coincide in both models. Equilibrium crystallization drives SiO_2 in liquid towards depletion, which can be more than 2wt% in intermediate stages of crystallization, while in fractional crystallization, the decrease of silica is negligible. In both cases, the liquid reaches 64wt% SiO_2 at late stages.

With respect to the genesis and evolution of quartz-tholeiites -- the crucial peculiarity is how to explain the enrichment in Ti and Fe at nearly constant silica content. The FeTi-enrichment might be a major magmatic differentiation processes, and can not be easily explained through assimilation or mixing. As shown in Figures 18. and 19., the evolving tholeiitic liquid becomes remarkably enriched in TiO_2 (2.5 times), and FeO, following an equilibrium crystallization, while with fractional crystallization Ti-enrichment stops at the temperature 1150 C°. These differences are more precisely expressed by the Fe/Mg ratio of the liquid (Fig. 20.). This calculation leads to an assumption, that equilibrium crystallization at QFM+1 buffer (NNO) is the more likely in case of the Thverartindur quartz-tholeiites and is consistent with the general idea of sill crystallization.

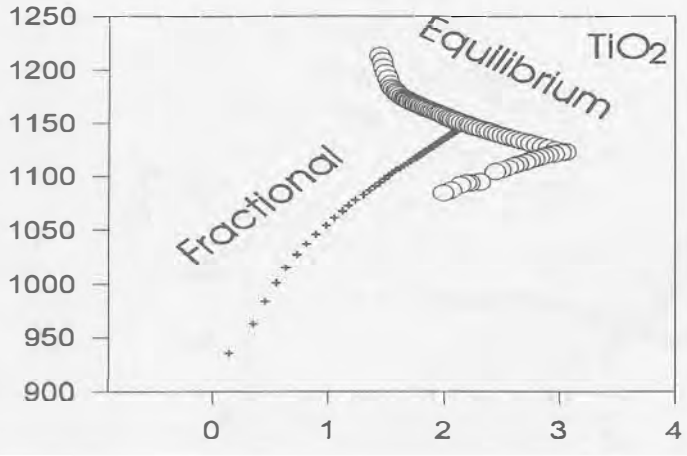

Figure 18. TiO_2 content (wt%) in liquid, modeled through the equilibrium and fractional crystallization of primitive gabbro composition (FE045). Notice the Ti-enrichment of equilibrium crystallization. QFM+1 buffer, water-0.2 wt%. Discussion in text.

In Figure 21., SiO_2, TiO_2 contents and FeO/MgO ratio of the two compositions -- FE045 and HV012 are shown. The crossing point of two compositions is in the temperature range 1140-1120° C, indicating the point, where primitive tholeiitic liquid has reached pseudoinvariant Fe/Mg, which resembles the properties of quartz-tholeiite. This temperature interval is where the magma density is at maximum and where oxide mineral precipitation begins at 5.5 -- 6.0 wt% MgO.

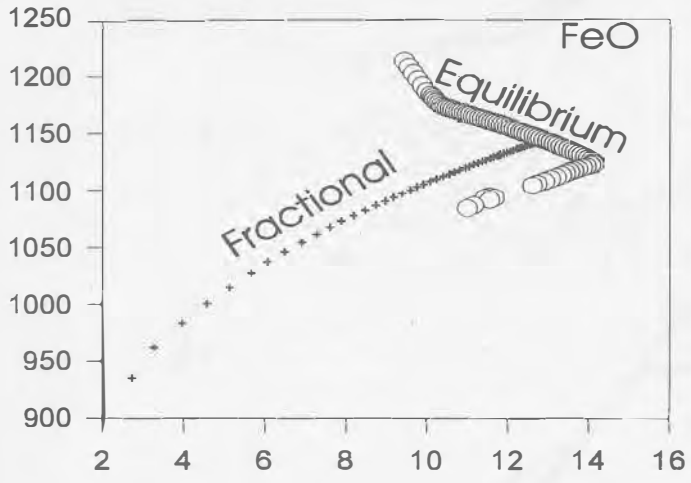

Figure 19. FeO content (wt%) in liquid, modeled through the equilibrium and fractional crystallization of primitive gabbro composition (FE045). Notice the higher iron-enrichment of equilibrium crystallization. QFM+1 buffer, water-0.2 wt%. Discussion in text.

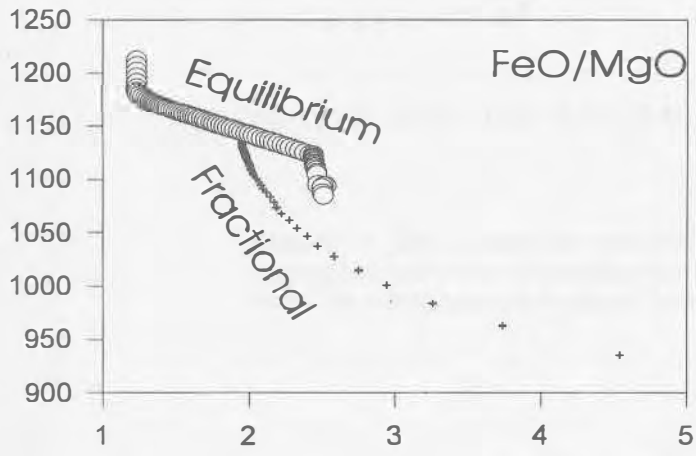

Figure 20. FeO/MgO ratio in liquid, modeled through the equilibrium and fractional crystallization of primitive gabbro composition (FE045). QFM+1 buffer, water-0.2 wt%. Discussion in text.

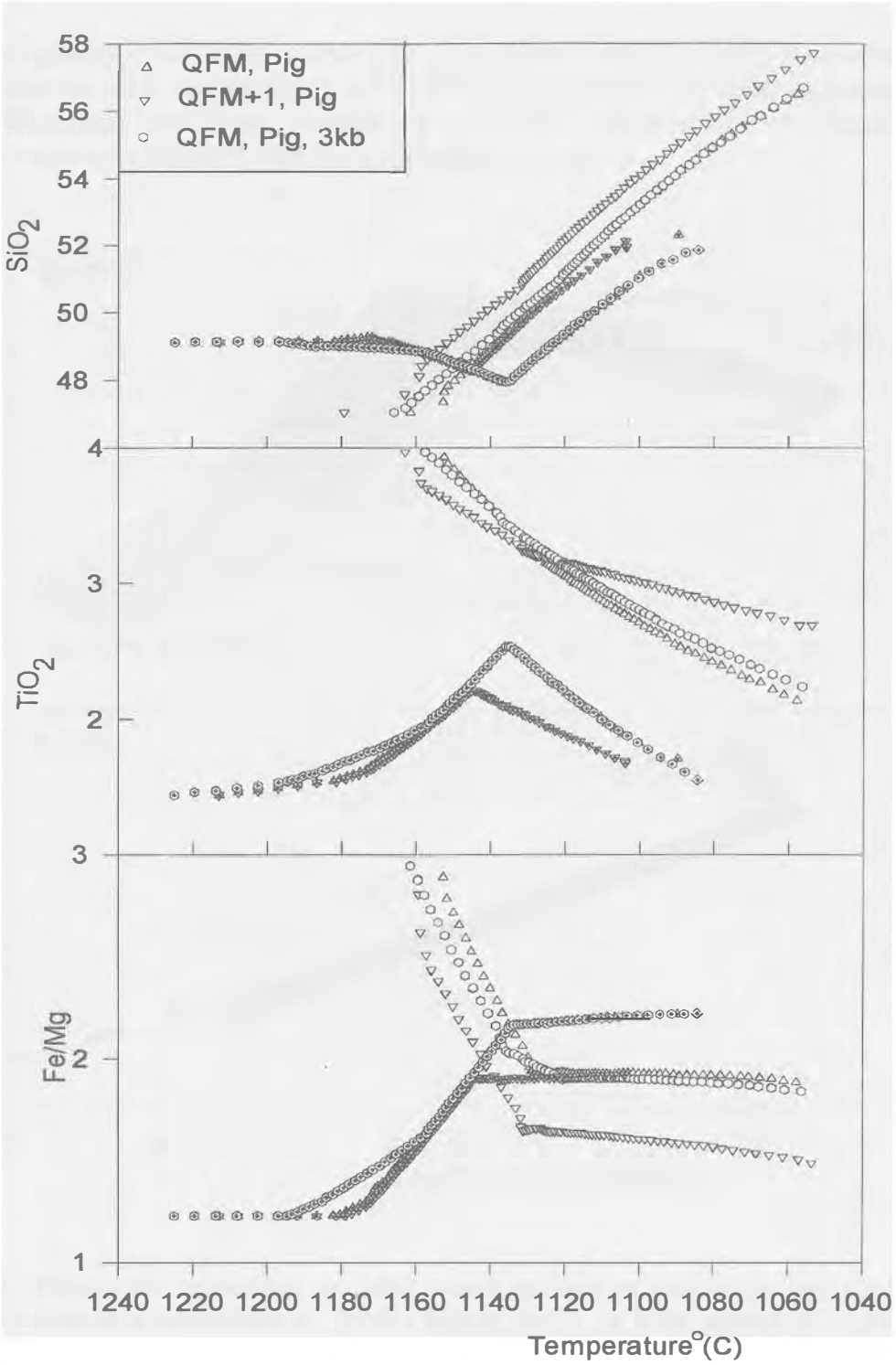

Figure 21. Silica, titanium and Fe/Mg ratio in liquid modeled through equilibrium crystallization . Filled and empty symbols indicate primitive and evolved basaltic compositions, respectively.

Mineral proportions and compositions, and composition with decreasing temperature, were studied for both fractional and equilibrium crystallization over different pressure, oxygen fugacities, and water content of 0,2 wt%. Subsequently, the modeled compositions were compared with the actual compositions.

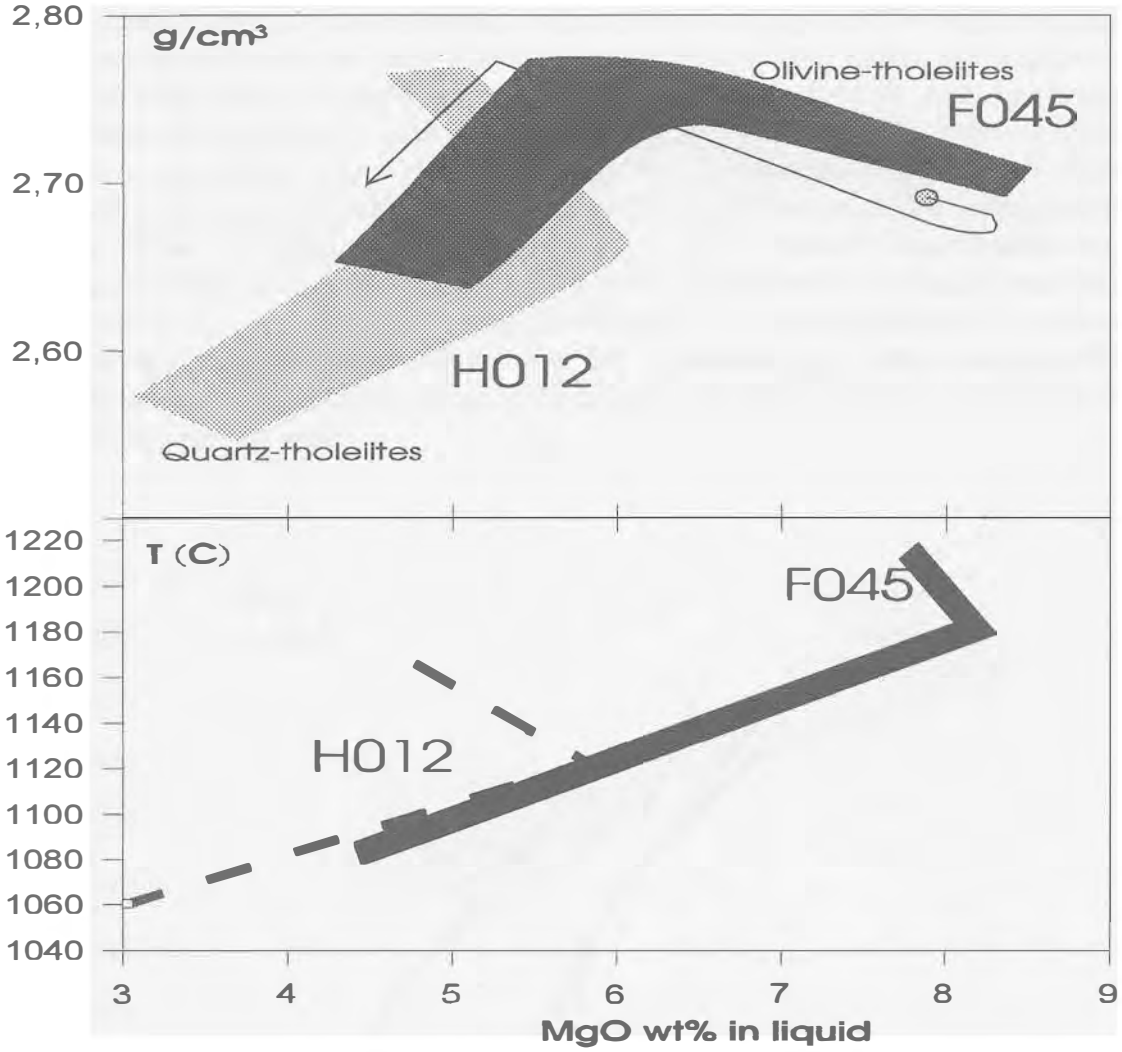

Figure 22. Density and temperature vs. MgO content in liquid as modeled through the low pressure equilibrium crystallization in QFM+1 oxygen buffer, at water content 0.2 wt% of primitive tholeiitic and evolved tholeiitic (basaltic) compositions. Notice the density decrease at early stage crystallization of olivine-tholeiitic composition followed by rapid increase and drop after oxide precipitation at 5.5-6.0wt% MgO. This process is restricted within magmatic temperatures of 1140 -- 1120° C.

There are no drastic differences in mineral compositions comparing the two crystallizational models. Low pressure fractional crystallization of olivine -tholeiitic magma in QFM buffer is somewhat difficult to complete because the olivine dissolution

at 1170° C changes mass balance between liquid and crystallized phases. Modeled primitive composition display some olivine crystallization at the QFM+1 buffer starting from 1190° C, and reaching 5 wt% later followed by complete dissolution being consistent with modal mineralogy of natural samples. The primitive composition (FE045) contains plagioclase gradually changing from An_{64} to An_{53}, and separate generation of An_{81} with normal, reverse and homogeneous zoning patterns. Compositional zoning is usually weak, reaching maximum up to 3-4% of An number, which may likely be due to normal mineral heterogeneity from cation site occupancy and analytical error. Evolved gabbro sample (HV012) displays two distinctive generations of plagioclase -- An_{46-51}, and An_{57-59}. As shown in Figure 23., the modeled compositions show regularly higher An components compared to those observed. Experimental results indicate, that calcic plagioclase reacts very slowly with melts in which the equilibrium plagioclase is more sodic. However, one possible way involves polybaric fractionation, which could to be an explanation for highly anorthitic plagioclases (An_{80-81}). As clearly seen from Figure 23., neither primitive nor evolved composition offers satisfying model-solution, but a combination of both trends modeled provides solutions significantly close to the natural at high temperatures but leaves no proof of an actual process.

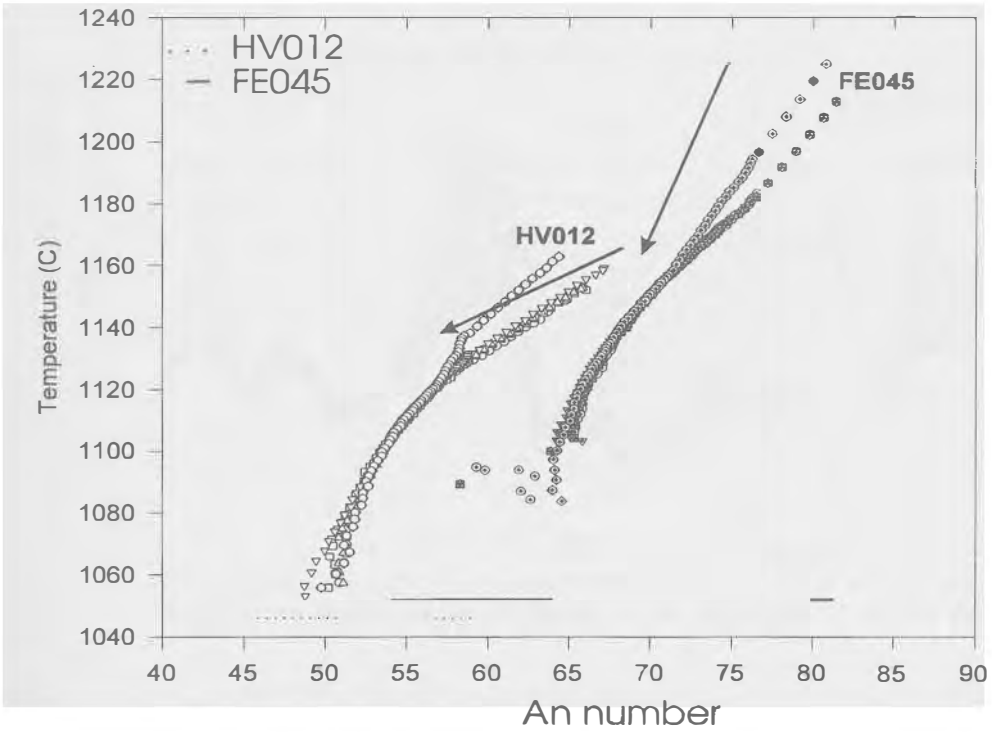

Figure 23. Modeled plagioclase compositions of primitive (FE045) and evolved (HV012) gabbros. Different parameters of equilibrium crystallization are used (see symbols in Fig. 21.). Initial water content is 0,2 wt%. Observed compositions are shown as a range.

Clinopyroxene crystallizing from a primitive melt shows slightly different trends depending on oxygen fugacity, and accompanying low-Ca pyroxene (not shown). Clinopyroxenes from evolved gabbros display much large En-Fs-Wo range as compared to the primitive variety. This may indicate that at lower temperature the clinopyroxenes have suffered from local modification of composition. Sometimes, compositional differences appear on the grain-size scale in the sample.

The major compositional differences within the natural samples appears in the Ca contents. Repeated heating followed by slow cooling offers a special conditions favourable for homogenization of clinopyroxene and gradual plagioclase modification through the Ca-Na exchange.

Composition of the evolved gabbros were normalized against the primitive gabbro sample (FE045) (Fig. 23). Modeled compositions of sample FE045 at the crystallinity of 40 and 70%, respectively, are shown in the same compositional space.

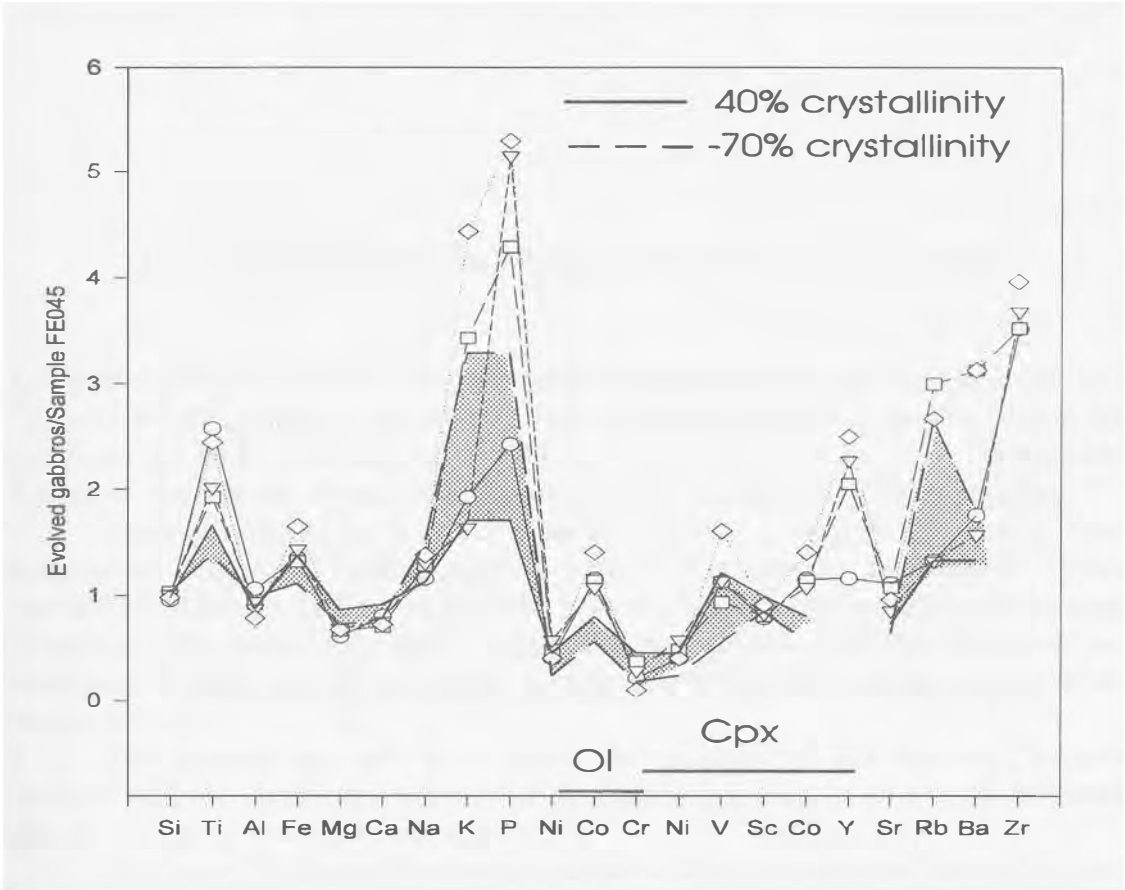

Figure 24. Thverartindur evolved gabbros normalized against the primitive gabbro composition. Dashed and solid lines indicate the modeled compositions at 70 and 40% crystallinity, respectively, of primitive tholeiitic sample (FE045). Olivine and clinopyroxene controlled trace elements are also shown.

It is evident from Figure 24., the bulk distribution of major and some trace elements can be described by over the 40-70% crystallization of primitive magma. The contents of titanium and iron manifest higher concentrations as modeled at 40% crystallinity, indicating, that FeTi-oxide precipitation in early stages of magmatic fractionation. Higher cobalt content compared to modeled is a good argument to support an early FeTi-oxide fractionation idea, since, the distribution coefficient is highest for Ti-magnetite. Phosphorus and potassium contents can not be described adequately because the model limitations. The fact, that evolved gabbros show a wide spectrum of trace elements, particularly incompatible elements, extends an assumption the mixing and contamination may act as a gabbro modifiers with a different magnitudes.

It can be concluded, that based on the present calculations, the closest fit is obtained assuming equilibrium crystallization of a Ol-tholeiitic magma to produce quartz-tholeiitic gabbros. This composition may be derived after a 40-70% low pressure crystallization accompanied with less, but different extent of mixing and assimilation-contamination processes.

10. Multiple Parental Magmas of a Rift Zone Volcano

Different definitions have used to distinguish a primary and parental magmas. The term "primary magma" indicates the magma which composition has not changed since it was generated by partial melting in its source region. In case of the Thverartindur formation, the primary magma is unknown as clearly manifested in earlier sections.

Parental magma has a wider meaning denoting a magma from which other magmas are derived. Usually, parental magma is regionally constrained. Typical parental MORBs may be derived from the most primitive liquids by complex processes. Sometimes, it is not entirely clear, whether the most primitive MORBs observed have undergone fractionation or are derived by separate, deep, high pressure melting of the mantle source.

The present approach is to show the relativity of the meaning "parental magma", and the complexity of involved the magmatic processes of a single magmatic lineage of single primary/parental magma.

In Figure 26, a simplified cross-section of the Thverartindur central volcanic complex is suggested. Fractional melting of mantle source and liquid accumulation is followed by upward migration of magma. Number of dikes supply small magma bodies. The first modification of a parental liquid take place within the dike formation. Usually, these modifications are minor, but in certain case, particularly when small temporary magma bodies begin to fractionate, a unique magmatic system based on single parental magma diverges. Some batches of magma may not been transported upwards immediately, they will fractionate and residual liquid can mix with later batches.

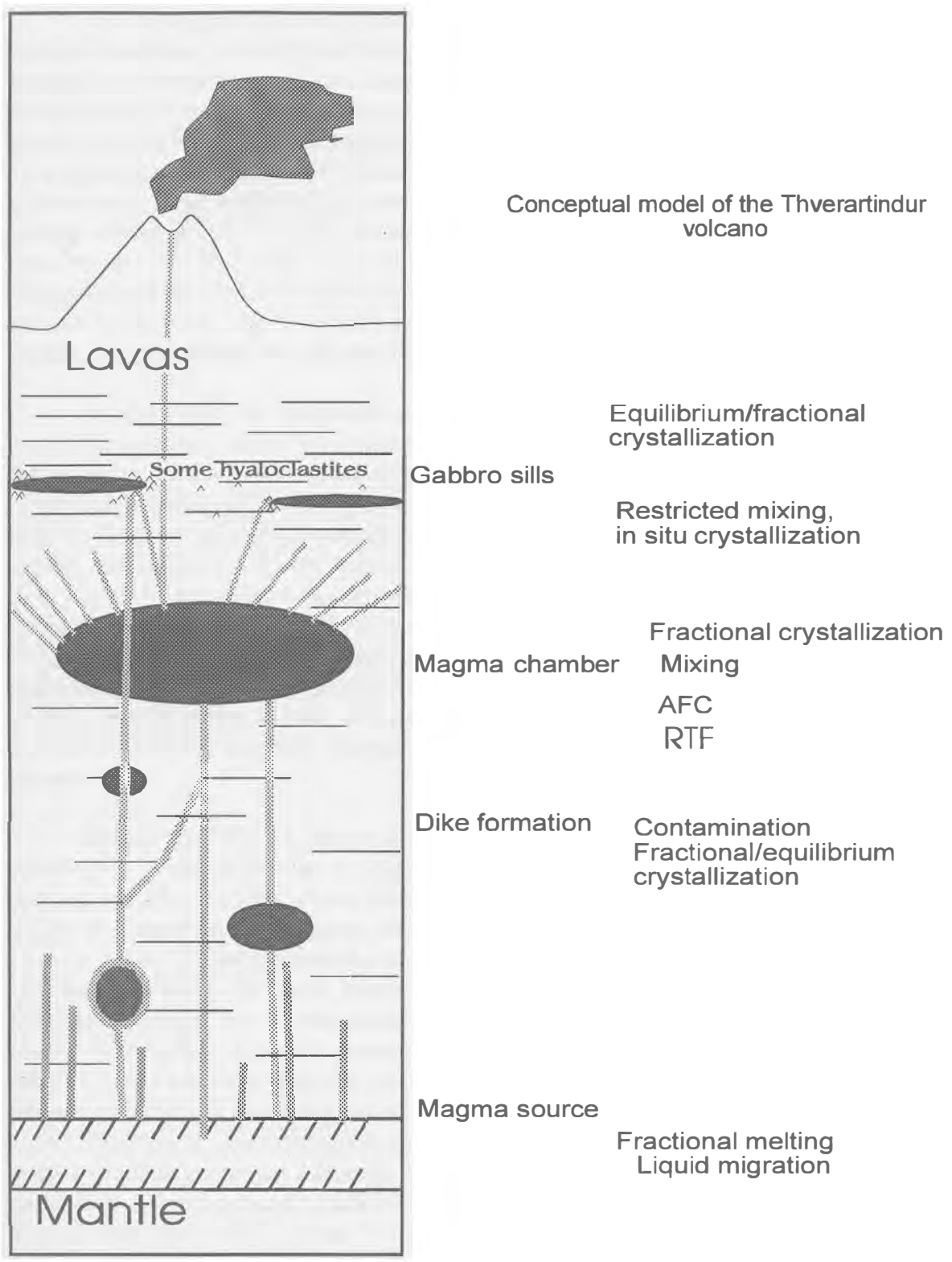

Figure 25. Simplified cross-section through Thverartindur central volcano showing possible processes involved in the liquid modification. Depending on scale, the parental magma may have a relative meaning. Discussion in text.

On the magma chamber level, commonly in the upper part of the crust at plate margin conditions, at neutral buoyancy, more complex processes are involved. This is referred to as second stage of modification (Fig. 25). Undoubtedly, the magma chamber is replenished, tapped, at least temporarily and continuously heated. Due to a good thermal connection, different mechanical mixing and stratification process may play very significant role. Roof and wall-rock assimilation, digesting of xenoliths and blocks incorporated from surroundings, enhance chemical heterogeneity and obscures the genetic relationship between some trace and major elements. Magma chambers feed cone sheets and dikes, but also, the chamber will loose the magma, and therefore energy through the volcanic eruptions. Third stage of modification is confined to the sill formation. Parental magma for sills has undergone several processes and will only be slightly changed during the sill crystallization.

In this frame, the magmatic evolution of a single volcanic system exhibits an array of processes caused by concurrent existence of multiple magmas, which may, depending on the scale, be referred to as parental for separate plutonic structures.

An erupted and intruded rock represents a stage of liquid evolution at certain time t_X. Several different situations occur: rock can solidify from a liquid through mineral separation in a closed-system equilibrium crystallization; crystals can separate from liquid leaving residual liquid to crystallize somewhere else or mix; crystals can be carried by other liquid and further separated again; liquids can mix together in addition to liquid -- crystal mixing etc. Thus, an infinite number of cases may contribute to a single magmatic formation in mid-ocean ridge environments. Sometimes, artificially relating samples to each other, a misinterpretation could be easily made because the existence of several magmatic lineages, all of which may initially be related to a single parent.

Figure 26. offers a simple conceptual outline. An initial magma, derived by partial melting within the mantle, evolves towards a more evolved compositions. The simplest evolution trend is shown from 1 to 2 (Fig. 26). The trends over 3, 4, 5 and 6 display the cases, when the magma subordinate in the extensive fractional crystallization producing very primitive cumulate rocks, and evolved liquid. Notice, that within the common time scale, the initial points 1 and 3 have different values. Second trend is followed by several new magma pulses from the mantle, up to the very rapidly evolving trend 7 to 2, which closes the entire evolutionary space described in Figure 26. Each batch of liquid extracted from the original mantle melts, has its own life-cycle outlined by different extent of modifying processes.

Particularly, this corresponds to the early stages of a central volcano and central magma chamber evolution. Later, when increasing magma supply and subsequently the decreasing thermal gradient within the system (i.e. with establishment of thermal control over the entire system), a higher homogenization rate results, and may contribute to compositional unification on the scale of a single volcanic magma system. Considering a plutonic formation of central volcano (like the Thverartindur), the question arises, whether the rocks really belong to a single magmatic lineage, and if we can juxtapose these rocks expecting evolutionary links between them. In other words,

an arbitrary section in Figure 26, A -- B indicates an arbitrary plutonic complex with four separate rock compositions, but they lie on different evolutionary lines shifted by a time - factor. However, if the ideal fractionation happens in nature, our modeling will give discrepancies we would like to explain involving more sophisticated processes, which in spite of a genuine solution would imply just the time-factor controlling different "starting points". Unfortunately, the real picture is much more complicated because this simple sketch (Fig. 26.) offers two-dimensional model where the most important dimension -- space is not indicated. Involving three additional space coordinates [X, Y, Z], as a third dimension, the model can be applied on real magmatic systems.

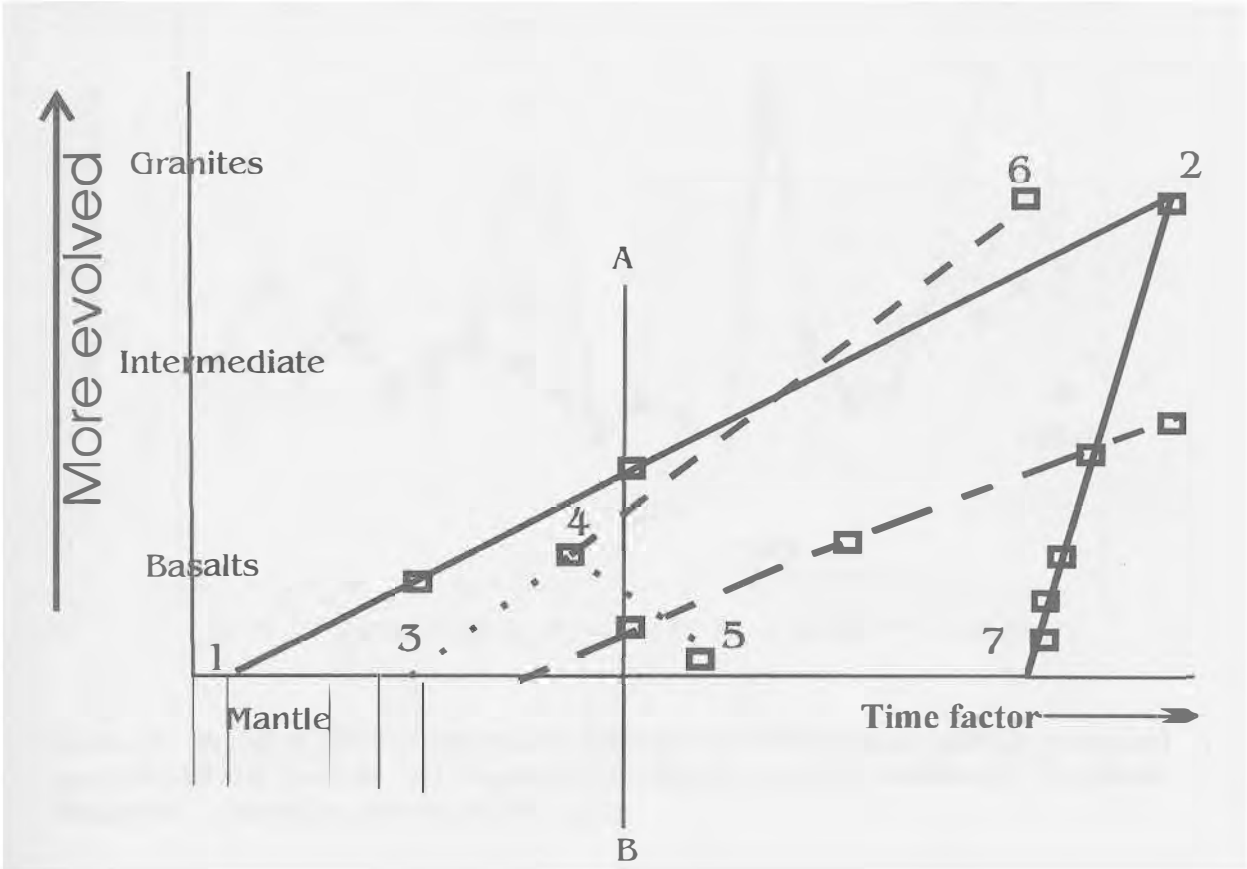

Figure 26. Graphical solution explaining the relativity and diversity of magma evolutionary trends. Each magma batch may act as a separate magmatic system, which description depends just on the scale investigated. An arbitrary line A -- B shows an artificial (can be natural) plutonic formation, which include rocks resulting from distinctive evolutionary sub-systems, magmatic lineages.

The Thverartindur gabbro and dike compositions can be compared with MORB compositions. In the Figure 27, the primitive and evolved gabbros have been generalized. Only one primitive gabbro sample (FE045) is used, because there are no drastic differences within primitive compositions. Evolved gabbros show somewhat larger scatter. Lower Ni, Co and Cr compared to typical MORB is a characteristic

feature for the majority of the Thverartindur rocks indicating mainly that these compositions have been depleted in olivine-philic elements. Positive V anomaly is also evident, which is likely related to the magnetite phase.

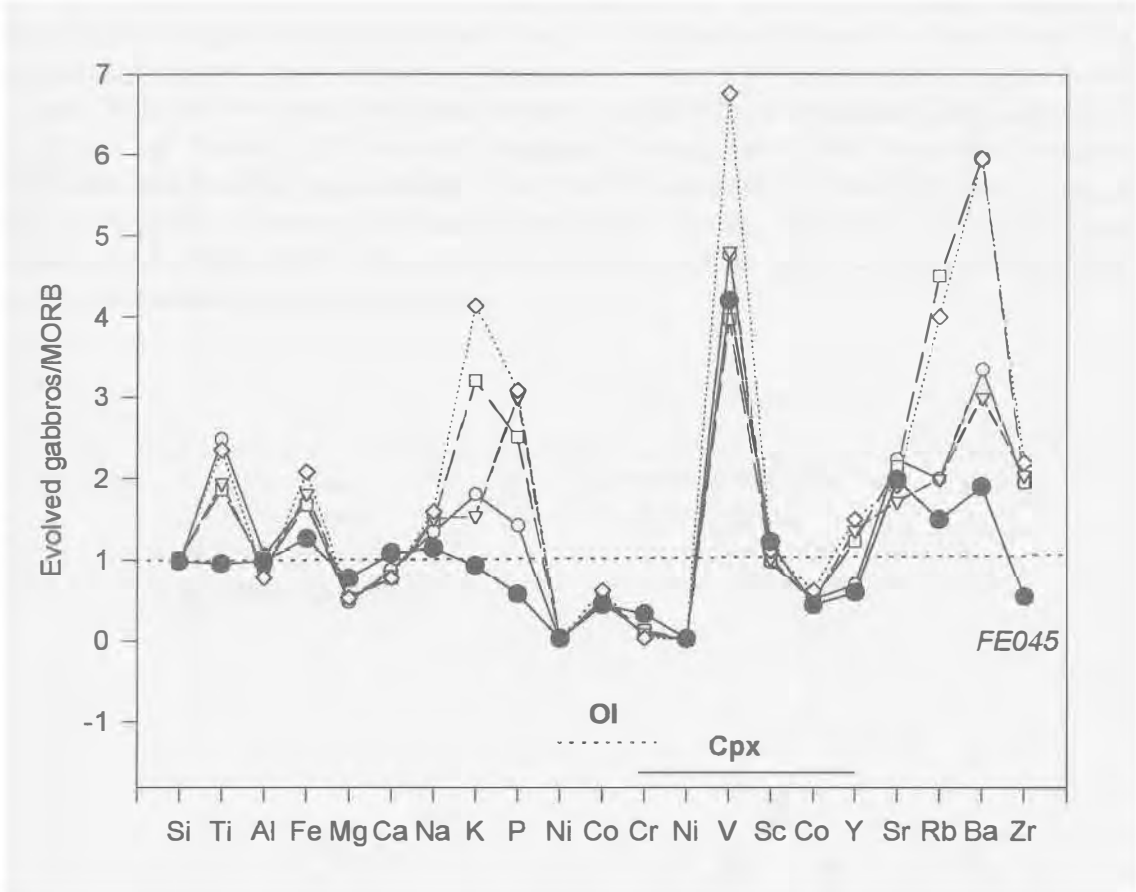

Figure 27. Primitive (FE045) and evolved gabbros from Thverartindur complex normalized against the MORB (see Tab. 19.). Negative Ni-Co-Cr and positive V anomalies are a common features for Thverartindur gabbros and dike rocks.

In order to avoid some anomalous distribution of elements comparing Thverartindur major and minor intrusive rocks, the gabbro and dike compositions have been clustered into primitive (olivine-tholeiitic) and evolved (quartz-tholeiitic) groups. Calculated average compositions can be easily compared with each other by normalization against single primitive dike composition. The results are presented in the Figure 28, which shows that the closest chemical relation to classical MORB/primitive dike composition is noticed in olivine-tholeiitic gabbros. In contrast, the highest scatter, particularly of mobile elements is evident for the quartz-tholeiitic dikes. It is also obvious from this Figure, that the chemistry of evolved dikes and plutonics is closer compared with the primitive varieties. A more detail study of magnitude and character of scatter convince that plutonics do not exhibit extensive crystal fractionation which is

consistent with petrographical study. In contrast, dike compositions manifest much higher variability which support an assumption, that they describe a multi-array of chemical evolution, and are good candidates to study and comprehend the entire range of time scattered evolutionary processes of the Thverartindur complex.

Most characteristic feature of the Thverartindur gabbros and dikes, compare to the MORB major compositions (see Tab. 19.), is higher Ti and Fe, and lower Mg contents. However, these average compositions do not represent parental magma *sensu stricto*, it is evident that Ti-Fe enrichment has played an important role during the evolution of "secondary" parental magma. Relying upon the Ni-Cr-Co negative anomaly, one possible explanation is that the Thverartindur original (primary) magma has undergone a olivine fractionation at deeper level, which causes a significant depletion of olivine-philic trace elements and Mg. Other explanation, more unlikely, may be a specific source composition.

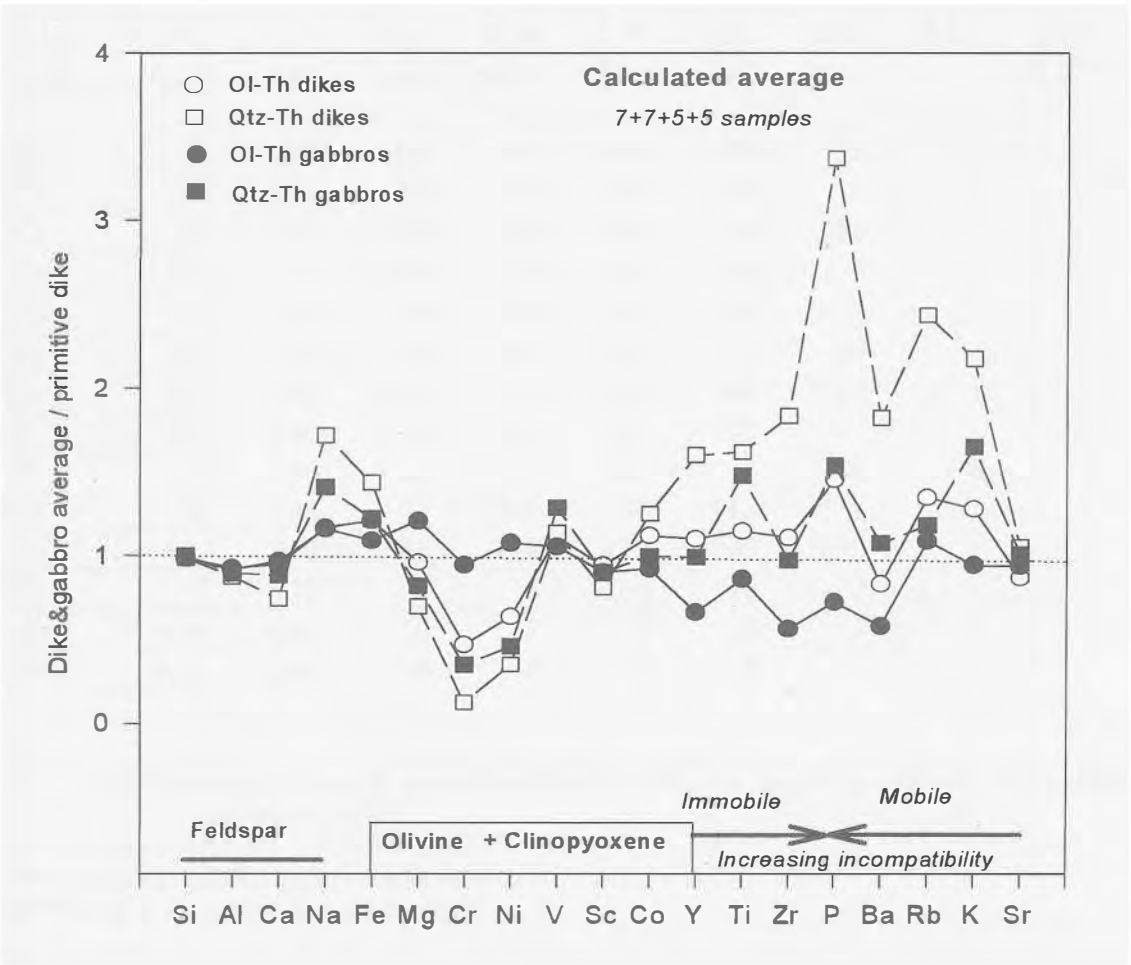

Figure 28. Average compositions of Thverartindur gabbros and dikes normalized against the primitive dike composition showing mutual relationship between both olivine- and quartz-tholeiitic compositions. The major and trace elements are arranged by minerals and according to the mobility and incompatibility features.

Table 19. Average chemical composition of Thverartindur olivine- and quartz-tholeiitic dikes and gabbros. MORB composition for comparison.

	Dike	Dike	Gabbro	Gabbro	Total	Total	MORB	MORB	MORB	MORB
	Ol-Thol	Qtz-Thol	Ol-Thol	Qtz-Thol	Ol-Thol	Qtz-Thol	*	**	***	****
	7 samples	7 samples	5 samples	5 samples						
SiO_2	48,27	48,43	48,60	49,12	48,44	48,78	49,40	48,96	49,30	50,30
TiO_2	2,35	3,30	1,76	3,02	2,06	3,16	1,50	0,82	0,76	0,73
Al_2O_3	15,46	14,56	15,27	14,90	15,36	14,73	15,60	15,75	16,90	16,60
FeO	12,10	14,35	10,91	12,21	11,50	13,28	7,50	8,52	7,20	7,99
MnO	0,20	0,25	0,20	0,20	0,20	0,23	0,20	0,13	0,14	0,12
CaO	12,17	9,56	12,43	11,36	12,30	10,46	13,00	11,92	11,20	13,20
MgO	6,27	4,57	7,89	5,36	7,08	4,96	10,00	9,79	11,10	10,20
Na_2O	2,36	3,47	2,35	2,85	2,35	3,16	2,00	1,97	2,27	2,00
K_2O	0,42	0,72	0,31	0,54	0,37	0,63	0,50	0,11	0,03	0
P_2O_5	0,28	0,64	0,14	0,29	0,21	0,47	0,12		0,07	
Ba	75	163	53	96	64	130	20			
Co	64	71	53	57	58	64				
Cr	91	25	181	67	136	46	250			
Cu	154	77	276	111	215	94				
Ni	55	30	93	40	74	35				
Sc	42	36	41	41	41	39	40			
Sr	220	266	238	255	229	260	120			
V	353	360	334	407	343	383				
Y	34	50	21	31	28	40	30			
Zn	96	124	93	108	94	116				
Zr	159	262	81	139	120	201	90			
Rb	7	13	6	6	6	10	2			
Nb	n.m.	n.m.	0	3	0	3	4			
Ga	n.m.	n.m.	8	8	8	8				

* MORB composition used in normalization of Thverartindur samples is compiled from Sullivan, (1991) and Pearce, (1983)

** Bryan and Moore, (1977); FAMOUS

*** Sullivan, (1991); melt inclusion in olivine

**** Frey et al., (1974); South Atlantic

11. Episodic Magmatism and the Formation of the Thverartindur Magma Chamber

Field and laboratory evidence suggests that the basaltic magmatism at Thverartindur (but also in other places around the central volcanoes) has an episodic character. These comprises:

i) a multitude of regional dike and cone sheet injections with apparently random alternation of primitive tholeiitic and more evolved basaltic compositions;
ii) several basaltic injections forming gabbroic sills with different thickness and composition;
iii) late emplacement of highly evolved basalt concurrent with granitic magmatism.

There is no direct evidence preserved of volcanism at Thverartindur because an extensive glaciation. However, the following geologic considerations suggest a volcanic activity of the central type:

i) The local occurrence of rhyolitic intrusions and sheets is a first order criterion to detect a partly buried volcanic system; these granophyric bodies normally indicate that a magma chamber was present at shallow crustal level (Walker, 1974; Jakobsson, 1979).

ii) Vertical dikes within complex indicate the upward transport of magma.

iii) The Thverartindur complex is situated on the volcanic lineament parallel to the Eastern neovolcanic zone supporting an idea of distribution of the volcanic complexes at spreading centres. The size of complex is comparable with other recent and extinct volcanic systems in Iceland.

Usually, central volcanoes at spreading centres are thought to have a feeder chamber at shallow level, which are commonly lens-shaped or spherical bodies. It was *suggested, that the Thverartindur volcano has an ellipsoidal chamber with size up to* $2 \times 7 \times 8$ km, because the maximum counted dip direction of inclined sheets outlining the magma chamber/source (Bromann and Soesoo, 1994).

Several investigators have proposed models for shallow magma chamber formation, where the rate of intrusion of magma is sufficiently high to melt the host rock (Hardee, 1982). Walker (1974) proposed that this mechanism may explain the formation of gabbro intrusions, many of which, presumably, acted as a magma chambers in Iceland. Gudmundsson (1986) suggested that crustal magma chambers in Iceland may form as a result of thick sills in the upper part of the crust. When basaltic magma which flows along a vertical dike meets a crustal layer in which the horizontal compressive stresses are higher than the vertical stress, a sill forms. If the resulting sill is thick enough (over 100 m) it may take hundreds of years for it to solidify and while liquid, it absorbs the magma in all dikes that enter it. The sill may evolve into a magma

chamber by expansion and magmatic stopping, its expansion resulting is partly elastic and partly plastic deformation of the host rock.

Detailed studies of the active Krafla volcano in northern Iceland indicate that the roof of Krafla magma chamber is at depth of 2-3 km, and the bottom at 7 km (Gudmundsson, 1987). Below that chamber is another and much larger chamber which supplies magma to the shallower Krafla magma chamber. Gudmundsson (1987) proposed that double chamber arrangement, where an upper chamber is located in the crust and lower is located in the magma layer is common in Iceland.

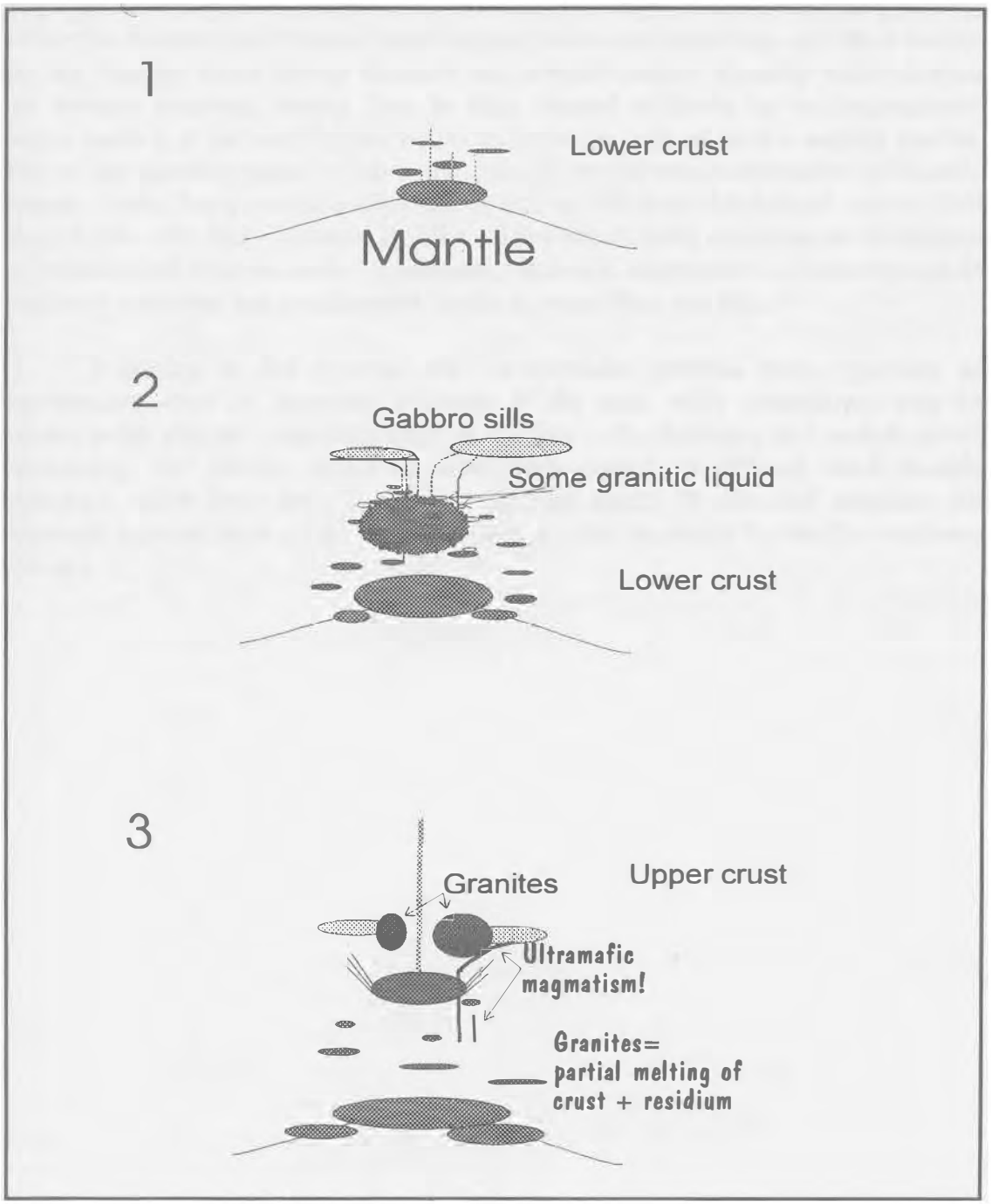

Figure 29. Three - stage evolution of the Thverartindur formation. Discussion in text.

In order to describe the evolution of the Thverartindur complex, a three-stage evolution has been suggested in Figure 29. The first stage indicates a partial melting of upper mantle resulting in a several magma batches and early propagation of dikes. When more extensive melting occurs, several small magma bodies are formed representing a variation of basaltic magmas modified by fractional/equilibrium crystallization, some assimilation, and mixing between two liquids and liquid plus solidified phases. This stage is likely to be responsible for the gabbroic sill formation studied at Thverartindur. However, some small chambers may differentiate up to the granitic melts, later can under the fertile conditions form dikes. The third stage is characterized by episodic but intensive basic magmatism. Within the thermal epicentre, where the densest distribution of small magma bodies and chambers, and dikes occurs, the big chamber forms having chemical and probably density diversity inherited from the primary magmatic bodies. Due to high thermal gradients (active magmatism), partial melting of the crust begins to play an important role of granitic magma genesis. Part of the granitic magma is generated through the extreme fractionation of basaltic magma bodies being mechanically isolated and cut off from the thermal source. This stage is also very likely indicated by bimodal volcanic activity producing an alternation of primitive and evolved basalts. Eventually, ultramafic magmatism, as a latest phase of magmatic evolution has partaken and results in some dikes and sills.

According to this scenario, the Thverartindur gabbroic rocks represent an intermediate stage of magmatic evolution of the area, while granophyres may be related to the mature completing stage. According to the chemistry and mutual spatial relationship, the gabbros could be most easily related to different small basaltic chambers, which have been evolved at different stages. It does not eliminate the magmatic imprints from a large magma chamber which is source for the Thverartindur volcano.

12. Conclusive Remarks

Different methods, such like Pearce element ratio diagrams, and thermodynamical modeling (not related to each other), indicate, that Thverartindur evolved basaltic compositions are not derived from the primitive one through olivine fractionation. Neither Pearce' diagrams nor thermodynamic modeling consider the mixing effects. Thus, the discrepancies between modeled and natural composition are evident. One handicap arises from an unknown composition of primary magma, which in turn, needs to involve a concept of multiple parental magmas. As shown earlier, the most primitive dike compositions can not be a parental magma for gabbro formation, and can not be directly related to the surrounding lavas. It is likely, that the olivine fractionation is important mechanism in the parental magma modification only at a deeper level. Later assumption does not have any direct evidence but the negative anomaly of olivine-philic trace elements compared to those for MORB compositions.

Comprehensive model, involving mineral separation, liquid-liquid mixing, liquid-crystal mixing, and assimilation of wallrock and earlier crystallized rocks may not survive the magma chamber mixing constraints established from a number of experimental chamber simulations. It is well-known, that all of the magma chamber models assume *a priori* the trace elements will distribute ideally inside the chamber and the resulting liquid is always homogenous. When we are dealing with replenished magma chambers producing episodic eruptions or repeated magmatism, the homogenization mechanism is important constraint. Further modeling of central volcano' magmatic system could be consider constraints arising from the unknown character of magma chamber homogenization, multi-stage mixing and assimilation through the concurrent existence of several magmas.

Some basic conclusions can be listed below:

1. The Tertiary Thverartindur plutonic formation reveals signs of repeated episodic magmatic activity. Major basic intrusions are represented by sill-like bodies which may not be related to a single shallow magma chamber, but may have formed partly before and during the shallow magma chamber formation. Granites are the latest phase accompanied by evolved basic envelope rock and restricted ultramafic magmatism. Generally, gabbros do not exhibit cumulate textures, indicating that they are chemically close to the liquid composition.

2. Field evidence indicate that the magmatic emplacement has rather wide time span. The contemporaneous existence of primitive and evolved basic magmas is evident.

3. Evolved gabbros (MgO<5) are derived from more primitive gabbroic liquid (MgO>7) by low pressure equilibrium crystallization in QFM+1 oxygen buffer with minor influence from assimilation and magma-magma mixing, and magma-solidified crystals mixing. Olivine separation has not affected the evolved gabbro formation. Olivine crystallization may have been important at deeper levels.

4. At least two types of hybridization mechanisms were active: (1) acid-basic magma mixing; and (2) evolved basic magma and captured crystals mixing. It is likely, that late ultramafic magma emplacement has caused back-veining, which in turn has created the third type of hybrid rocks. Two hybrid rock types can also be distinguished by clinopyroxene compositions.

5. There are no direct evidences for a common parental magma. No simple magmatic lineages between primitive dikes and primitive gabbro compositions has been found.

Acknowledgements:

This project was undertaken during the Nordic Scholarship at Nordic Volcanological Institute, Reykjavik. I am thankful for Martin Bromann for successful field co-operation through two field seasons. I thank Karl Grönvold for assistance in microprobe studies and Nils Oskarsson for help in whole rock chemistry. The ideas were kept evolving by both Nils Oskarsson and Karl Grönvold who have done a lot for improvement of present report. I thank Agust Gudmundsson for an introduction into the field area and comments. Gudmundur Sigvaldasson is thanked for useful comments and help during my study in Iceland.

References

Aitchison, J. 1981. A new approach to null correlation of proportions. Journal of Mathematical Geology., 13, 175-189.

Aitchison, J. 1984. The statistical analysis of geochemical compositions. Journal of Mathematical Geology., 16, 532-564.

Annels, A.E. 1967. The geology of the Hornafjordur region. Ph.D., University of London.

Ariskin, A.; Frenkel, M.; Barmina, G. & Nielsen, R., 1993. COMAGMAT: a FORTRAN program to model magma differentiation processes. Comp. Geosci., 19, 1150-1170.

Bacon, C.R. & Hirschmann, M.M., 1988. Mg/Mn partitioning as a test for equilibrium between coexisting Fe-Ti oxides. Am. Mineral., 73, 5-61.

Bernstein, S.; Rosing, T.M.; Brooks, C.K. & Bird, K.D, 1992. An ocean-ridge type magma chamber at passive volcanic, continental margin: the Kap Edvard Holm layered gabbro complex, East Greenland. Geol. Mag., 129, 437-456.

Biggar, G.M., 1983. Crystallization of plagioclase, augite and olivine in synthetic systems and in tholeiites. Mineral. Mag., 47, 161-176.

Blake, D.H., 1964. The volcanic geology of the Austurhorn area, south-eastern Iceland. Ph.D. Thesis, University of London.

Blake, D.H., 1966. The net-veined complex of the Austurhorn intrusion, south-eastern Iceland. Journal of Geology, 76, 891-907.

Bromann, M. & Soesoo, A. (1994): Structure and petrology of a central volcanic complex in SE. Iceland. (Abstract) *In:* Journal of Icelandic Geological Society, 29-30

Bryan, W.B. & Moore, J.G., 1977. Compositional variation of young basalts in the Mid-Atlantic Ridge rift valley near lat. 36° 49´N. Geol. Soc. Am. Bull., 88, 556-570.

Cox, K.G.; Bell, J.D. & Pankhurst, R.J., 1989. The interpretation of igneous rocks. 450.

DePaolo, D.J., 1981. Trace element and isotopic effects of combined wallrock assimilation and fractional crystallization. Earth. Planet. Sci. Lett., 53, 189-202.

Dugan, M.A. & Rhodes, J.M., 1978. Residual glasses and melt inclusions in basalts from DSDP Legs 45 and 46: Evidence for magma mixing. Contrib. Mineral. Petrol., 67, 417-431.

Duke, J.M., 1976. Distribution of the period four transition elements among olivine, calcic pyroxene and mafic liquid: experimental results. J. Petrol., 17, 499-521.

Elthon, D., 1987. Petrology of gabbroic rocks from Mid-Cayman Rise Center. J Geophys. Res., 92, 658-682.

Fridleifsson, G., 1983. The geology and the alteration history of the Geitafell central volcano, SE Iceland. PhD. Thesis, University of Edinburgh.

Fujimaki, H.; Tatsumoto, M. & Aoki, K., 1984. Partition coefficients of Hf, Zr and REE between phenocrysts and groundmasses. Proceedings of the fourteenth lunar and planetary science conference, Part 2. J. Geophys. Res., 89. B662-B672.

Furman, T., Frey, A.F. & Meyer, P.S. 1992a. Petrogenesis of evolved basalts and rhyolites at Austurhorn, Southeastern Iceland: the role of fractional crystallization. J. Petrol.., 33, 1405-1445.

Furman, T., Meyer, P.S. & Frey, A.F. 1992b. Evolution of Icelandic central volcanoes: evidence from the Austurhorn intrusion, southeastern Iceland. Bull. Volcanol., 55, 45- 62.

Gale, N.H.; Moorbath, S.; Simons, J. & Walker, G.P.L., 1966. K-Ar ages of acid intrusive rocks from Iceland. Earth Planet. Sci. Lett., 1, 284-288.

Gill, J.B., 1981. Orogenic andesites and plate tectonics. Springer, Berlin.
Grove, T.L. & Bryan, W.B., 1983. Fractionation of pyroxene-phyric MORB at low pressure: an experimental study. Contr. Miner. Petrol., 84, 293-309.
Gudmundsson, A., 1986. Formation of crustal magma chambers in Iceland. Geology, 14, 164-166.
Gudmundsson, A., 1987. Formation and mechanics of magma reservoirs in Iceland. Geophys. J. R. Astr. Soc., 91, 27-41.
Hardee, H.C., 1982. Incipient magma chamber formation as a result of perspective intrusions. Bull. Volcanol., 45, 41-49.
Huppert, H. & Sparks, R., 1980. The fluid dynamics of a basaltic magma chamber replenished by influx of hot, dense ultrabasic magma. Contrib. Mineral. Petrol., 75, 279-289.
Huppert, H.; Sparks, R.; Whitehead, J. & Hallworth, M., 1986. Replenishment of magma chambers by light inputs. J. Geophys. Res., 91, B6, 6113-6122.
Imsland, P., 1984. Petrology, mineralogy and evolution of the Jan Mayen magma system. 332p. Reykjavik.
Irvine, T.N., 1980. Rocks whose composition is determined by crystal accumulation and sorting. *In:* The evolution of the igneous rocks., 245-306, Princeton University Press.
Irvine, P., 1982. Terminology of layered intrusions. J. Petrol., 23, 127-162.
Jakobsson, S.P.; Pedersen, A.K.; Ronsbo, J.G. & Larsen, C.M., 1973. Petrology of mugearite-hawaiite: early extrusives in the 1973 Heimaey eruption, Iceland. Lithos, 6, 203-214.
Jakobsson, S.P.; Jonsson, J. & Shido, F., 1978. Petrology of the western Reykjanes Peninsula, Iceland. J. Petrol., 19, 669-705.
Jakobsson, S.P., 1979. Outline of the petrology of Iceland. Jökull, 29, 57-73.
Kristjansson, L.; Helgason, J., 1988. Some properties of basalt lava sequences and volcanic centres in a plate-boundary environment. *In*: Early Tertiary volcanism and opening of the NE Atlantic, Geological Society Special Publication, 39, 147-155.
Mattson, S.R.; Vogel, T.A. & Wilbrand, J.T., 1986. Petrochemistry of the silicic-mafic complexes at Vesturhorn and Austurhorn, Iceland: evidence for zoned/stratified magma. J. Volcanol. Geotherm. Res., 28, 197-223.
McBirney, A.R.; Baker, B.H. & Nilson, R.H., 1985. Liquid fractionation, I, basic principles and experimental simulations. J. Volcanol. Geotherm. Res., 24, 1-24.
McBirney, A.R. & Naslund, H.L., 1990. The differentiation of the Skaergaard intrusion. Contrib. Mineral.Petrol., 104, 235-247.
Meyer, P.S., 1978. Petrology of basaltic dikes from Vestfirdir: Iceland's Northwest Peninsula. M.S.Thesis, University of Rhode Island, Kingston (unpublished).
Meyer, P.S., Dick, J.B. & Thompson, G., 1989. Cumulate gabbros from the southwest Indian ridge, 54° S-7° 16' E: implications for magmatic processes at slow spreading ridge. Contrin. Mineral. Petrol., 103, 44-63.
Michael, P.J. & Chase, R.L., 1987. The influence of primary magma composition, H_2O and pressure on Mid-Ocean Ridge basalt differentiation. Contib. Mineral. Petrol., 96, 254-263.
Moorbath, S.; Sigurdsson, H. & Goodwin, R., 1968. K-Ar ages of the oldest exposed rocks in Iceland. Earth Planet. Sci. Lett., 4, 197-205.
Morse, S.A., 1990. The differentiation of the Skaergaard intrusion. Contrib. Mineral. Petrol., 104, 235-247.

Mullen, E.D., 1983. $MnO/TiO_2/P_2O_5$: a minor element discriminant for basaltic rocks of oceanic environment and its implications for petrogenesis. Earth. Planet. Sci. Lett., 62, 53-62.
Newman, T.C.M., 1967. The geology of some igneous intrusions in the Hornafjordur region, S.E. Iceland. Ph.D., Victoria University of Manchester.
Nicholls, J., 1988. The statistics of Pearce element diagrams and the Chayes closure problem. Contrib. Mineral. Petrol. 98, 11-24.
Nicholson, H. & Latin,D., 1992. Olivine tholeiites from Krafla, Iceland: evidence for variations in melt fraction within a plume. J. Petrol. 33, 1105-1124.
Oskarsson, N.; Steinthorsson, S. & Sigvaldason, G.E., 1985. Iceland geochemical anomaly: Origin, volcanotectonics, chemical fractionation and isotope evolution of the crust. J.Geophys. Res., 90, 10 011-10 025.
Pearce, J.A. & Norry, M.J., 1979. Petrogenetic implications of Ti, Zr, Y and Nb variations in volcanic rocks. Contrib. Mineral. Petrol. 69, 33-47.
Pearce, T.H., 1987., The identification and assessment of spurious trends in Pearce-type ratio variation diagrams: a discussion of some statistical arguments. Contrib. Mineral. Petrol., 97, 529-534.
Perfit, M.J. & Fonaris, D., 1983. Geochemical studies of abyssal lavas recovered by DSRV Alvin from Eastern Galapagos Rift, Inca transform, and Ecuador rift, 2. Phase chemistry and crystallization history. J. Geophys. Res. 88, 10530-10550.
Roeder, P.L. & Emslie, R.F., 1970. Olivine-liquid equilibrium. Contrib. Miner. Petrol., 29, 275-289.
Roeder, P.L., 1974. Activity of iron and olivine solubility in basaltic liquids. Earth. Planet. Sci. Lett., 23, 397-410.
Russell, J.K & Nicholls,J., 1987. Early crystallization history of alkali olivine basalts, Diamond Craters, Oregon. Geochim. Cosmochim. Acta., 51, 143-154.
Russell, J.K & Nicholls, J.K., 1988. Analysis of petrologic hypotheses with Pearce element ratios. Contrib. Mineral. Petrol., 25-35.
Russell, J.K.; Nicholls, J.; Stanley, C.R. & Pearce, T.H., 1990. Pearce element ratios. A paradigm for testing hypotheses. Eos, 71, 234-247.
Saemundsson, K., 1979. Outline of the geology of Iceland. Jökull, 29, 7-28.
Schönharting, G. & Petersen, K., 1979. The Hvannadalur and Geitafell intrusions, SE Iceland: Magnetic anomalies, structure and the magnetic layer problem. Jökull, 28, 32-41.
Shibata, T., 1976. Phenocryst-bulk rock composition relations of abyssal tholeiites and their petrogenetic significance. Geochim. Cosmochim. Acta 40, 1407-1417.
Sigurdsson, H., 1981. First-order major element variation in basalt glasses from the Mid-Atlantic Ridge: 29°N to 73°N. J. Geophys. Res. 86, 9483-9502.
Sigurdsson, H. & Sparks, R.S., 1981. Petrology of rhyolitic and mixed-magma ejecta from the 1875 eruption of Askja, Iceland. J.Petrol., 22, 41-84.
Skala, W., 1979. Some effects of the constant-sum problem in geochemistry. Chem. Geol., 27, 1-9.
Sparks, R.; Meyer, J. & Sigurdsson, H., 1980. Density variations amongst mid-ocean ridge basalts: Implications for magma mixing and the scacity of primitive lavas. Earth. Planet. Sci. Lett., 46, 419-430.
Sparks, R.S.J. & Huppert, H.E., 1984. Density changes during fractional crystallization of basaltic magmas: fluid dynamic implications. Contrib. Mineral. Petrol., 85, 300-309.

Sullivan, G., 1991. Chemical evolution of basalts from 23° N along the mid-Atlantic ridge: evidence from melt inclusions. Contrib. Mineral.Petrol., 106, 296-308.
Takahashi, E. & Kushiro, I., 1983. Melting of dry peridotite at high pressure and basalt magma genesis. Am. Mineral. 68, 859-879.
Torfason, H., 1979. Investigations into the structure of southeastern Iceland. Ph.D. Thesis, University of Liverpool.
Toplis, M.J.; Libourel, G.; Carroll, M.R., 1994. The role of phosphorus in crystallization of basalt: An experimental study. Geochem. Cosmoschim. Acta 58, 797-810.
Tormey, D.R., Grove, T.L., Bryan, W.B., 1987. Experimental petrology of normal MORB near the Kane Fracture Zone:22° - 25° N, mid-Atlantic ridge. Contr. Miner. Petrol., 96, 121-139.
Wager, L.R.; Brown, G.M., 1968. Layered igneous rocks. 588.
Walker, G.P.L. 1964. Geological investigations in eastern Iceland. Bull. Volcanol., 27, 3-15.
Walker, G.P.L., 1974. The structure of eastern Iceland. *In:* Geodynamics of Iceland and the North Atlantic area.
Ward, P.L., 1971. New interpretation of the geology of Iceland. Geol. Soc. Am. Bull., 82, 2991-3012.
White, R.S., 1990. Initiation of the Iceland plume and opening of the North Atlantic. - *In:* Extensional tectonics and stratigraphy of the North Atlantic margin, 149-154.
White, R.S.; McKenzie, D. 1989. Magmatism at rift zones: the generation of volcanic continental margins and flood basalts. J. Geophys. Res., 94, 7685-7729.

Appendix 1

Whole rock chemical analyses of the Thverartindur formation.

	FE063	FE065	HV028	**dike**
SiO_2	37,24	42,00	44,13	**47.24**
TiO_2	0,81	0,74	0,82	**1.06**
Al_2O_3	5,76	6,71	8,11	**10.08**
FeO	19,07	19,32	10,43	**10.17**
MnO	0,24	0,29	0,17	**0.15**
CaO	4,24	6,59	5,74	**7.09**
MgO	31,85	23,75	29,00	**22.98**
Na_2O	0,32	0,32	0,73	**0.51**
K_2O	0,12	0,05	0,54	**0.31**
P_2O_5	0,07	0,04	0,06	**0.10**
Total	99,72	99,81	99,73	**99.69**
Ba	13	9	38	**15**
Co	124	118	82	**98**
Cr	727	480	1102	**1392**
Cu	516	331	70	**84**
Ni	995	423	1119	**834**
Sc	22	29	20	**21**
Sr	67	95	92	**96**
V	209	214	190	**321**
Y	10	10	13	**16**
Zn	111	125	87	**98**
Zr	44	39	56	**55**
Rb	3,5	2	12	**10**
Ga	7	5	8	**n.m.**
Nb	--	--	--	**n.m.**
Mg#	**0,75**	**0,69**	**0,83**	**0.80**

Table 1. Whole-rock chemical analyses from Thverartindur ultramafic rocks. The representative dike composition is bold. Mg# = MgO/(MgO+FeO). FE- Fellsa; HV- Hvannadalur plutons.

Key to the samples: **FE063-** Central part, slightly digested (by margins) xenolith in gabbro; **FE065-** North-western part, medium grained ultramafic sheet in association with pegmatitic gabbros; **HV028-** Central part, coarse grained ultramafic sill.

Table 2. Whole rock chemical analyses of olivine-tholeiitic gabbros and sheets. The representative dike composition (in bold) shows a restricted modification of liquid composition within plutonic rocks. Mg# = MgO/(MgO+FeO). FE- Fellsa; HV- Hvannadalur, VD-Vedhurardalur plutons.

	HV010	HV017	HV018	VD139	FE044	FE045	FE053	FE059	FE078	FE081	**dike**	HV161 lava
SiO_2	51,54	48,17	49,59	48,32	51,32	49,07	46,39	48,78	49,81	47,41	**47.33**	49,36
TiO_2	2,12	1,71	1,49	1,55	1,64	1,44	1,70	2,18	2,12	1,99	**1.99**	2,18
Al_2O_3	14,50	14,87	15,41	17,10	16,39	15,47	13,92	14,48	15,33	16,11	**16.40**	15,31
FeO	9,32	10,87	10,12	9,33	9,18	9,43	14,60	11,63	11,02	12,48	**12.08**	11,28
MnO	0,16	0,24	0,20	0,15	0,16	0,15	0,24	0,19	0,18	0,19	**0.18**	0,19
CaO	12,37	12,25	12,45	13,78	12,32	14,03	9,80	11,96	11,85	11,46	**10.83**	10,64
MgO	6,12	8,88	7,84	7,58	5,74	7,77	11,12	7,73	6,52	7,21	**7.85**	6,97
Na_2O	2,75	2,22	2,16	1,78	2,55	2,30	1,66	2,43	2,56	2,63	**2.33**	2,87
K_2O	0,75	0,50	0,45	0,21	0,36	0,14	0,22	0,28	0,28	0,20	**0.57**	0,83
P_2O_5	0,22	0,14	0,14	0,07	0,23	0,07	0,24	0,19	0,20	0,14	**0.31**	0,22
Total	99,85	99,85	99,85	99,87	99,89	99,87	99,89	99,85	99,87	99,82	**99.87**	99,85
Ba	120	55	56	35	63	38	35	61	59	52	**176**	161
Co	47	51	47	48	45	49	69	**56**	43	60	**71**	61
Cr	216	249	249	103	50	84	28	100	87	220	**202**	129
Cu	129	199	206	188	194	190	134	202	158	84	**85**	134
Ni	42	109	97	72	59	63	85	82	57	113	**124**	96
Sc	45	38	40	41	36	49	29	40	42	36	**30**	41
Sr	248	232	219	262	245	239	177	248	256	251	**296**	242
V	339	324	331	322	300	344	256	321	338	349	**278**	390
Y	29	22	19	17	28	18	27	**26**	28	19	**27**	27
Zn	79	112	123	86	82	71	111	94	111	64	**85**	193
Zr	131	74	75	52	117	50	123	117	121	90	**161**	122
Rb	13	13	8	3	4	2,5	2	4	3	2	**6**	28
Ga	n.m.	12	13	n.m.	14	13	n.m.	n.m.	15	n.m.	**n.m.**	n.m.
Nb	n.m.	1	--	n.m.	3	--	n.m.	n.m.	1	n.m.	**n.m.**	n.m.
Mg#	**0,54**	**0,59**	**0,58**	**0,59**	**0,53**	**0,59**	**0,57**	**0,54**	**0,51**	**0,51**	**0,51**	**0,52**

Key to the samples: **HV010-** Northern part, medium to coarse grained gabbro; **HV017-** Northern-central part, fine grained, in association with coarse massive ultramafic rock; **HV018-** Northern-central part, basal part of coarse massive ultramafic rock related to **HV017**; **VD139-** Northern end, medium to coarse grained gabbro; **FE044-** Western part, coarse grained leucogabbro forming veins in gabbro-pegmatite; **FE045-** Western part, coarse grained gabbro-pegmatite forming the lowermost section of an exposure; **FE053-** Southern-central part, dark medium grained sheet cutting gabbros; **FE059-** Western part, dark coarse grained gabbro; **FE078-** Western part, fine to medium grained cone sheet; **FE081-** North-eastern part, medium to coarse grained melanogabbro; **HV161-** Southern part, a huge lava block in gabbro.

Table 3. Representative whole rock chemical analyses of quartz-tholeiitic gabbros and lavas. A sheet composition (in bold) shows the restricted modification of liquid composition within plutonic rocks. Notice the similar chemistry between Fellsa, Hvannadalur and Vedhurardalur gabbros. Mg# = MgO/(MgO+FeO). FE- Fellsa; HV-Hvannadalur, VD-Vedhurardalur plutons.

	FE047	VD147	FE073	FE079	VD138	HV012	**sheet**	FE133	FE132 lava	FE131 lava	FE130 lava
SiO_2	48,44	48,93	47,32	50,87	51,01	47,00	**47.17**	47,67	45,90	47,53	50,26
TiO_2	3,52	3,64	3,71	2,78	2,63	4,11	**3.60**	3,33	4,08	3,35	2,81
Al_2O_3	12,31	12,45	16,52	14,43	14,71	14,80	**13.55**	13,90	14,01	12,33	14,33
FeO	15,59	15,68	12,77	12,50	11,61	14,19	**15.93**	14,68	15,11	17,91	12,18
MnO	0,24	0,25	0,20	0,22	0,19	0,26	**0.29**	0,24	0,30	0,31	0,19
CaO	10,24	9,58	11,45	10,05	9,96	10,40	**9.72**	10,39	10,07	8,12	10,91
MgO	5,34	4,94	4,81	5,27	5,20	4,81	**5.02**	6,03	4,02	5,45	5,36
Na_2O	3,18	3,24	2,68	2,97	3,24	3,09	**3.56**	2,67	4,54	3,62	2,94
K_2O	0,62	0,75	0,27	0,48	1,00	0,72	**0.52**	0,59	0,07	0,70	0,53
P_2O_5	0,37	0,39	0,17	0,30	0,31	0,48	**0.49**	0,36	1,78	0,52	0,34
Total	99,85	99,85	99,90	99,87	99,86	99,86	**99.85**	99,86	99,88	99,84	99,85
Ba	119	154	67	119	257	114	**158**	100	67	257	134
Co	69	76	57	56	53	67	**82**	73	64	78	71
Cr	9	14	19	32	89	42	**29**	40	6	12	63
Cu	115	172	76	84	113	39	**81**	120	34	59	109
Ni	26	32	26	31	39	46	**38**	45	20	24	57
Sc	45	39	39	40	38	38	**41**	38	35	30	36
Sr	231	242	268	258	256	285	**234**	253	303	343	320
V	554	484	390	325	341	454	**448**	456	291	362	360
Y	45	45	21	37	35	32	**49**	37	66	45	33
Zn	130	168	101	119	149	149	**125**	131	163	149	113
Zr	198	221	90	176	162	161	**250**	160	280	217	170
Rb	8,3	18	4,1	8,7	18	2	**10**	3	2	8	6
Ga	14	n.m.	n.m.	16	n.m.	14	**n.m.**	n.m.	n.m.	n.m.	n.m.
Nb	6	n.m.	n.m.	5	n.m.	6	**n.m.**	n.m.	n.m.	n.m.	n.m.
Mg#	**0,38**	**0,36**	**0,40**	**0,43**	**0,31**	**0,38**	**0,36**	**0,42**	**0,32**	**0,35**	**0,44**

Key to the samples: **FE047-** Western part, fine to medium grained leucogabbro; **VD147-** Central part, by lake, medium grained melanogabbro; **FE073-** North-western part, massive big-spotted gabbro forming upper section; **FE079-** Northern Ridge, separate body, even-grained leucogabbro; **VD138-** Northern end, dike-possibly a feeder of the separate medium grained gabbro body; **HV012-** Northern part, coarse grained melanogabbro; **FE133-** Northern part, coarse to medium grained gabbro-dike; **FE132, FE131, FE130-** three lava flows from the bank of Fellsa river.

Table 4. Representative whole rock chemical analyses of hybrid rocks. The representative dike composition (in bold) is shown for reference. Mg# = MgO/(MgO+FeO). FE- Fellsa; HV- Hvannadalur, plutons.

	FE046	FE048	FE068	HV001	HV029	HV036	HV033	HV039	HV179	HV035	**dike**
SiO_2	49,98	55,20	60,00	65,05	63,90	70,91	54,53	64,18	63,17	58,01	**58.57**
TiO_2	1,94	2,11	1,96	1,20	1,34	0,66	1,57	1,19	1,30	1,70	**1.77**
Al_2O_3	19,54	14,25	13,78	14,55	14,14	12,84	14,57	14,62	14,01	13,98	**13.66**
FeO	9,07	12,71	9,44	5,88	7,23	4,33	8,85	7,34	7,31	10,91	**11.63**
MnO	0,15	0,28	0,20	0,13	0,15	0,16	0,19	0,15	0,13	0,24	**0.24**
CaO	12,31	6,97	6,03	4,39	4,28	2,10	9,44	4,75	4,33	5,69	**7.09**
MgO	3,40	2,51	2,39	1,51	1,53	0,53	6,71	1,37	2,22	1,92	**2.24**
Na_2O	2,82	3,77	2,39	4,09	5,12	5,42	3,10	4,02	5,09	5,19	**2.85**
K_2O	0,41	0,92	2,95	2,74	1,74	2,70	0,69	1,78	1,96	1,51	**0.97**
P_2O_5	0,26	1,15	0,66	0,35	0,38	0,14	0,17	0,40	0,31	0,67	**0.86**
Total	99,88	99,87	99,80	99,89	99,81	99,79	99,82	99,80	99,83	99,82	**99.88**
Ba	80	209	800	428	409	500	124	347	488	388	**206**
Co	38	43	26	17	14	4	49	18	28	17	**32**
Cr	27	8	18	14	28	30	305	12	24	14	**12**
Cu	97	20	30	22	33	12	118	6	32	11	**14**
Ni	28	11	11	4	38	28	138	9	35	29	**4**
Sc	26	22	21	12	13	12	30	15	17	23	**26**
Sr	294	269	242	196	211	150	205	229	199	291	**185**
V	269	137	179	78	194	164	242	44	157	144	**66**
Y	28	72	75	54	70	102	42	81	73	91	**98**
Zn	82	154	130	85	67	133	103	91	84	93	**151**
Zr	124	334	462	301	739	874	314	1208	500	647	**494**
Rb	6	14,9	57,8	53	30	60	9	30	34	24,5	**17**
Ga	15	16	n.m.	n.m.	20	20	n.m.	21	18	17	n.m.
Nb	3	17	n.m.	n.m.	33	55	n.m.	14	31	27	n.m.
Mg#	**0,40**	**0,26**	**0,31**	**0,31**	**0,27**	**0,18**	**0,57**	**0,25**	**0,35**	**0,24**	**0,25**

Key to the samples: **FE046-** Western part - coarse grained leucogabbro; **FE048-** Western part, medium to coarse grained spotted gabbro with some pegmatoidal pockets; **FE068-** North-western part, greenish-grey medium grained vertical dike; **HV001-** Northern end, medium grained hybrid rock; **HV029-** Central part, grey rock associated with melanogabbros; **HV036-** Southern part, bed of canyon, dark acid hybrid rock; **HV033-** Central part, dark fine to medium grained rock closely related to the ultramafic rocks; **HV039-** Southern part, fine grained melanocratic rock penetrating gabbros; **HV179-** Central part, dark-gray rock related to the ultramafic and granitic association; **HV035-** Central part, medium grained grey rock.

Table 5. Representative whole rock chemical analyses of granitic rocks (granophyres). The representative dike composition (in bold) is shown for reference. Mg# MgO/(MgO+FeO). FE- Fellsa; HV- Hvannadalur, VD-Vedhurardalur plutons.

	HV013	HV041	HV159	HV165	VD144	FE043	FE067	FE084	FE080	**dike**
SiO_2	67,90	80,40	71,57	74,26	70,23	71,16	74,51	69,94	71.38	**73.18**
TiO_2	0,78	0,42	0,64	0,34	0,77	0,58	0,42	0,60	0.59	**0.40**
Al_2O_3	14,32	13,65	12,74	12,80	13,40	13,25	12,95	13,75	12.96	**13.10**
FeO	5,65	1,04	4,26	3,76	5,05	5,21	2,02	5,34	4.63	**4.78**
MnO	0,10	0,01	0,15	0,14	0,04	0,16	0,05	0,09	0.14	**0.05**
CaO	2,93	0,82	2,03	1,44	2,49	2,70	3,31	2,81	2.31	**1.84**
MgO	0,54	0,17	0,50	0,10	0,55	0,27	0,45	0,58	0.27	**0.31**
Na_2O	5,17	0,07	5,13	4,44	4,02	4,28	4,28	4,02	4.88	**3.78**
K_2O	2,28	3,23	2,69	2,52	3,09	2,13	1,77	2,57	2.45	**2.32**
P_2O_5	0,16	0,04	0,12	0,04	0,15	0,09	0,07	0,14	0.12	**0.09**
Total	99,83	99,85	99,83	99,84	99,79	99,83	99,83	99,84	99.89	**99.89**
Ba	518	332	489	561	902	432	452	472	477	**473**
Co	6	1	4	3	8	0	5	13	8	--
Cr	9	7	10	15	15	16	20	10	18	**7**
Cu	7	1	5	7	40	18	65	13	17	**4**
Ni	13	10	6	7	29	15	0	10	31	**2**
Sc	12	5	9	4	8	12	7	12	11	**7**
Sr	198	54	137	125	230	159	167	132	146	**106**
V	61	19	7	37	122	155	28	31	123	--
Y	77	129	111	109	98	101	93	95	100	**102**
Zn	66	26	113	**138**	59	157	35	72	119	**38**
Zr	663	785	716	665	760	695	670	680	569	**797**
Rb	46	45	50	64	55	48,6	28	46	50	**36**
Ga	23	33	22	24	n.m.	21	17	n.m.	46	**n.m.**
Nb	39	85	54	74	n.m.	52	53	n.m.	18	**n.m.**
Mg#	**0,15**	**0,23**	**0,17**	**0.05**	**0,16**	**0,08**	**0,28**	**0,16**	**0,12**	**0,10**

Key to the samples: **HV013-** Northern-central part, medium grained granitic rock; **HV041-** South-eastern part, medium grained light-coloured granitic rock; **HV159-** South-western part, grey granitic rock; **HV165-** fresh medium grained granite; **VD144-** Central part, microgranite penetrating gabbros; **FE043-** South-western part, medium grained, grey granite with some layering features; **FE067-** North-western part, fine grained, grey granite; **FE084-** Eastern part, fine grained granite forming veins; **FE080-** Eastern part, medium grained granitic rock.

Table 6. Representative whole rock chemical analyses of fine grained basaltic envelope´ rock. Mg# = MgO/(MgO+FeO). FE- Fellsa; HV- Hvannadalur, VD- Vedhurardalur plutons. HV162 -- gabbroic sample, shown as reference.

	HV153	HV154	HV155	HV156	HV157	HV162	VD148	VD149	VD150	FE085
SiO_2	49,16	50,12	48,87	50,19	49,22	49,73	53,83	50,93	54,16	49,79
TiO_2	3,02	2,96	2,96	2,95	2,89	2,77	2,95	3,63	2,66	2,91
Al_2O_3	13,47	13,91	13,10	13,40	13,56	13,97	13,63	13,04	12,79	13,64
FeO	13,91	13,32	14,28	13,34	13,74	12,75	12,43	14,32	13,05	13,58
MnO	0,22	0,23	0,24	0,23	0,23	0,21	0,25	0,25	0,28	0,24
CaO	10,24	10,19	10,28	10,06	10,42	11,02	7,40	8,29	7,09	10,70
MgO	5,93	5,43	5,94	5,79	5,75	6,01	3,20	4,32	3,27	5,41
Na_2O	2,93	2,68	3,27	2,97	3,08	2,68	4,31	3,46	4,10	3,00
K_2O	0,63	0,67	0,62	0,63	0,66	0,45	0,92	0,99	1,25	0,23
P_2O_5	0,34	0,36	0,31	0,30	0,32	0,27	0,95	0,62	1,19	0,36
Total	99,85	99,87	99,87	99,86	99,87	99,86	99,87	99,85	99,84	99,86
Ba	124	113	121	120	117	77	221	200	288	60
Co	66	63	70	56	64	55	37	68	42	53
Cr	59	69	61	56	55	30	10	24	11	25
Cu	162	153	141	147	133	154	31	62	24	105
Ni	42	39	34	38	36	43	9	33	6	37
Sc	41	46	41	45	38	41	25	33	26	41
Sr	206	234	233	225	209	200	252	247	281	207
V	334	338	326	325	325	371	211	348	188	394
Y	39	42	40	41	38	38	76	53	88	41
Zn	130	146	138	122	126	108	154	130	159	128
Zr	178	189	172	187	166	176	384	285	426	184
Rb	14	15	13	13	13	15	26	23	26	4
Ga	n.m.	n.m.	13	n.m.	n.m.	n.m.	n.m.	n.m.	n.m.	n.m.
Nb	n.m.	n.m.	7	n.m.	n.m.	n.m.	n.m.	n.m.	n.m.	n.m.
Mg#	**0,43**	**0,42**	**0,43**	**0,44**	**0,43**	**0,46**	**0,31**	**0,35**	**0,31**	**0,42**

Key to the samples: **HV153, HV154, HV155, HV156, HV157-** South-western part, profile across basaltic envelope from granophyric rocks by step of 5cm; **HV162-** South-western part, light-coloured gabbroic rock, very closely related to basaltic envelope, *presented for comparison* ; **VD148, VD149, VD150-** Central part, section across the envelope by the lake, samples taken in 5cm, 90cm and 150cm from a granophyric body, respectively; **FE085-** Southern-central part, homogenous rock.

Appendix 2

Chemical analyses of the Thverartindur minerals.

Table 7. Representative olivine analyses from Fellsa (FE) and Hvannadalur (HV) ultramafic dikes and sills. Cations on the basis of 4 oxygens.

Sample	**HV101**	**FE065**	**FE065**	**FE063**	**FE063**	**HV028**	**HV028**
	Core	Core	Core	Rim	Core	Rim	Core
SiO_2	39,35	36,02	36,93	38,09	38,90	41,04	41,10
FeO	13,26	26,73	27,68	24,46	24,43	11,70	9,75
MnO	0,14	0,37	0,37	0,25	0,17	0,14	0,11
MgO	46,45	36,63	34,27	36,33	36,49	48,08	49,25
CaO	0,14	0,00	0,65	0,00	0,00	0,00	0,00
NiO	0,28	0,12	0,09	0,17	0,20	0,37	0,38
Total	99,62	99,87	99,99	99,30	100,19	101,33	100,59
Si	0,987	0,965	0,991	1,009	1,018	1,002	1,002
Fe^{2+}	0,278	0,598	0,620	0,541	0,534	0,238	0,198
Mn	0,003	0,008	0,008	0,006	0,004	0,003	0,002
Mg	1,736	1,462	1,370	1,433	1,422	1,748	1,788
Ca	0,004	0,000	0,019	0,000	0,000	0,000	0,000
Ni	0,006	0,003	0,002	0,004	0,004	0,007	0,007
Sum	3,013	3,035	3,009	2,991	2,982	2,998	2,998
Fo #	**86,21**	**70,97**	**68,84**	**72,60**	**72,72**	**88,00**	**90,01**

Table 8. Representative plagioclase analyses from Fellsa (FE) and Hvannadalur (HV) ultramafic rocks. C-core, R-rim analyzed. Letters denote grains; X-analyzed core only. Cations on the basis of 8 oxygens.

Sample	FE065	FE065	FE065	FE065	FE065	FE065	FE065	FE065	FE065	FE063	HV028
spot	C	Incl	C	R	C	R	R	C	C	C	C
grain	C	A	B	B	D	D	D	D	X	A	X
SiO_2	48,90	52,25	52,41	51,91	49,43	50,72	52,99	48,30	50,55	50,36	50,57
Al_2O_3	31,96	31,37	28,89	29,56	31,28	31,46	30,67	32,14	31,66	29,26	29,21
FeO	0,72	0,69	0,72	0,30	0,62	0,71	0,64	0,66	0,51	0,36	0,29
CaO	13,52	11,74	11,04	10,64	12,61	13,38	12,21	13,16	13,35	14,17	13,01
Na_2O	4,31	5,39	5,52	5,55	4,73	4,10	5,14	4,33	4,55	3,62	4,69
K_2O	0,05	0,13	0,13	0,27	0,15	0	0,03	0,06	0,03	0,50	0,02
Total	99,46	101,57	98,71	98,23	98,82	100,37	101,70	98,65	100,60	98,27	97,79
Si	2,250	2,339	2,410	2,393	2,284	2,302	2,367	2,239	2,291	2,342	2,355
Al	1,742	1,664	1,573	1,614	1,712	1,692	1,623	1,765	1,700	1,612	1,612
Fe^{2+}	0,028	0,026	0,028	0,012	0,024	0,027	0,024	0,026	0,019	0,014	0,011
Ca	0,666	0,563	0,544	0,525	0,624	0,650	0,584	0,653	0,648	0,706	0,649
Na	0,384	0,468	0,492	0,496	0,423	0,361	0,445	0,389	0,400	0,326	0,423
K	0,003	0,007	0,008	0,016	0,009	0,000	0,002	0,004	0,002	0,030	0,001
Sum	5,073	5,067	5,053	5,056	5,076	5,032	5,045	5,075	5,060	5,030	5,051
An	**63**	**55**	**53**	**51**	**60**	**64**	**57**	**63**	**62**	**68**	**61**

Table 9. Representative plagioclase analyses from Fellsa (FE) and Hvannadalur (HV) olivine-tholeiitic gabbros. Cations on the basis of 8 oxygens.

Sample	FE045	FE045	FE045	FE045	FE045	FE045	FE045	FE045	FE045	FE045	FE045
spot	R	R	C	R	C	C	C	C	R	R	C
grain	B18	B19	B20	B22	B23	C26	C27	C28	D32	E37	E38
SiO_2	52,61	53,31	54,49	52,94	54,76	52,02	54,09	54,96	55,37	54,80	53,09
Al_2O_3	29,77	30,22	29,88	30,71	29,13	30,81	29,25	27,34	28,65	28,73	29,79
FeO	0,74	0,73	0,69	0,69	0,68	0,67	0,65	0,49	0,94	0,70	0,81
CaO	12,41	12,45	11,79	13,35	11,50	12,78	11,91	11,24	11,53	12,60	12,63
Na_2O	4,34	4,43	4,95	4,26	5,09	4,22	4,94	5,09	5,26	4,69	4,46
K_2O	0,17	0,11	0,16	0,17	0,22	0,17	0,17	0,20	0,25	0,22	0,17
Total	100,04	101,25	101,96	102,12	101,38	100,67	101,01	99,32	102,00	101,74	100,95
Si	2,387	2,388	2,419	2,359	2,444	2,348	2,426	2,498	2,460	2,444	2,389
Al	1,600	1,603	1,572	1,621	1,540	1,647	1,554	1,472	1,508	1,518	1,588
Fe^{2+}	0,028	0,027	0,026	0,026	0,025	0,025	0,024	0,019	0,035	0,026	0,030
Ca	0,603	0,597	0,561	0,637	0,550	0,618	0,572	0,547	0,549	0,602	0,609
Na	0,382	0,384	0,426	0,368	0,440	0,369	0,429	0,448	0,453	0,405	0,389
K	0,010	0,006	0,009	0,010	0,013	0,010	0,010	0,012	0,014	0,013	0,010
Sum	5,009	5,006	5,012	5,020	5,012	5,018	5,016	4,996	5,019	5,007	5,016
An	**61**	**61**	**57**	**63**	**56**	**63**	**57**	**55**	**55**	**60**	**61**

Table 9. (Continued)

Sample	FE045	FE045	FE045	FE045	FE045	FE045	FE045	FE045	FE081	FE081	FE081
spot	C	C	R	C	C	C	C	C	C	C	R
grain	E40	E41	F45	F46	X	X	X	X	H63	H64	H65
SiO_2	52,94	53,54	53,24	52,77	53,19	52,63	52,24	53,05	51,87	50,35	50,95
Al_2O_3	30,51	27,06	28,03	27,21	28,78	29,31	27,95	29,00	30,94	30,23	28,93
FeO	0,52	0,59	0,62	0,60	0,65	0,75	0,65	0,81	0,58	0,54	0,57
CaO	13,00	12,19	13,03	12,61	11,54	12,80	12,32	13,22	14,74	14,76	14,16
Na_2O	4,37	4,87	4,81	4,49	5,49	4,23	4,84	4,12	3,57	3,31	3,56
K_2O	0,14	0,17	0,24	0,12	0,28	0,14	0,42	0,16	0,15	0,17	0,09
Total	101,48	98,42	99,97	97,80	99,93	99,86	98,42	100,36	101,80	99,36	98,26
Si	2,369	2,468	2,426	2,450	2,419	2,394	2,418	2,404	2,324	2,315	2,364
Al	1,617	1,478	1,513	1,496	1,550	1,579	1,533	1,557	1,642	1,647	1,590
Fe^{2+}	0,019	0,023	0,024	0,023	0,025	0,028	0,025	0,031	0,022	0,021	0,022
Ca	0,623	0,602	0,636	0,627	0,562	0,624	0,611	0,642	0,707	0,727	0,703
Na	0,379	0,435	0,425	0,404	0,484	0,373	0,434	0,362	0,310	0,295	0,320
K	0,008	0,010	0,014	0,007	0,016	0,008	0,025	0,009	0,009	0,010	0,005
Sum	5,016	5,015	5,037	5,007	5,056	5,007	5,045	5,003	5,014	5,014	5,004
An	**62**	**58**	**60**	**61**	**54**	**63**	**58**	**64**	**70**	**71**	**69**

Table 9. (Continued)

Sample	FE081	FE081	FE081	FE081	FE081	FE081	FE081	FE081	FE081	FE081	FE081
spot	C	R	R	C	C	C	C	R	R	R	C
grain	I68	I69	J77	J79	J82	J83	J84	K85	K88	K89	K90
SiO_2	55,34	54,40	55,11	52,34	50,67	54,80	53,65	55,46	53,08	53,34	50,06
Al_2O_3	29,24	28,19	27,37	27,47	29,20	25,46	28,92	26,70	30,86	31,04	31,90
FeO	0,53	0,49	0,53	0,62	0,84	0,67	0,70	0,60	0,66	0,62	0,51
CaO	11,71	12,20	10,75	13,41	14,67	11,55	11,83	11,35	11,92	12,71	15,39
Na_2O	5,25	5,03	5,36	4,05	3,16	5,04	5,15	5,36	5,21	4,60	3,00
K_2O	0,29	0,29	0,16	0,14	0,05	0,26	0,18	0,15	0,29	0,16	0,08
Total	102,36	100,60	99,28	98,03	98,59	97,78	100,40	99,62	102,00	102,40	100,90
Si	2,447	2,453	2,504	2,429	2,347	2,537	2,424	2,516	2,365	2,364	2,267
Al	1,532	1,506	1,473	1,510	1,602	1,396	1,548	1,435	1,629	1,629	1,711
Fe^{2+}	0,020	0,018	0,020	0,024	0,032	0,026	0,026	0,023	0,025	0,023	0,019
Ca	0,555	0,589	0,523	0,666	0,728	0,573	0,572	0,552	0,569	0,603	0,746
Na	0,450	0,439	0,472	0,364	0,284	0,452	0,451	0,471	0,450	0,395	0,263
K	0,016	0,017	0,009	0,008	0,003	0,015	0,010	0,009	0,016	0,009	0,005
Sum	5,020	5,022	5,001	5,002	4,995	4,999	5,032	5,006	5,054	5,023	5,012
An	**55**	**57**	**53**	**65**	**72**	**56**	**56**	**54**	**56**	**60**	**74**

Table 9. (Continued)

Sample	FE081	FE081	FE044	FE044	FE044	FE044	FE044	FE044
spot	C	C	C	R	C	C	C	C
grain	H	K	C	D	D	X	X	X
SiO_2	51,55	52,41	50.11	52.73	48.83	53.75	55.74	50.96
Al_2O_3	28,43	28,63	31.73	29.23	32.98	30.04	27.94	30.32
FeO	0,57	0,57	0.63	0.68	0.56	0.63	0.60	0.75
CaO	14,23	12,50	13.55	11.56	15.01	12.03	9.65	14.36
Na_2O	3,61	4,37	2.81	4.16	2.21	4.10	5.49	3.10
K_2O	0,11	0,23	0.11	0.15	0.09	0.17	0.23	0.06
Total	98,50	98,71	98.94	98.51	99.68	100.70	99.65	99.55
Si	2,385	2,411	2.298	2.418	2.232	2.411	2.513	2.332
Al	1,558	1,560	1.724	1.588	1.786	1.596	1.492	1.643
Fe^{2+}	0,022	0,022	0.024	0.026	0.021	0.024	0.023	0.029
Ca	0,705	0,616	0.666	0.568	0.735	0.578	0.466	0.704
Na	0,324	0,389	0.250	0.370	0.196	0.356	0.480	0.275
K	0,006	0,013	0.006	0.009	0.005	0.010	0.013	0.004
Sum	5,001	5,011	4.968	4.978	4.975	4.974	4.987	4.986
An	**69**	**61**	**72**	**60**	**78**	**62**	**49**	**72**

Table 10. Representative plagioclase analyses from Fellsa (FE) and Hvannadalur (HV) quartz-tholeiitic gabbros and xenolith (FE050). C-core, R-rim analyzed. Letters denote grains; X-analyzed core only. Cations on the basis of 8 oxygens.

Sample	FE047	FE047	FE047	FE047	FE047	FE047	FE047	FE047	FE047	FE079	FE079
spot	R	C	C	C	C	R	R	C	C	C	R
grain	D	D	E30	E32	E34	E35	F	F	F	A	A
SiO_2	54,79	55,95	63,01	67,15	57,86	57,41	57,34	54,49	56,82	53,06	53,68
Al_2O_3	27,37	25,79	22,60	20,01	24,01	25,80	27,58	25,60	26,75	28,59	28,84
FeO	0,72	0,69	0,24	0,10	0,68	0,59	0,15	0,67	0,53	0,53	0,57
CaO	11,28	11,64	4,31	2,64	9,72	10,29	11,10	11,75	10,71	10,32	10,04
Na_2O	5,51	5,93	6,40	11,70	6,11	6,56	6,52	5,74	6,17	4,75	5,11
K_2O	0,20	0,16	5,50	0,09	0,23	0,18	0,04	0,17	0,17	0,14	0,33
Total	99,87	100,16	102,06	101,69	98,61	100,83	102,73	98,42	101,15	97,39	98,57
Si	2,485	2,534	2,790	2,917	2,639	2,571	2,520	2,516	2,537	2,452	2,454
Al	1,471	1,384	1,185	1,030	1,297	1,369	1,436	1,400	1,415	1,565	1,562
Fe^{2+}	0,027	0,026	0,009	0,004	0,026	0,022	0,006	0,026	0,020	0,020	0,022
Ca	0,548	0,565	0,204	0,123	0,475	0,493	0,522	0,581	0,512	0,511	0,492
Na	0,484	0,520	0,549	0,985	0,540	0,569	0,555	0,514	0,534	0,425	0,453
K	0,012	0,009	0,310	0,005	0,013	0,010	0,002	0,010	0,010	0,008	0,019
Sum	5,027	5,039	5,048	5,063	4,990	5,035	5,041	5,046	5,027	4,982	5,001
An	**53**	**52**	**27**	**11**	**47**	**46**	**48**	**53**	**49**	**55**	**52**

Table 10. (continued)

Sample	FE079	FE079	FE079	FE079	FE079	FE079	FE079	FE079	FE079	FE079	FE079
spot	R	C	C	R	R	C	R	C	C	C	R
grain	B	B	D	D	D	D	E	E	E	F	F
SiO_2	53,25	54,69	55,03	61,89	57,86	55,23	53,46	53,04	56,04	53,80	54,47
Al_2O_3	29,21	28,28	29,41	24,16	28,64	27,98	27,78	29,66	27,94	27,94	27,22
FeO	0,69	0,54	0,72	0,41	0,62	0,71	0,71	0,71	0,44	0,52	0,57
CaO	11,52	10,07	11,51	5,06	8,66	10,40	11,41	11,17	9,00	10,44	9,85
Na_2O	4,33	5,21	4,36	7,76	5,56	4,84	4,57	4,56	5,78	5,07	5,65
K_2O	0	0,07	0,20	0,58	0,18	0,11	0,27	0,33	0,32	1,09	0,30
Total	99,00	98,86	101,23	99,86	101,52	99,27	98,20	99,47	99,52	98,86	98,06
Si	2,427	2,486	2,451	2,745	2,545	2,501	2,462	2,411	2,525	2,467	2,504
Al	1,577	1,523	1,552	1,269	1,492	1,501	1,516	1,597	1,491	1,518	1,483
Fe^{2+}	0,026	0,020	0,027	0,015	0,023	0,027	0,027	0,027	0,017	0,020	0,022
Ca	0,562	0,490	0,549	0,240	0,408	0,504	0,563	0,544	0,434	0,513	0,485
Na	0,382	0,459	0,376	0,667	0,474	0,425	0,408	0,402	0,505	0,450	0,503
K	0,000	0,004	0,011	0,033	0,010	0,006	0,016	0,019	0,018	0,064	0,018
Sum	4,975	4,983	4,967	4,970	4,951	4,964	4,992	5,000	4,991	5,031	5,015
An	**60**	**52**	**59**	**26**	**46**	**54**	**58**	**58**	**46**	**53**	**49**

Table 10. (continued)

Sample	FE079	FE079	FE079	FE079	FE079	HV012	HV012	HV012	HV012	HV012	HV012
spot	C	R	C	C	C	R	C	C	R	C	C
grain	H	I	X	X	X	A	A	B	C	C	D
SiO_2	50,52	61,80	51,50	57,30	52,17	57,98	55,20	55,56	55,74	54,13	54,08
Al_2O_3	29,87	22,74	29,19	27,44	28,57	21,63	25,88	26,01	25,50	27,94	28,43
FeO	0,67	0,36	0,84	0,54	0,73	2,56	0,45	0,52	1,16	0,65	0,66
CaO	12,91	3,79	11,34	9,01	11,80	8,74	9,89	9,51	9,06	11,77	11,68
Na_2O	4,17	8,58	5,31	5,83	4,93	5,95	5,54	6,11	6,11	5,02	4,80
K_2O	0,11	0,73	0,09	0,03	0,06	0,55	0,42	0,52	0,55	0,28	0,29
Total	98,25	98,00	98,27	100,15	98,26	97,41	97,38	98,23	98,12	99,79	99,94
Si	2,341	2,791	2,383	2,559	2,410	2,697	2,553	2,551	2,567	2,459	2,450
Al	1,640	1,217	1,600	1,452	1,564	1,192	1,418	1,415	1,391	1,504	1,526
Fe^{2+}	0,026	0,014	0,032	0,020	0,028	0,099	0,017	0,020	0,045	0,025	0,025
Ca	0,641	0,183	0,562	0,431	0,584	0,435	0,490	0,468	0,447	0,573	0,567
Na	0,374	0,751	0,476	0,505	0,441	0,536	0,496	0,544	0,545	0,442	0,421
K	0,007	0,042	0,005	0,002	0,004	0,033	0,025	0,030	0,032	0,016	0,017
Sum	5,029	4,997	5,058	4,968	5,031	4,992	4,999	5,028	5,027	5,018	5,006
An	**63**	**20**	**54**	**46**	**57**	**45**	**50**	**46**	**45**	**56**	**57**

Table 10. (continued; xenolith sample)

Sample	FE050	FE050	FE050	FE050	FE050	FE050	FE050	FE050	FE050	FE050	FE050
spot	C	R	C	C	C	C	R	C	R	C	C
grain	A	A	B	D	E	E	K	K	L	L	X
SiO_2	55,07	56,42	55,76	56,32	53,22	57,09	55,46	54,89	56,10	56,56	58,05
Al_2O_3	26,58	26,36	26,50	26,16	27,87	27,58	26,50	29,14	26,73	28,42	26,47
FeO	0,64	0,37	0,67	0,72	0,64	0,64	0,56	0,74	0,75	0,60	0,64
CaO	11,02	9,65	10,09	11,18	12,32	11,23	10,84	12,06	10,04	10,82	9,97
Na_2O	4,89	5,49	5,42	4,76	4,44	4,87	4,95	4,65	5,35	5,17	5,59
K_2O	0,03	0,02	0,03	0,01	0	0,05	0	0,03	0,04	0,03	0,08
Total	98,23	98,31	98,47	99,15	98,49	101,40	98,31	101,50	99,01	101,60	100,80
Si	2,525	2,570	2,545	2,555	2,447	2,530	2,537	2,445	2,546	2,504	2,583
Al	1,444	1,422	1,433	1,406	1,518	1,448	1,436	1,537	1,437	1,490	1,395
Fe^{2+}	0,025	0,014	0,026	0,027	0,025	0,024	0,021	0,028	0,028	0,022	0,024
Ca	0,541	0,471	0,493	0,543	0,607	0,533	0,531	0,575	0,488	0,513	0,475
Na	0,434	0,485	0,479	0,419	0,396	0,418	0,439	0,401	0,470	0,443	0,482
K	0,002	0,001	0,002	0,001	0,000	0,003	0,000	0,002	0,002	0,002	0,005
Sum	4,971	4,962	4,979	4,951	4,992	4,956	4,964	4,988	4,972	4,974	4,963
An	**55**	**49**	**51**	**56**	**61**	**56**	**55**	**59**	**51**	**54**	**50**

Table 11. Representative plagioclase analyses from Fellsa (FE) and Hvannadalur (HV) hybrid rock types. C-core, R-rim analyzed. Letters denote grains; X-analyzed core only. Cations on the basis of 8 oxygens.

Sample	HV035	HV035	HV035	HV035	HV035	HV035	FE046	FE046	FE046	FE046	FE046
spot	C	C	R	C	C	C	C	R	R	C	C
grain	A	B	B	X	X	X	A	A	B	B	C
SiO_2	61,66	61,74	66,97	62,34	62,86	62,33	54,49	51,23	56,25	52,98	54,40
Al_2O_3	25,38	26,23	19,84	24,19	24,94	23,85	28,94	31,67	25,84	28,54	27,96
FeO	0,26	0,40	0,26	0,24	0,26	0,26	0,77	0,94	0,56	0,72	0,81
CaO	7,07	7,16	2,34	5,40	5,54	5,46	13,29	13,86	9,52	13,36	12,11
Na_2O	7,05	7,34	9,04	8,11	7,87	7,99	4,60	3,90	6,82	4,37	4,95
K_2O	0,09	0,09	0,26	0,14	0,19	0,20	0,14	0,18	0,24	0,09	0,16
Total	101,51	102,96	98,71	100,42	101,66	100,09	102,23	101,78	99,23	100,06	100,39
Si	2,694	2,666	2,963	2,746	2,734	2,755	2,424	2,299	2,559	2,410	2,458
Al	1,314	1,342	1,039	1,262	1,285	1,249	1,525	1,684	1,393	1,538	1,497
Fe^{2+}	0,009	0,014	0,010	0,009	0,009	0,010	0,029	0,035	0,021	0,027	0,031
Ca	0,331	0,331	0,111	0,255	0,258	0,258	0,633	0,666	0,464	0,651	0,586
Na	0,597	0,614	0,775	0,692	0,663	0,684	0,397	0,339	0,601	0,385	0,433
K	0,005	0,005	0,015	0,008	0,011	0,011	0,008	0,010	0,014	0,005	0,009
Sum	4,950	4,973	4,912	4,973	4,960	4,968	5,016	5,034	5,052	5,016	5,015
An	**36**	**35**	**13**	**27**	**28**	**27**	**61**	**66**	**44**	**63**	**57**

Table 11. (continued)

Sample	FE046	FE046	FE046	FE046	FE046	FE048	FE048	FE048	FE048	FE048	FE048
spot	C	R	R	R	C	C	R	R	R	C	R
grain	A	A	B	D	D	J	J	K	K	L	M
SiO_2	46,98	48,02	51,92	56,67	55,00	56,28	59,10	61,33	56,24	61,33	56,67
Al_2O_3	34,43	34,05	29,42	25,64	25,88	26,85	27,31	25,22	28,11	23,96	27,13
FeO	0,63	0,64	0,69	0,78	0,54	0,29	0,52	0,25	0,72	0,36	0,35
CaO	16,95	16,66	14,59	10,84	11,19	8,48	8,81	4,08	8,83	5,66	9,46
Na_2O	2,09	1,89	3,96	5,45	5,69	6,03	6,08	8,05	5,72	7,60	5,96
K_2O	0,05	0,04	0,11	0,23	0,19	0,29	0,06	1,67	0,63	1,18	0,11
Total	101,13	101,30	100,69	99,61	98,49	98,22	101,88	100,60	100,25	100,09	99,68
Si	2,137	2,173	2,357	2,567	2,528	2,564	2,590	2,712	2,522	2,730	2,550
Al	1,855	1,825	1,582	1,376	1,409	1,449	1,418	1,321	1,493	1,263	1,446
Fe^{2+}	0,024	0,024	0,026	0,030	0,021	0,011	0,019	0,009	0,027	0,013	0,013
Ca	0,826	0,807	0,709	0,526	0,551	0,414	0,414	0,193	0,424	0,270	0,456
Na	0,184	0,166	0,348	0,478	0,507	0,532	0,516	0,690	0,497	0,656	0,520
K	0,003	0,002	0,006	0,013	0,011	0,017	0,003	0,094	0,036	0,067	0,006
Sum	5,029	4,998	5,029	4,991	5,026	4,986	4,961	5,019	4,998	4,999	4,990
An	**82**	**83**	**67**	**52**	**52**	**44**	**44**	**22**	**46**	**29**	**47**

Table 11. (continued)

Sample	FE048	FE048	FE048	FE048	FE048	FE048	FE048	FE048	FE048	FE048	FE048
spot	C	C	C	C	R	C	R	R	C	C	C
grain	M	N	O	R	R	S	S	T	T	X	X
SiO_2	55,87	57,72	60,64	56,88	57,80	60,51	61,72	61,39	58,04	57,47	57,28
Al_2O_3	26,66	27,37	25,30	27,93	25,61	24,13	24,19	24,59	27,87	27,20	27,00
FeO	0,34	0,36	0,34	0,48	0,37	0,26	0,20	0,27	0,43	0,34	0,38
CaO	8,77	9,82	6,08	9,30	6,82	5,41	4,18	5,17	8,28	8,48	8,50
Na_2O	6,29	5,91	7,85	6,09	7,65	7,87	7,92	7,84	6,26	6,44	6,32
K_2O	0,28	0	0	0	0	0,26	0,37	0,27	0,24	0,06	0,74
Total	98,21	101,18	100,21	100,68	98,25	98,44	98,58	99,53	101,12	99,99	100,22
Si	2,553	2,557	2,686	2,533	2,625	2,724	2,759	2,728	2,565	2,570	2,566
Al	1,443	1,436	1,327	1,473	1,378	1,287	1,281	1,295	1,459	1,441	1,433
Fe^{2+}	0,013	0,013	0,013	0,018	0,014	0,010	0,007	0,010	0,016	0,013	0,014
Ca	0,429	0,466	0,288	0,444	0,332	0,261	0,200	0,246	0,392	0,406	0,408
Na	0,557	0,507	0,674	0,525	0,673	0,687	0,686	0,675	0,536	0,558	0,549
K	0,016	0,000	0,000	0,000	0,000	0,015	0,021	0,015	0,014	0,003	0,042
Sum	5,012	4,979	4,988	4,993	5,022	4,983	4,954	4,970	4,981	4,991	5,013
An	**44**	**48**	**30**	**46**	**33**	**28**	**23**	**27**	**42**	**42**	**43**

Table 12. Representative clinopyroxene analyses from the Thverartindur ultramafic rocks. R-rim, C-core. FE and HV indicate Fellsa and Hvannadalur intrusions, respectively. Letters denote the grains analysed. X-analysed core only. Cations on the basis of six oxygens.

Sample	FE063	FE063	FE063	FE063	FE063	FE063	FE065	FE065	FE065	FE065
grain	A	A	C	C	B	B	A	A	C	G
spot	R	C	R	C	C	M	M	M	C	M
SiO_2	53,05	52,48	53,09	53,26	51,43	52,26	52,05	51,89	50,62	50,96
TiO_2	0,91	1,12	0,82	0,74	1,24	1,35	0,97	1,02	1,09	1,02
Al_2O_3	1,77	1,81	1,64	1,35	1,77	1,60	1,30	1,37	1,68	1,02
Cr_2O_3	0,19	0,24	0,36	0,27	0,15	0,09	0,03	0,09	0,34	0,01
FeO	7,44	7,74	6,36	6,99	8,38	7,92	9,66	9,83	8,43	10,63
MnO	0,24	0,17	0,13	0,17	0,15	0,22	0,28	0,21	0,17	0,28
MgO	15,58	15,68	15,97	15,77	15,48	15,34	15,94	15,64	15,78	16,09
CaO	20,53	19,68	21,16	20,68	20,69	20,78	19,73	19,52	20,85	19,32
Na_2O	0,26	0,29	0,31	0,25	0,33	0,25	0,40	0,29	0,32	0,26
Total	99,97	99,21	99,84	99,48	99,62	99,81	100,36	99,86	99,28	99,59
Si	1,956	1,950	1,955	1,970	1,920	1,940	1,934	1,937	1,903	1,919
Ti	0,025	0,031	0,023	0,021	0,035	0,038	0,027	0,029	0,031	0,029
Al	0,077	0,080	0,072	0,059	0,078	0,070	0,057	0,061	0,075	0,046
Cr	0,006	0,007	0,010	0,008	0,004	0,003	0,001	0,003	0,010	0,000
Fe2+	0,229	0,240	0,196	0,216	0,261	0,245	0,300	0,306	0,265	0,334
Mn	0,007	0,005	0,004	0,005	0,005	0,007	0,009	0,007	0,005	0,009
Mg	0,856	0,868	0,876	0,869	0,861	0,848	0,882	0,870	0,884	0,903
Ca	0,811	0,783	0,835	0,819	0,827	0,826	0,785	0,780	0,839	0,779
Na	0,019	0,021	0,022	0,018	0,024	0,018	0,029	0,021	0,023	0,019
Total	3,986	3,986	3,992	3,985	4,016	3,995	4,024	4,013	4,035	4,038
En	**45**	**46**	**46**	**46**	**44**	**44**	**45**	**44**	**44**	**45**
Fs	**12**	**13**	**10**	**11**	**13**	**13**	**15**	**16**	**13**	**17**
Wo	**43**	**41**	**44**	**43**	**42**	**43**	**40**	**40**	**42**	**39**

Table 12. (Continued)

Sample	FE065	FE065	HV028	HV028	HV028
grain	G	X	X	X	X
spot	C	C	C	C	C
SiO_2	51,30	52,52	48,73	49,73	49,84
TiO_2	1,02	1,00	1,42	1,41	0,15
Al_2O_3	1,07	1,34	2,83	2,66	0,50
Cr_2O_3	0,03	0,11	0,13	0,15	0,06
FeO	10,72	10,21	8,62	7,73	8,75
MnO	0,27	0,26	0,16	0,12	0,19
MgO	16,37	15,64	14,26	14,17	13,90
CaO	19,45	19,33	20,32	20,19	21,50
Na_2O	0,29	0,30	0,33	0,27	0,35
Total	100,52	100,71	96,80	96,43	95,24
Si	1,915	1,944	1,881	1,912	1,962
Ti	0,029	0,028	0,041	0,041	0,004
Al	0,047	0,059	0,129	0,121	0,023
Cr	0,001	0,003	0,004	0,005	0,002
Fe2+	0,334	0,316	0,278	0,248	0,288
Mn	0,009	0,008	0,005	0,004	0,006
Mg	0,910	0,862	0,820	0,812	0,815
Ca	0,778	0,766	0,840	0,831	0,907
Na	0,021	0,022	0,025	0,020	0,027
Total	4,043	4,008	4,023	3,994	4,034
En	**45**	**44**	**42**	**43**	**41**
Fs	**17**	**16**	**14**	**13**	**14**
Wo	**38**	**39**	**43**	**44**	**45**

Table 13. Representative clinopyroxene analyses from the Thverartindur olivine-tholeiitic gabbros. R-rim, C-core. FE and HV indicate Fellsa and Hvannadalur intrusions, respectively. Letters denote the grains analysed. X-analysed core only . Cations on the basis of six oxygens.

Sample	FE044	FE044	FE044	FE044	FE045	FE045	FE045	FE045	FE045	FE045
grain	D	E	E	X	A	A	A	B	C	D
spot	C	R	C	C	C	R	C	C	R	R
SiO_2	52,76	53,20	51,57	51,54	50,98	50,86	51,76	52,54	52,77	52,06
TiO_2	0,99	0,70	1,02	0,77	1,11	1,08	1,02	0,91	1,02	1,00
Al_2O_3	2,72	1,48	2,52	1,74	2,19	1,74	1,66	1,46	1,70	1,69
Cr_2O_3	0,02	0	0,01	0,06	0,01	0	0,01	0,03	0	0,01
FeO	9,03	12,27	9,43	10,63	9,17	9,80	9,58	10,27	9,61	9,88
MnO	0,21	0,37	0,21	0,32	0,20	0,28	0,22	0,27	0,19	0,23
MgO	15,61	13,80	15,28	14,61	14,27	14,90	14,50	14,89	14,70	14,34
CaO	19,28	18,13	20,01	19,23	20,92	20,91	20,15	20,33	20,15	20,02
Na_2O	0,28	0,28	0,31	0,20	0,31	0,28	0,33	0,24	0,30	0,25
Total	100,90	100,23	100,36	99,10	99,16	99,85	99,23	100,94	100,44	99,48
Si	1,933	1,984	1,913	1,944	1,920	1,911	1,945	1,945	1,954	1,951
Ti	0,027	0,020	0,028	0,022	0,031	0,030	0,029	0,025	0,028	0,028
Al	0,118	0,065	0,111	0,078	0,098	0,077	0,074	0,064	0,075	0,075
Cr	0,001	0,000	0,000	0,002	0,000	0,000	0,000	0,001	0,000	0,000
Fe2+	0,276	0,382	0,292	0,335	0,288	0,307	0,300	0,317	0,297	0,309
Mn	0,007	0,012	0,007	0,010	0,006	0,009	0,007	0,008	0,006	0,007
Mg	0,852	0,767	0,845	0,821	0,801	0,834	0,811	0,821	0,811	0,800
Ca	0,757	0,724	0,795	0,777	0,844	0,841	0,811	0,806	0,799	0,803
Na	0,020	0,020	0,022	0,015	0,023	0,020	0,024	0,017	0,022	0,018
Total	3,990	3,974	4,014	4,002	4,011	4,030	4,001	4,006	3,991	3,993
En	**45**	**41**	**44**	**42**	**41**	**42**	**42**	**42**	**43**	**42**
Fs	**15**	**20**	**15**	**17**	**15**	**16**	**16**	**16**	**16**	**16**
Wo	**40**	**39**	**41**	**40**	**44**	**42**	**42**	**41**	**42**	**42**

Table 13. (Continued)

Sample	FE045	FE045	FE081	FE081	FE081	FE081	FE081	FE081	FE081
grain	E	F	H	I	K	K	K	K	M
spot	C	C	C	C	R	C	C	C	C
SiO_2	53,26	51,44	53,04	55,72	54,31	54,42	49,67	52,40	53,60
TiO_2	1,05	1,09	0,44	0,30	0,33	1,11	0,36	1,09	0,97
Al_2O_3	1,76	2,12	2,95	1,75	2,78	2,10	6,96	1,72	1,69
Cr_2O_3	0,01	0,08	0,22	0,03	0,06	0,05	0,42	0,20	0,27
FeO	9,50	8,51	8,69	13,71	16,81	8,50	19,17	9,52	7,68
MnO	0,21	0,17	0,13	0,25	0,34	0,17	0,17	0,27	0,19
MgO	14,58	14,82	15,05	14,34	11,74	13,97	10,44	14,18	14,51
CaO	20,14	20,66	19,07	13,34	12,31	19,99	12,32	20,71	21,20
Na_2O	0,27	0,27	0,29	0,15	0,62	0,28	0,58	0,25	0,24
Total	100,78	99,16	99,88	99,59	99,30	100,59	100,09	100,34	100,35
Si	1,962	1,928	1,956	2,058	2,040	1,991	1,884	1,947	1,972
Ti	0,029	0,031	0,012	0,008	0,009	0,031	0,010	0,030	0,027
Al	0,077	0,094	0,129	0,077	0,124	0,091	0,313	0,076	0,074
Cr	0,000	0,002	0,006	0,001	0,002	0,001	0,013	0,006	0,008
Fe2+	0,292	0,266	0,267	0,423	0,527	0,260	0,607	0,295	0,236
Mn	0,007	0,005	0,004	0,008	0,011	0,005	0,005	0,008	0,006
Mg	0,800	0,827	0,827	0,789	0,657	0,761	0,590	0,785	0,795
Ca	0,794	0,829	0,753	0,528	0,495	0,783	0,500	0,824	0,835
Na	0,019	0,020	0,021	0,011	0,045	0,020	0,043	0,018	0,017
Total	3,980	4,003	3,975	3,901	3,910	3,943	3,965	3,990	3,969
En	**42**	**43**	**45**	**45**	**39**	**42**	**35**	**41**	**43**
Fs	**15**	**14**	**14**	**24**	**31**	**14**	**36**	**16**	**13**
Wo	**42**	**43**	**41**	**30**	**29**	**43**	**29**	**43**	**45**

Table 14. Representative clinopyroxene analyses from the Thverartindur quartz-tholeiitic gabbros. R-rim, C-core. FE and HV indicate Fellsa and Hvannadalur intrusions, respectively. Letters denote the grains analysed. X-analysed core only . Cations on the basis of six oxygens.

Sample	FE047	FE047	FE047	FE079	FE079	FE079	FE079	FE079	FE079	FE079
grain	A	B	X	I	I	X	X	X	X	X
spot	C	R	C	C	R	C	C	C	C	C
SiO_2	50,48	50,39	50,96	51,52	51,39	51,06	51,12	51,43	51,71	51,44
TiO_2	1,03	0,61	1,01	0,82	1,05	0,87	1,07	0,90	0,91	0,98
Al_2O_3	1,61	0,99	1,54	1,02	1,13	0,99	1,51	0,93	0,69	1,09
Cr_2O_3	0,01	0,02	0,01	0,05	0	0,01	0,08	0,01	0	0,05
FeO	10,47	15,17	13,62	9,86	10,31	12,81	9,07	11,49	12,91	9,94
MnO	0,24	0,48	0,32	0,20	0,24	0,34	0,21	0,26	0,35	0,22
MgO	14,47	12,98	13,52	15,69	15,12	13,79	15,26	14,72	14,33	15,40
CaO	20,48	19,15	18,52	19,78	20,38	19,11	20,57	19,27	18,25	19,61
Na_2O	0,29	0,24	0,22	0,32	0,29	0,30	0,34	0,29	0,28	0,28
Total	99,08	100,03	99,72	99,26	99,91	99,28	99,23	99,30	99,43	99,01
Si	1,916	1,930	1,935	1,939	1,929	1,945	1,923	1,946	1,961	1,941
Ti	0,029	0,018	0,029	0,023	0,030	0,025	0,030	0,026	0,026	0,028
Al	0,072	0,045	0,069	0,045	0,050	0,045	0,067	0,042	0,031	0,049
Cr	0,000	0,001	0,000	0,001	0,000	0,000	0,002	0,000	0,000	0,001
Fe2+	0,332	0,485	0,432	0,310	0,323	0,407	0,285	0,363	0,409	0,313
Mn	0,008	0,016	0,010	0,006	0,008	0,011	0,007	0,008	0,011	0,007
Mg	0,818	0,741	0,765	0,880	0,846	0,783	0,855	0,830	0,809	0,865
Ca	0,832	0,786	0,753	0,797	0,819	0,780	0,829	0,781	0,741	0,792
Na	0,021	0,018	0,016	0,023	0,021	0,022	0,025	0,021	0,021	0,020
Total	4,029	4,038	4,009	4,026	4,026	4,018	4,024	4,018	4,008	4,017
En	**41**	**37**	**39**	**44**	**43**	**40**	**43**	**42**	**41**	**44**
Fs	**17**	**24**	**22**	**16**	**16**	**21**	**14**	**18**	**21**	**16**
Wo	**42**	**39**	**39**	**40**	**41**	**40**	**42**	**40**	**38**	**40**

Table 14. (Continued)

Sample	HV012	HV012	HV012	HV012	HV012	FE050	FE050	FE050	FE050	FE050
grain	A	C	D	E	X	D	D	G	X	X
spot	R	C	R	R	C	C	R	R	C	C
SiO_2	50,85	51,58	49,81	50,95	50,78	51,52	52,69	52,39	52,47	51,95
TiO_2	1,02	1,08	1,52	1,18	1,33	1,28	0,93	0,79	1,05	1,05
Al_2O_3	1,31	1,15	1,87	1,58	1,56	2,72	1,83	1,66	1,94	2,35
Cr_2O_3	0,01	0,04	0,02	0	0,01	0	0,01	0	0,01	0,02
FeO	9,39	9,39	9,34	9,28	9,07	10,30	10,68	10,92	10,23	9,76
MnO	0,23	0,24	0,27	0,24	0,21	0,21	0,32	0,29	0,27	0,22
MgO	15,86	16,19	14,78	14,73	14,74	14,07	14,55	14,46	14,94	14,67
CaO	20,66	20,45	21,10	20,68	21,02	19,66	18,94	19,14	18,29	19,96
Na_2O	0,32	0,29	0,32	0,34	0,33	0,31	0,32	0,26	0,27	0,28
Total	99,65	100,41	99,03	98,98	99,05	100,07	100,27	99,91	99,47	100,26
Si	1,911	1,920	1,889	1,924	1,918	1,921	1,958	1,958	1,957	1,930
Ti	0,029	0,030	0,043	0,034	0,038	0,036	0,026	0,022	0,029	0,029
Al	0,058	0,051	0,084	0,071	0,070	0,120	0,081	0,073	0,086	0,103
Cr	0,000	0,001	0,001	0,000	0,000	0,000	0,000	0,000	0,000	0,001
Fe2+	0,295	0,292	0,296	0,293	0,286	0,321	0,331	0,341	0,319	0,303
Mn	0,007	0,008	0,009	0,008	0,007	0,007	0,010	0,009	0,009	0,007
Mg	0,888	0,898	0,835	0,829	0,829	0,782	0,805	0,805	0,830	0,812
Ca	0,831	0,815	0,857	0,837	0,850	0,785	0,754	0,766	0,731	0,794
Na	0,023	0,021	0,024	0,025	0,024	0,022	0,023	0,019	0,020	0,020
Total	4,043	4,035	4,037	4,019	4,022	3,994	3,988	3,993	3,980	3,999
En	**44**	**45**	**42**	**42**	**42**	**41**	**43**	**42**	**44**	**43**
Fs	**15**	**15**	**15**	**15**	**15**	**17**	**18**	**18**	**17**	**16**
Wo	**41**	**41**	**43**	**43**	**43**	**42**	**40**	**40**	**39**	**42**

Table 15. Representative clinopyroxene analyses from the Thverartindur hybrid rocks. R-rim, C-core. FE indicate Fellsa intrusion. Letters denote the grains analysed. X-analysed core only . Cations on the basis of six oxygens.

Sample	FE046	FE046	FE046	FE046	FE046	FE048	FE048
grain	A	A	B	B	C	F	G
spot	R	C	R	C	R	C	C
SiO_2	50,73	51,07	49,44	49,88	50,87	51,46	49,64
TiO_2	0,80	1,02	0,80	1,02	1,17	0,64	0,57
Al_2O_3	1,74	1,60	1,72	1,87	1,91	0,63	0,61
Cr_2O_3	0	0	0	0,01	0,01	0	0
FeO	11,89	12,70	12,89	10,14	10,94	15,78	16,45
MnO	0,27	0,36	0,36	0,26	0,33	0,47	0,49
MgO	13,91	13,72	13,52	13,89	12,67	12,06	11,50
CaO	19,69	18,10	18,24	20,56	20,75	18,7	18,92
Na_2O	0,21	0,28	0,23	0,28	0,32	0,23	0,23
Total	99,24	98,85	97,20	97,91	98,97	99,97	98,41
Si	1,927	1,945	1,925	1,915	1,935	1,969	1,947
Ti	0,023	0,029	0,023	0,029	0,033	0,018	0,017
Al	0,078	0,072	0,079	0,085	0,086	0,029	0,028
Cr	0,000	0,000	0,000	0,000	0,000	0,000	0,000
Fe2+	0,377	0,404	0,419	0,325	0,347	0,504	0,539
Mn	0,009	0,012	0,012	0,008	0,011	0,015	0,016
Mg	0,787	0,778	0,784	0,794	0,718	0,687	0,672
Ca	0,801	0,738	0,761	0,845	0,845	0,766	0,795
Na	0,015	0,021	0,017	0,021	0,024	0,017	0,017
Total	4,018	4,000	4,021	4,023	4,000	4,007	4,031
En	**40**	**41**	**40**	**40**	**38**	**35**	**34**
Fs	**19**	**21**	**21**	**17**	**18**	**26**	**27**
Wo	**41**	**38**	**39**	**43**	**44**	**39**	**40**

Table 15. (Continued)

Sample	FE048	FE048	FE048	FE048	FE048	FE048	FE048	FE048
grain	X	X	X	X	X	X	X	X
spot	C	C	C	C	C	C	C	C
SiO_2	50,64	52,16	51,52	51,74	51,37	50,82	52,56	50,79
TiO_2	0,49	0,63	0,53	0,54	0,56	0,52	0,50	0,53
Al_2O_3	0,57	0,88	0,59	0,55	0,62	0,49	0,79	0,57
Cr_2O_3	0	0	0	0	0,03	0	0	0
FeO	17,35	14,34	15,73	17,88	15,93	17,69	15,94	16,39
MnO	0,56	0,42	0,47	0,52	0,47	0,55	0,50	0,51
MgO	10,59	12,81	11,79	10,87	10,85	11,19	11,17	11,13
CaO	19,57	18,66	19,72	18,37	19,12	18,16	19,01	18,96
Na_2O	0,26	0,25	0,21	0,23	0,23	0,28	0,26	0,25
Total	100,03	100,15	100,56	100,70	99,18	99,70	100,73	99,13
Si	1,961	1,975	1,965	1,981	1,985	1,968	1,993	1,971
Ti	0,014	0,018	0,015	0,016	0,016	0,015	0,014	0,015
Al	0,026	0,039	0,027	0,025	0,028	0,022	0,035	0,026
Cr	0,000	0,000	0,000	0,000	0,001	0,000	0,000	0,000
Fe2+	0,561	0,453	0,501	0,571	0,514	0,572	0,505	0,531
Mn	0,018	0,013	0,015	0,017	0,015	0,018	0,016	0,017
Mg	0,611	0,722	0,670	0,620	0,625	0,646	0,631	0,643
Ca	0,811	0,757	0,806	0,753	0,791	0,753	0,772	0,788
Na	0,020	0,018	0,016	0,017	0,017	0,021	0,019	0,019
Total	4,022	3,997	4,014	4,000	3,993	4,016	3,985	4,010
En	**31**	**37**	**34**	**32**	**32**	**33**	**33**	**33**
Fs	**28**	**23**	**25**	**29**	**27**	**29**	**26**	**27**
Wo	**41**	**39**	**41**	**39**	**41**	**38**	**40**	**40**

Table 17. Representative chemical analyses of cromian spinels from Thverartindur ultramafic rocks. AA101- a olivine-rich dike from Hvannadalur; FE indicate Fellsa and HV Hvannadalur intrusions, respectively. Cations on the bases of 32 oxygens.

	AA101	AA101	FE063	FE063	FE063	HV028	HV028	HV028	HV028
Grain	A	D	X	P	P	X	G	G	X
TiO_2	1,45	1,81	0,75	2,76	2,89	1,19	1,60	1,72	1,62
Al_2O_3	30,04	29,15	13,05	15,25	15,32	16,99	19,03	19,21	13,71
Cr_2O_3	30,02	29,86	37,76	30,78	29,34	42,61	40,64	39,82	30,73
FeO	24,88	23,45	41,22	44,14	44,98	29,33	28,59	28,60	46,49
MnO_2	0,28	0,32	0,48	0,43	0,35	0,33	0,55	0,45	0,46
MgO	14,62	14,64	5,69	7,01	6,80	8,84	8,33	8,47	5,40
Total	101,29	99,23	98,95	100,37	99,68	99,29	98,74	98,27	98,41
Ti	0,260	0,335	0,165	0,575	0,608	0,244	0,318	0,343	0,357
Al	8,503	8,496	4,136	5,010	5,080	5,107	5,955	6,029	4,761
Cr	5,668	5,805	8,718	6,745	6,489	9,192	8,483	8,335	6,863
Fe	4,963	4,447	10,055	10,220	10,511	6,391	6,306	6,325	11,378
Mn	0,057	0,067	0,119	0,101	0,083	0,076	0,123	0,101	0,114
Mg	5,204	5,365	2,215	2,896	2,835	3,595	3,278	3,342	2,358
Total	24,654	24,515	25,408	25,547	25,607	24,606	24,463	24,475	25,831
Cr/Al+Cr	**0,40**	**0,41**	**0,68**	**0,57**	**0,56**	**0,64**	**0,59**	**0,58**	**0,59**

Table 18. Representative FeTi - oxide analyses from Thverartindur ultramafic rocks, gabbros and hybrid rock types. FE and HV indicate Fellsa and Hvannadalur intrusions, respectively. Analyses from separate big crystals, enclosed by olivine and plagioclase; and small groundmass crystals.

Sample	Phase	Note	TiO_2	Al_2O_3	Cr_2O_3	FeO	MnO_2	MgO	Total
FE063	Ilm	Separate	49,08	0,06	0,04	47,17	1,18	1,56	99,09
FE063	Ilm	In Ol	51,01	0,08	0,28	44,78	1,45	1,88	99,48
FE063	Ilm	Ol-Px	50,30	0,20	0,34	45,43	1,44	2,09	99,80
FE065	Ilm	Separate	47,55	0,10	0,05	48,20	2,49	1,49	99,88
FE065	Ilm	Separate	49,00	0,08	0,09	47,05	3,01	1,37	100,60
HV028	Ilm	Separate	47,88	0,03	0,02	49,25	3,45	0,12	100,75
HV028	Ilm	Ground	48,02	0,03	0,10	48,34	3,29	0,36	100,14
FE044	Ilm	Separate	47,49	0,18	0,01	48,49	2,44	0,16	98,77
FE045	Mt	In Pl	24,61	1,16	0,05	72,42	1,45	0,1	99,79
FE081	Ilm	In Pl	46,35	0,05	0,01	46,01	8,87	0,18	101,47
FE047	Ilm	Separate	47,16	0,39	0,02	50,95	1,82	0,12	100,46
FE047	Mt	Separate	14,22	0,81	0,03	85,78	0,75	0,07	101,66
FE047	Ilm	In Pl	48,43	0,11	0	50,67	1,76	0,07	101,04
FE047	Mt	In Pl	22,77	0,67	0,01	76,43	0,86	0,07	100,81
FE079	Mt	Separate	27,88	0,80	0,02	71,50	1,11	0,08	101,39
FE079	Mt	Separate	11,17	1,93	0,03	85,97	0,55	0,06	99,71
FE079	Mt	Separate	33,34	1,39	0,04	63,33	1,41	0,03	99,54
FE079	Ilm	Pl-Px	47,97	0,13	0	48,72	2,00	0,05	98,87
HV012	Ilm	Separate	45,88	0,06	0	51,75	1,96	0,18	99,83
HV012	Ilm	Separate	45,81	0,04	0,03	51,38	1,96	0,16	99,38
FE050	Mt	Altered	30,23	0,16	0,04	69,28	1,43	0,04	101,18
FE050	Ilm	Ground	46,96	0,09	0,01	50,64	1,84	0,05	99,59
FE 046	Mt	Separate	28,20	1,11	0,02	68,34	1,66	0,08	99,41
FE 046	Ilm	Separate	43,38	1,03	0	52,57	2,38	0,11	99,47
FE048	Ilm	Separate	49,81	0,03	0	44,38	4,52	0,09	98,83
FE048	Ilm	Separate	49,31	0,05	0	47,48	4,91	0,05	101,80
FE048	Mt	Ground	17,56	0,25	0,02	78,92	1,71	0,02	98,48
FE048	Mt	In Pl	29,47	0,49	0	66,45	2,81	0,09	99,31
HV035	Ilm	Separate	48,25	0,08	0,02	44,63	6,84	0,07	99,89
HV035	Ilm	In Pl	47,89	0,17	0,01	44,70	5,43	0,39	98,59